Copyright Warning & Restrictions

The copyright law of the United States (Title 17, United States Code) governs the making of photocopies or other reproductions of copyrighted material.

Under certain conditions specified in the law, libraries and archives are authorized to furnish a photocopy or other reproduction. One of these specified conditions is that the photocopy or reproduction is not to be "used for any purpose other than private study, scholarship, or research." If a, user makes a request for, or later uses, a photocopy or reproduction for purposes in excess of "fair use" that user may be liable for copyright infringement,

This institution reserves the right to refuse to accept a copying order if, in its judgment, fulfillment of the order would involve violation of copyright law.

Please Note: The author retains the copyright while the New Jersey Institute of Technology reserves the right to distribute this thesis or dissertation

Printing note: If you do not wish to print this page, then select "Pages from: first page # to: last page #" on the print dialog screen

ABSTRACT

EXPLORING FUSED DEPOSITION MODELING (FDM) THREE-DIMENSIONAL PRINTING TABLET DESIGN OPTIONS FOR PHARMACEUTICAL DOSAGE FORMS

by
Guluzar Gorkem Buyukgoz

This dissertation examines the use of Fused Deposition Modeling (FDM) based three-dimensional (3D) printing approach for developing patient-specific dosage forms and addressing related technical challenges in such drug delivery systems. The first main objective is to explore pharmaceutical tablet design options using novel FDM 3D printing technology as the drug delivery platform such that drug form and tablet properties are tailored by considering patient age-specific formulations and dissolution control. Of the five different design options, two proposed options meet the main objective of providing similar drug release, whereas the popular option of fixed drug concentration but differing tablet size could not. These two options are, (1) varying drug-concentration feed materials at fixed tablet size, and (2) fixed-sized duo-tablet with internal varying size placebo regions. The tablet surface area to volume (SA/V) ratio is identified as the controlling factor for drug release, while Hydroxymethyl cellulose (HPC) as the matrix yields near zero-order release. For the duo-tablet design, placebo shell thickness governs long lag times. Next, miniature tablets containing very low drug concentration (1 wt%) are manufactured via FDM 3D printing for targeting the pediatric patient population, who have difficulty in swallowing large tablets, while the dosage is dictated by their body weight/age. It is demonstrated that the use of multi-unit mini-tablets, allows flexible dose titration, leads to similar release profiles

for varying drug doses, could serve the purpose of micro-dosed therapy, and minimize the difficulties in swallowing. As a unique new contribution, the feed materials containing the drug in largely crystalline form are produced via hot-melt extrusion (HME) at relatively low processing temperatures. This approach is intended to reduce the adverse effects of recrystallization of the amorphous drug, including uncontrolled drug crystal growth. In addition, this approach is shown to better maintain adequate filament mechanical properties, which is crucial for their printability. In addition, this technique, called fusion-assisted amorphous solid dispersion (ASD) conversion during printing is shown to be a one-step printing process alternative to the conventional HME-compounded ASDs for solubility enhancement of poorly water-soluble drugs. By avoiding the use of HME for preparing the amorphous filaments, this approach also minimizes the confounding effects arising from drug recrystallization, being a common challenge for HME compounded ASDs. Finally, process analytical technology (PAT) is implemented for predicting drug concentration of the feed materials using chemometric methods based solely on Raman spectroscopy. This is intended for addressing regulatory concerns for point of care printed on-demand products without requiring testing of the resulting product. In summary, this dissertation makes major advances in several areas for developing patient-specific dosage forms and addressing related technical challenges in such drug delivery systems, including addressing regulatory issues typical for on-demand products.

EXPLORING FUSED DEPOSITION MODELING (FDM) THREE-DIMENSIONAL PRINTING TABLET DESIGN OPTIONS FOR PHARMACEUTICAL DOSAGE FORMS

by
Guluzar Gorkem Buyukgoz

A Dissertation
Submitted to the Faculty of
New Jersey Institute of Technology
in Partial Fulfillment of the Requirements for the Degree of
Doctor of Philosophy in Chemical Engineering

Otto H. York Department of
Chemical and Materials Engineering

August 2021

APPROVAL PAGE

EXPLORING FUSED DEPOSITION MODELING (FDM) THREE-DIMENSIONAL PRINTING TABLET DESIGN OPTIONS FOR PHARMACEUTICAL DOSAGE FORMS

Guluzar Gorkem Buyukgoz

Dr. Rajesh N. Davé, Dissertation Advisor — Date
Distinguished Professor of Chemical and Materials Engineering, NJIT

Dr. Ecevit A. Bilgili, Committee Member — Date
Associate Professor of Chemical and Materials Engineering, NJIT

Dr. Xiaoyang Xu, Committee Member — Date
Associate Professor of Chemical and Materials Engineering, NJIT

Dr. Murat Guvendiren, Committee Member — Date
Assistant Professor of Chemical and Materials Engineering, NJIT

Dr. Rodolfo J. Romañach, Committee Member — Date
Research Professor of Analytical Chemistry, University of Puerto Rico at Mayagüez (UPRM), Puerto Rico

BIOGRAPHICAL SKETCH

Author: Guluzar Gorkem Buyukgoz

Degree: Doctor of Philosophy

Date: August 2021

Undergraduate and Graduate Education:

- Doctor of Philosophy in Chemical Engineering
  New Jersey Institute of Technology, Newark, NJ, 2021

- Master of Science in Food Engineering
  Hacettepe University, Ankara, Turkey, 2014

- Bachelor of Science in Food Engineering
  Hacettepe University, Ankara, Turkey, 2012

Major: Chemical Engineering

Presentation and Publications

Patent and journal articles:

Davé, R. N., Zhang, L., **Gorkem Buyukgoz, G**., and Cetindag, E (2021). Compositions and methods for preparing polymeric films loaded with uniformly distributed drug particles. U.S. Patent 10,918,602.

Gorkem Buyukgoz, G., Castro, J. N., Atalla, A. E., Pentangelo, J. G., Tripathi, S., & Davé, R. N. (2021). Impact of mixing on content uniformity of thin polymer films containing drug micro-doses. Pharmaceutics, 13, 812.

Gorkem Buyukgoz, G., Soffer, D., Defendre, J., Pizzano, G. M., & Davé, R. N. (2020). Exploring tablet design options for tailoring drug release and dose via fused deposition modeling (FDM) 3D printing. International Journal of Pharmaceutics, 591, 119987.

Gorkem Buyukgoz, G.,Ji, S., Guvendiren, M., & Davé, R. N. Dose titration via 3D printed mini-tablets*. In preparation*.

Gorkem Buyukgoz, G., Kossor, C., & Davé, R. N. FDM 3D printed tablets loaded with fusion-assisted amorphous solid dispersions*. In preparation*.

Gorkem Buyukgoz, G., Cetindag, E., Quirie, S., Manoj, P. R., Montarrayos, M., & Davé, R. N. Real-time monitoring of critical quality attributes (CQAs) of polymer films laden with engineered drug particles. *In preparation*.

Gorkem Buyukgoz, G., Castro, J., Atalla, A. A., Pentangelo, J., & Davé, R. N. Enhanced content uniformity from thin polymer films containing micron-sized Fenofibrate through improved mixing. *In preparation*.

Conference proceedings:

Gorkem Buyukgoz, G. Continuous mixing of film precursor containing engineered particles (2019). American Association of Pharmaceutical Scientists *PHARMSCI 360*.

Gorkem Buyukgoz, G., Castro, J., Velmurugan, K., & Davé, R. (2018). Towards continuous manufacturing (CM) of drug loaded strip films: Continuous mixing of dry micronized drug particles with film precursor via twin screw extruder (TSE). *American Institute of Chemical Engineers Annual Meeting.*

Gorkem Buyukgoz, G., Abdelmalak, M., Kapoor, R., Castro, J., Ji, S., Quirie, S., . . . Davé, R. (2018). 3D printed complex dosage forms embedded with engineered BCS class II drug particles. *American Institute of Chemical Engineers Annual Meeting.*

Castro, J., **Gorkem Buyukgoz, G.,** & Davé, R. (2018). The effects of mixing processes on critical quality attributes of strip films. In *8th World Congress on Particle Technology*. American Institute of Chemical Engineers.

Gorkem Buyukgoz, G., Abdelmalak, M., Kapoor, R., Castro, J., Ji, S., Quirie, S., Guvendiren, M., & Davé, R. (2018). Additive manufacturing of high drug loaded extended-release tablets via FDM 3D Printing. In *8th World Congress on Particle Technology*. *American Institute of Chemical Engineers*.

To my family

ACKNOWLEDGMENT

I would like to express my gratitude to my dissertation advisor, Dr. Rajesh N. Davé, for his expert guidance, patience, financial support, and encouragement through my graduate studies. I am always grateful for his help in mentoring me and encouraging me to think from various aspects, which helped me to reach my personal best.

I would like to thank my committee members, Dr. Rodolfo J. Romañach, Dr. Ecevit A. Bilgili, Dr. Murat Guvendiren, and Dr. Xiaoyang Xu for accepting to serve on my committee, reading previous drafts of this dissertation, and providing valuable comments that greatly improved the contents of this dissertation.

I would like to extend special thanks to Dr. Bilgili, Dr. Guvendiren, Dr. Romañach, and Dr. Zafar Iqbal for allowing me to use their laboratories as well as their constructive comments, guidance, and intellectual contribution through my graduate studies. I would like to extend acknowledgment to Dr. Edward Dreizin for allowing me to use his laboratories and to Dr. Mirko Schoenitz for his remarks and guidance with the use of instruments necessary for my research.

I would like to thank Dr. Mardan Niyaz, who is an account manager in Nisso America Inc., for donating materials, essential for my research.

I am thankful for partial financial support from National Science Foundation under grants [EEC-0540855] and [IIP-1919037].

I would like to thank the following members of our group and friends for their spiritual and physical support to my research: Dr. Eylul Cetindag, Semih Cetindag,

Dr. Kuriakose Kunnath, Dr. Mahbubur Rahman, Dr. Kai Zheng, Dr. Liang Chen, Dr. Lu Zhang, Sangah Kim, Zhixing Lin, Ruosong Dong, Siddharth Tripathi, Nathaniel Parker, Gulenay Guner, and Dr. Shen Ji. I would like to extend special thanks to Dr. Eylul Cetindag for supporting me with her enthusiasm, pride, curiosity, and importantly her sincere friendship throughout my Ph.D. I would like to thank my respectful friend, Cemile Kanalka, who stood by me through thick and thin.

Finally, I would like to express my deepest gratitude to my family. To my mother, Ayfer Gorkem, to my father, Yasar Gorkem, and my brother Resul Metehan Gorkem for their endless love and support at every stage of my life. A special thanks to my beloved husband and priceless friend, Dr. Cihangir Buyukgoz for being always there for me.

TABLE OF CONTENTS

TABLE OF CONTENTS
(Continued)

Chapter **Page**

TABLE OF CONTENTS
(Continued)

Chapter **Page**

TABLE OF CONTENTS
(Continued)

Chapter **Page**

LIST OF TABLES

Table **Page**

LIST OF TABLES
(Continued)

Table **Page**

LIST OF FIGURES

Figure **Page**

LIST OF FIGURES
(Continued)

Figures **Page**

LIST OF FIGURES
(Continued)

Figures **Page**

CHAPTER 1

INTRODUCTION

1.1 Background

Developing and implementing new, state of the art technologies to meet the individual patient's need is one of the most important objectives in drug development; hence it is an active area of pharmaceutical research. The main areas of research in novel pharmaceutical designs are: (i) improving drug administration, (ii) improving drug bioavailability, and more importantly, (iii) enhancing dosage flexibility. All of these are very important, and have a big impact on patient compliance and adherence to required medications, which ultimately dictate the success of any therapy. Further, because of the differing needs of the patients, stemming from different reasons including their age, weight, and genetic make-up, relying on a single dosage form is less than ideal and is the motivation for the development of more flexible, on-demand dosage platforms (Breitkreutz et al., 2007; Lopez et al., 2015). Towards that objective, there is an increasing research activity towards developing vehicles for personalized medicine for drug delivery, while addressing issues such as flexible dosing and increased bioavailability, which are all generally lacking in the conventional dosages.

It is a known fact that traditional oral dosage forms (e.g., tablets and capsules) cannot cater to on-demand production and fabrication of tailored dosage forms, particularly when dose variations and drug combinations are required. In addition, the large footprint of inherently complex manufacturing processes

including milling, sieving, compressing, and coating limits the level of agility and flexibility in dosing (Alhnan et al., 2016). The conventional approach is also not very suitable for achieving enhanced bioavailability through producing complex dosage geometries (Li et al., 2017b; Sadia et al., 2018a; Zhang et al., 2017a).

Fortunately, the emerging field of three-dimensional (3D) printing technology, in particular through Fused Deposition Modeling (FDM), is capable of the increased flexibility of manufacturing along with achieving drug product shape complexity by digital control over the arrangement of printed matter that includes drug (Norman et al., 2017). Consequently, creating advanced geometries to manipulate drug release behavior with an adjustable surface area/volume ratio of the final product (Alhnan et al., 2016; Norman et al., 2017; Sadia et al., 2018a), and accurately controlling the spatial distribution of active pharmaceutical ingredients (APIs) within the product, hence allowing for rapid fabrication of combination drugs along with a tailored dosage form are some of these advantages of 3D printing technology (Khaled et al., 2015a, 2015b; Norman et al., 2017). Further, the recent approval by the U.S. Food and Drug Administration (FDA) for the first 3D printed medication (Zipdose®, 2015), has also triggered growing interest in 3D printing technology (Alhnan et al., 2016; Goyanes et al., 2017).

It is useful to mention that besides FDM technique, (Goyanes et al., 2015d; Long et al., 2017; Melocchi et al., 2015; Pietrzak et al., 2015) 3D printing technologies in oral dosage forms include several other techniques; mainly i.e., semi-solid extrusion (EXT) printing (Khaled et al., 2014; Khaled et al., 2015a,

2015b; Rattanakit et al., 2012) and powder bed (PB) printing (Rowe et al., 2000; Yu et al., 2009). Although these technologies have their strengths and weaknesses, FDM printing is considered highly promising for developing and producing 3D printed industrial oral dosage forms (Goyanes et al., 2015b; Goyanes et al., 2016). This is largely due to FDM not requiring lengthy post-printing processes such as drying or powder removal. Another advantage of FDM printing is that it makes use of solid feed materials which have better shelf-life than the liquids and pastes used in PB and EXT printing. This means that there is less waste due to expired feed at the factory level. In FDM technique, a polymer filament is fed through a heated nozzle and deposited on a build plate layer-by-layer (Goyanes et al., 2014; Melocchi et al., 2015). The thermoplastic polymers used to create the filaments must be heated to a temperature above the polymer glass transition temperature (T_g) before the printing process can start (Melocchi et al., 2015; Okwuosa et al., 2016). This requirement of elevated temperatures during the process limits the use of this technique for heat-sensitive compounds (Alhnan et al., 2016).

Recent literature in FDM 3D printing has focused on, but is not limited to, two main categories: (i) improvements in flexible dosage dispensing and, (ii) enhancement of bioavailability. The most prevalent approaches to achieve desired drug therapy through FDM 3D printing involve manipulating the tablet sizes, structure, or shape (Goyanes et al., 2015c; Goyanes et al., 2015d; Pietrzak et al., 2015; Sadia et al., 2018a; Skowyra et al., 2015; Solanki et al., 2018b). However, scrutiny of the results also reveals that it is not easy to produce

prescribed dosages by manipulating tablet properties while keeping the percentage drug release profiles similar. Regarding controlling drug dissolution, creating advanced geometries (Goyanes et al., 2015c) and solid dispersions (Solanki et al., 2018b) are the main techniques. Recent reports have shown the potential for embedding a drug in amorphous form into 3D printed structures (Solanki et al., 2018b; Wei et al., 2020). However, that approach requires sufficient drug-polymer miscibility, suitable polymer type, and has drug to polymer ratio limitations (Solanki et al., 2018b). In addition, if these criteria are not adequately addressed, recrystallization of the drug can occur within the matrix during storage and throughout the dissolution, adversely impacting the product performance (Gupta et al., 2004). Therefore, it is important to investigate expanded design options for novel FDM 3D printing drug delivery platform, to improve both the bioavailability and flexibility of dosing.

1.2 Objectives

In response to the aforementioned challenges and issues, the major objective of this dissertation is to explore pharmaceutical tablet design options for the novel drug delivery platform, FDM 3D printing, such that drug form and tablet properties are tailored by considering age-specific formulations and bioavailability enhancement. First, achieving simultaneous tailoring of drug release and dose is considered through manipulating the tablet size and structure of FDM 3D printed tablets. Next, options for the dose titration, necessary for patient age and weight specific dosages, via FDM 3D printed mini-sized tablets containing very low drug

concentration are examined. Subsequently, an innovative design option is investigated towards enhancing the solubility of poorly water-soluble drugs. That approach takes advantage of FDM 3D printing capability of producing transient heat energy along with advanced geometries to produce fusion-assisted ASDs. Finally, process analytical technology (PAT) to enhance manufacturability is considered. Towards that goal, chemometric models are developed for predicting the printed tablet drug concentration at the point of care through Raman spectroscopy of the feed materials, for addressing regulatory concerns related to on-demand products.

1.3 Outline

This dissertation has been organized into six chapters. Chapter 1 discusses relevant background concepts and literature, followed by the objective and outline of the dissertation. Chapter 2 investigates the tablet design options for FDM 3D printing for simultaneous tailoring of drug release and dose. Chapter 3 examines the manufacturing of low-dosed mini-tablets via FDM 3D printing, by targeting patient age-specific dose titration. Chapter 4 presents the 3D printed tablets loaded with fusion-assisted amorphous solid dispersions (ASDs) to enhance the solubility of poorly water-soluble drugs. Chapter 5 implements the process analytical technology (PAT) using Raman spectroscopy for determining the drug concentration from feed materials of FDM 3D printing. Chapter 6 provides an overall summary and conclusions of the dissertation, and offers a direction for future studies.

CHAPTER 2

TABLET DESIGN OPTIONS

2.1 Introduction

The need for patient-specific drug dosage development has been well recognized, in particular for pediatric and geriatric populations that differ from a ‘standard patient’ in many aspects (Breitkreutz et al., 2007; Kearns et al., 2003; Liu et al., 2014). The differing needs, stemming from individual’s age, gender, lifestyle, metabolic capacity, co-morbidity as well as therapeutic response to the medications (Breitkreutz et al., 2007; Sandler et al., 2016), may impact the efficacy of the dosage due to either the amount of delivered drug being insufficient or too much. Ideally, the drug formulations and dosages should meet the patient’s individual needs. The emerging technique of Fused Deposition Modeling (FDM) based 3D printing may address this need because it is capable of manufacturing patient-tailored dosage forms by digital control over the arrangement of printed matter (Norman et al., 2017). Recent work shows incorporation of different polymer types into formulation of filaments, used as the feed materials, usually produced via hot-melt extrusion (Melocchi et al., 2016; Solanki et al., 2018b; Zhang et al., 2017a). These papers demonstrate that the drug amount and its release rate may be tailored by exploiting differing polymer properties and by designing different formulations. The FDM printing also requires suitable mechanical properties for the feed materials (Zhang et al., 2017a), imposing an additional burden on adjusting the formulations to also assure printability. Thus, the success of this

approach becomes dependent on several factors such as thermal properties of the material used, miscibility/solubility between drug and polymer, mechanical properties of the feed materials, and 3D printing process parameters (Ilyés et al., 2019b; Wei et al., 2020). These potentially confounding factors could inherently limit the manufacturing flexibility of 3D printing, hence preventing its widespread use for manufacturing personalized dosages. The most prevalent approaches to achieve desired dosage and its release through FDM 3D printing involve manipulating the tablet sizes, structure, or shapes while utilizing the feedstock having fixed drug concentration (Goyanes et al., 2015c; Goyanes et al., 2015d; Skowyra et al., 2015; Solanki et al., 2018b). For example, Goyanes et al. (2015c) fabricated 3D printed forms having several geometries including cube, pyramid, cylinder, sphere, and torus by using polyvinyl alcohol (PVA) filament with 3.78 wt% drug concentration. They varied printed tablet dimensions to keep either (i) surface area constant, (ii) surface area to volume ratio constant (SA/V), or, (iii) the weight constant, for each shape. Their main conclusion was that the drug release showed little dependence on the surface area but more on either the SA/V or surface area to tablet mass ratio, which is expected from matrix erosion phenomena. However, they did not analyze the dissolution profiles using known drug release kinetic models. Another popular option to achieve dosages with varying drug amounts is to print tablets with increasing sizes/volumes. (Pietrzak et al., 2015; Skowyra et al., 2015). For instance, Skowyra et al. obtained the desired drug amounts through varying tablet volumes, where the smaller tablets containing lower drug amounts had faster drug release (Skowyra et al., 2015). In an interesting work, Sadia et al.

created 3D printed tablets, which were either solid or had channels within (Sadia et al., 2018a). The channels led to increased SA/V ratio as well as increased dissolution media perforation through the structure. Analysis of their dissolution testing results reveals that the dissolution from various tablets was a strong function of the SA/V ratio (Sadia et al., 2018a). In their well-planned study, the surface area was increased through internal channels or holes. Hence the importance of reducing the channel resistance to the flow of the dissolution media was also identified.

Papers such as these shed light on the dissolution behavior of printed tablets with several designs, sizes, and shapes. However, scrutiny of the results also reveals that it is not easy to produce patient-specific dosages with differing drug amounts while keeping the percentage drug release profile similar. This is due to the fact that the FDM-based 3D printed tablets inherently require relatively large amounts of matrix-forming polymers resulting in erosion-based dissolution that largely depends on the tablet SA/V ratio. Since that is likely to be the case for most 3D printed tablets, it is important to examine how tablets with fixed shape and size can provide similar dissolution behavior while having differing drug doses. Consequently, the main focus of this paper is to examine several design options and analyze the corresponding drug release profiles using appropriate models to determine the prevailing drug release mechanism. The underlying goal is to identify the options that allow designing tablets with desirable drug release while varying their drug dose that could help with patient-specific oral drug delivery.

Since the drug release is largely controlled by the tablet SA/V ratio, keeping it constant while varying the tablet drug amount using filaments containing different drug concentrations may be a logical choice to meet the main objective of this work. A shortcoming of this approach is the need for producing printable filaments in varying drug concentrations, e.g., 5–30 wt%, posing challenges due to varying filament mechanical properties. Another choice of tablet design that is worth studying is to use a placebo filament in conjunction with a fixed drug-concentration filament to create a fixed size tablet that has patterned regions within the tablet containing drug, also called drug reservoirs (Li et al., 2017b; Siepmann et al., 2012). The latter option may allow greater flexibility, whereas ultimately both of the proposed approaches could be combined for producing tablets with varying patterns of drug-containing and placebo regions to cover a wide range of drug concentrations while achieving nearly similar drug release profiles. As an interesting variation, 3D printing may be used to create duo-tablets, where either the drug-containing zone is internally formed as a core of the tablet or it is formed peripherally so that the placebo portion is the core. Such approaches are considered in this work, along with quantitative analysis of resulting dissolution profiles using mathematical models including Korsmeyer-Peppas and zero-order (Korsmeyer et al., 1983; Peppas et al., 1989). The focus of this paper is to examine the impact of the tablet design options on drug release from 3D printed tablets. The drug material and processing protocols are selected to avoid added complications and confounding effects arising from drug-polymer interactions during the feed-material preparation using hot-melt extrusion (HME), which

typically produces amorphous solid dispersions (ASDs) (Hancock et al., 1997; Li et al., 2018; Thommes et al., 2011; Wei et al., 2020). HME-based products require considerations of the individual drug and polymer properties as well as their interactions such as drug-polymer miscibility, melt rheology, degradation, and long-term stability, which are all greatly impacted by drug type, polymer type, drug weight percentage, and extrusion temperature (Solanki et al., 2018a; Solanki et al., 2019a; Solanki et al., 2019b; Wei et al., 2020). On one hand, improved miscibility and lower viscosity at higher processing temperature reduces the load on the equipment and could help mixing. On the other hand, a higher temperature could lead to polymer and drug degradation and it could adversely affect filament quality necessary for FDM 3D printing (Aho et al., 2017; Censi et al., 2018; Govender et al., 2020; Kempin et al., 2017; Solanki et al., 2018a; Yang et al., 2016). Moreover, the resulting ASDs have inherent stability problems due to the tendency for the amorphous forms to recrystallize in time that may influence the performance of the products such as drug dissolution behavior. For circumventing such problems associated with forming and maintaining ASDs, and the need for higher processing temperatures, it may be better to maintain the drug in its crystalline form (Hülsmann et al., 2000; Thommes et al., 2011). For example, when using a constant printing temperature for producing tablets with different drugs, either amorphous or crystalline forms appeared in the final products hence the effects from the physical form of the drug were confounded (Goyanes et al., 2015d; Sadia et al., 2016). Therefore, it is better to avoid formation of ASDs to meet the main objective of this work and select the model drug and polymer in a manner

that facilitates maintaining the drug in crystalline form. That requires the drug to have a sufficiently high melting point and minimal miscibility with the polymer at the HME and FDM processing temperatures. Another major advantage of keeping the drug in crystalline form is the reduced possibility of adverse effects on filament printability due to reduced processing temperature. Because this approach does not produce ASDs, it is useful for 3D printing of all Biopharmaceutics Classification System (BCS) class compounds that meet the melting point and miscibility requirements. As an example, theophylline, a BCS class I compound, that meets such requirements, was used to tailor dosage form via FDM 3D printing (Pietrzak et al., 2015).

Based on these considerations, model BCS class II drug, griseofulvin (GF) is used along with hydroxypropyl cellulose (HPC) as the matrix-forming polymer. GF and HPC are thermally stable at higher processing temperatures (Goyanes et al., 2019; Rahman et al., 2020c) and allow flexibility with setting the printing temperatures. Further, GF and HPC are poorly miscible and unlikely to form amorphous structure (Li et al., 2017a). A twin-screw extruder is used to prepare the required drug-loaded filaments at 5–30 wt% concentrations, subsequently used for FDM-based 3D printing of the options described below.

A. Using fixed drug-concentration filaments, varying tablet sizes at fixed geometry with varying drug amounts. This common approach (Pietrzak et al., 2015; Skowyra et al., 2015) also serves as the control design.

B. Using varying drug-concentration filaments, varying tablet sizes at fixed geometry with constant total drug amount. This option is another control that may allow for evaluating the impact of matrix and varying surface area for the same mass of drug in each tablet.

C. Using varying drug-concentration filaments, fixed tablet sizes at fixed geometry for varying drug amounts in each tablet. This option allows for maintaining a constant SA/V ratio, which is considered to be the main driver for dissolution. This option allows testing the hypothesis that since the dissolution rate is expected to be driven by matrix relaxation/erosion due to properties of the polymer, HPC, all dissolution profiles should be statistically similar.

D. Using fixed drug-concentration filaments, keeping tablet sizes and geometry (cylinder) fixed but patterning the tablet allowing for varying total tablet drug amounts by creating different sized internal drug reservoirs and peripherally printed placebo regions.

E. Similar to option D, but varying total tablet drug amounts by creating different sized internal placebo regions and peripherally printing drug-rich regions. It hypothesized that the dissolution profiles exhibit statistically similar release since the presence of important variables (i.e., varying surface area to volume ratio & drug concentration) in previous cases will be eliminated.

2.2 Materials and methods

2.2.1 Materials

Griseofulvin (GF; Letco Medical, Decatur, AL, USA) was selected as a model Biopharmaceutics Classification System (BCS) class II drug. GF is a crystalline drug with a melting point of 220 ºC. Pharmaceutical grade hydrophilic silica (M5P, Cabot Corporation, MA, USA) with a primary particle size of 16 nm was used for the surface modification of milled GF particles. Hydroxypropyl cellulose (HPC, SL grade, Nisso America Inc., New York, NY) is a semi-crystalline polymer with largely amorphous domains (Picker-Freyer et al., 2007; Rahman et al., 2020c; Sarode et al., 2013a). HPC has been used as a printing polymer for fused deposition modeling (FDM) due to its ability to produce filaments with appropriate mechanical properties for 3D printing (Öblom et al., 2019; Pietrzak et al., 2015; Zhang et al.,

2017a). In addition, it enhances the wettability of hydrophobic GF particles (Li et al., 2017a). Polylactic acid (PLA) was purchased as an extruded filament (ø: 1.75 mm, print temperature: 190–220 ºC, Flashforge Corp., China). PLA was used only for printing a marker to better monitor the morphological changes of the printed tablets under the dissolution medium. Sodium dodecyl sulfate (SDS) (Sigma-Aldrich, Saint Louis, MO, USA) was used as a solvent

2.2.2 Preparation methods

2.2.2.1 Preparation of milled and surface modified GF particles. Dry milling of GF particles was performed by following previously established works with continuous milling in a fluid energy milling (FEM; qualification model, Sturtevant Inc., Hanover, MA, USA) (Davé et al., 2011; Han et al., 2011). Powder feeding was controlled by a volumetric feeder (Model 102M, Schenck Accurate, WI, USA) at a rate of 1 g/min. A constant feeding pressure of 65 psi and constant grinding pressure of 60 psi were maintained. Surface modification of the milled particles was conducted using a high-intensity vibrational mixer (LabRAM, Resodyn Acoustic Mixers, Inc., Butte, MT, USA). The milled GF particles (99 g) and silica (1 g) were added to a plastic cylindrical jar and were mixed by LabRAM at a frequency of 61 Hz with an acceleration of 75 G for 5 min; these particles were referred to as MC-GF. The additional dry coating step was carried out to help with the feeding of drug and polymer powder mixture through gravity-driven screw feeder, found to be necessary for two higher drug concentration cases. Another reason was for the potential of coated GF particles to help ensure a very good distribution of GF particles within the polymeric matrix (Zhang et al., 2018).

2.2.2.2 Preparation of feed materials (filaments) of FDM 3D printer. The formulations to be extruded and their processing temperature are shown in Table 2.1. The polymer HPC-SL and MC-GF, in correct proportions to achieve the required drug concentrations, were mixed using LabRAM at a frequency of 61 Hz with an acceleration of 75 G for 5 min. Hot-melt extrusion was performed with an 11 mm diameter co-rotating twin-screw extruder (Thermo Fisher Scientific Inc., MA, USA). A round-shaped die having a 2 mm hole was used. The powder blends in Table 2.1 were fed into the extruder via a volumetric feeder (Model 102M, Schenck Accurate, WI, USA) at a feed rate of 0.6–0.7 g/min. The screw speed was kept at 30 rpm for all the formulations. To maintain the crystalline form of GF particles, the minimum extrusion temperatures, see Table 2.1, were defined as the temperatures at which the torque and pressure values would not create a problem throughout the processing. In the case of a drug having a higher softening value than that of a polymer, increased drug amount in the formulation requires higher energy input to soften the material. Thus, the extrusion temperature for the formulation having 30 wt% drug concentration was increased to 145 ºC.

Table 2.1 Composition of Powder Blends and Their Processing Temperature

Run #	Drug sample	Wt.% MC-GF	Wt.% HPC	HME Extrusion Temperature (ºC)	FDM Printing Temperature (ºC)
1	MC-GF	5	95	140	170
2	MC-GF	15	85	140	170
3	MC-GF	25	75	140	170
4	MC-GF	30	70	145	170
5	N/A	-	100	140	170

2.2.2.3 Design and printing of cylindrical tablets. It was aimed to study the five cases discussed in the introduction: Case A with varying tablet sizes printed using 15 wt% drug-concentration filament; case B with varying tablet size but total drug amount kept the same printed using varying drug-concentration (5–30 wt%) filaments; case C with fixed tablet size printed using varying drug-concentration (5–30 wt%) filaments; case D duo-tablets with varying drug amount by having different sized internal drug reservoir printed using 15 wt% drug-concentration filament while peripherally printing placebo shell; and, case E, reverse of case D where drug-rich regions are the shells. The details of the tablet dimensions and drug concentrations for each case are listed in Table 2.2. The drug release profiles for printed tablets of all five cases were examined. The aspect ratio was maintained similar (ø/H: 2.56 ± 0.08), and the cylindrical shape as the tablet geometry was used in all the cases. The tablets were designed using Autodesk® Fusion 360 Ultimate (Autodesk 3D design software). The design was recorded as an STL file and was converted to an X3G file using FlashPrint software (Version 3.18.0; Jinhua, China) as the slicer. The tablets were printed using FDM 3D printer (Flashforge®, Creator Pro 3D, 2016, China). The opening of the printer nozzle is 0.4 mm. In all of the cases, the following operating parameters were used; the printing temperature 170 ºC; printing speed, 35 mm/s; nozzle traveling speed, 80 mm/s; layer height, 0.10 mm; and the bed temperature 30 ºC. For case D and case E, the layer height of 0.2 mm was used to decrease the complexity of the printing process, where the printing process requires less amount of time with increased layer height. The 100% infill percentage was used for all of the printed

formulations. The cooling fans are controlled automatically. The general guideline of the operating temperatures was previously reported; the processing temperature of polymers in HME should be higher than the polymer glass transition temperature, T_g (Gupta et al., 2016; Solanki et al., 2018b). While HME imposes such limitations, FDM printing process itself requires a much higher processing temperature than that of HME due to low shear in FDM printing (Pietrzak et al., 2015). The printing temperature was selected below the melting temperature of GF (T_m: 220 ºC) to keep GF as its crystalline state and above the T_g of polymer HPC.

2.2.3 Characterization methods

2.2.3.1 Mechanical Properties. The mechanical properties of the filaments were tested to determine the printability of the filaments via a Texture Analyzer with a maximum force of 1 kN (3-point bender tester, Instron, Norwood, MA). Modulus of elasticity (ME) was calculated from the slope of the initial linear segment, of the stress-strain plot while tensile strength (TS) was calculated using Equation (2.1) (Callister, 2007).

$$\sigma_{fs} = \frac{F_f L}{\Pi R^3} \tag{2.1}$$

Here, the flexural strength (σ_{fs}) is defined for a sample having a circular cross-section, where F_f is the load at fracture, L is the distance between support points and R is the radius of the sample. To conduct the test, 5-6 extruded

filaments were randomly selected and cut into 1 cm segments. The gap on the probe was set up as 4 mm. Later, each filament was positioned on the sample holder, and the force was applied at a constant speed at 0.5 mm/min until the breaking point. The average values and standard deviation of TS and ME were computed over the 5-6 samples.

2.2.3.2 Solid-state characterization. To determine the crystallinity of the drug in the filaments and printed tablets, the formulation of 25 wt% drug concentration was examined via X-ray diffraction. Dry MC-GF particles, the physical mixture of the formulation, the extruded filament, and the 3D printed disk (model dimensions: ø: 15.5 mm x H: 1.7 mm) were tested. The printing parameters were kept the same as the printing parameters of 3D printed tablets. The reason for printing of a bigger size tablet (disk) was to fit the printed product on an XRD sample holder. The samples were scanned for 2θ angle in the range 5–35° (0.01° step) using PANanalytical (Westborough, MA, USA).

2.2.3.3 Thermo-gravimetric analysis (TGA). To assess the extent of thermal degradation and measure the moisture content of various GF-HPC samples, thermo-gravimetric analysis was performed using a TGA/DSC1/SF STARe system (Mettler Toledo Inc., OH, USA). The filaments and printed tablets containing 5 and 30 wt% drug concentrations, as well as as-received GF powder and HPC powder were examined. Each sample was placed in a standard ceramic crucible, heated from 25 ºC to 250 ºC at a rate of 10 ºC/min, and cooled back to 25 ºC under nitrogen flow. Varying moisture content could induce pseudo-crosslinking within the matrix (Zaldivar et al., 2018) or alter water uptake during

dissolution. Thus, the moisture content could eventually affect mechanical performance (Öblom et al., 2019; Zaldivar et al., 2018) and bioavailability of the product (Chowhan, 1980). Since HPC has a high affinity to water molecules and it was prepared at varying concentrations, the moisture contents of the filaments, as well as 3D printed tablets, were also analyzed through their moisture profile at 100 ºC, which allowed the determination of bound water (Tidau et al., 2019).

2.2.3.4 Determination of drug content of printed tablets. The printed tablets were tested from each formulation set. The thickness, diameter, and weight of the tablets were recorded to evaluate the variations among tablet samples. The thickness and diameter of the printed tablets were measured using a digital caliper. The printed tablets containing 5–30 wt% MC-GF were dissolved in 7.2 mg/ml SDS solution with continuous stirring for a minimum of 5h. A Thermo Scientific Evolution 300 UV–vis spectrophotometer (Thermo Fisher Scientific Inc., MA) was used to measure the UV absorbance at a wavelength of 297 nm. The average drug amounts were calculated for minimum of 3 samples from each set.

2.2.3.5 In-vitro drug dissolution. A flow-through cell dissolution apparatus (USP IV, Sotax, Switzerland) with cells of 22.6 mm diameter and 0.2 µm Pall HT Tuffryn membrane disc filters were used for printed tablets (Skowyra et al., 2015). For cases A–C, 4–6 samples from each set were tested. Due to the complexity of printing duo-tablets, 3–5 samples were tested for cases D and E. Additional glass microfiber filters (Whatman GF/D and, Whatman GF/F) were used for the tablets in case D and case E. Additional filters help to prevent clogging the cells due to the large amount of polymer within the cells. The samples from each formulation

were positioned in the cells having 5 g of glass beads. Deionized water (DI) was selected as a dissolution medium in order to obtain good discrimination between GF formulations (Bhakay et al., 2014; Li et al., 2017a), and DI was circulated for the printed tablets maintaining the sink conditions. The flow rate was 16 ml/min with a constant temperature of 37 ± 0.5 ºC. The average percentage of the dissolved drug was plotted as a function of time.

2.2.3.6 Dissolution kinetics of printed tablets and statistical analysis. To gain insight into the dissolution kinetics of printed tablets, the classical models that consider various transport mechanisms were utilized. In all cases, the models were fitted for about the first 60% of fractional release curves, the sink condition was maintained, and the cylindrical shape was kept as the tablet geometry. The tablets were designed by several variables, which may modulate the dissolution profiles. For example, varying surface area to volume ratio of tablet designs (i.e., case A, case B) may adjust the diffusion path length, while changing total drug amount for each tablet (i.e., all cases except case B) or drug concentration within the polymeric matrix (i.e., case B, case C) may change the matrix behavior in release transport. It was expected to see the impact of these variables on dissolution kinetics by fitting the following models. Briefly, Korsmeyer-Peppas model defines the release transport by considering Fickian diffusion, polymer relaxation/erosion. Since 3D printed tablets have inherently dense structures, where swellable/erodible polymer properties could be more pronounced, zero-order equation was considered, as one would expect polymer relaxation/erosion based release kinetics from the dense structures.

The Korsmeyer-Peppas model: This model, depicted in Equation (2.2), is a simple approach for describing the controlled drug release behavior from polymeric matrices (Ford et al., 1991; Korsmeyer et al., 1983).

$$F = k * t^n \tag{2.2}$$

Here, F is the percentage of the drug dissolved at time *t*, *k* is the kinetic constant intended to capture structural and geometric characteristics of the tablet, and, *n* is the release exponent indicative of release mechanism (Ford et al., 1991; Langer et al., 1981; Peppas et al., 2014). The exponent represents Fickian diffusion for $n = 0.45$, Case II transport with $n = 0.89$ and, anomalous transport with $0.45 < n < 0.89$ for cylindrical geometries (Ritger et al., 1987). Basically, several phenomena may appear by swellable/erodible polymers upon water uptake including water diffusion, polymer swelling, drug diffusion, and polymer erosion (Siepmann et al., 2000). Fickian diffusion refers to molecular diffusion of the drug presence of chemical gradient while zero-order means that release transport links with stresses and state-transitions in swellable polymers (Peppas et al., 1989). Anomalous transport simultaneously accounts for both drug diffusion and polymer relaxation/erosion (Sujja-Areevath et al., 1998).

The zero-order model: Equation (2.3) describes the constant drug release rate with time, where k_0 is the release constant (Mendyk et al., 2013; Paixão et al., 2017). This model is mostly applied to the matrix systems with poorly soluble drugs.

$$F = k_0 * t \quad (2.3)$$

For the tablet design of case D, drug release profiles are expected to have lag-times. Therefore, Korsmeyer-Peppas and zero-order models are not directly applicable without accounting for the lag-time. The lag-time estimates were found by first fitting a straight line to the dissolution profile data between 20% and 80% drug release. The slope of the fitted line provided the drug release rate constant for each constant, assuming the linear approximation was valid. The goodness of fit was tested based on examination of the R^2 values. The slope value was used to calculate the intercept on the time axis, which was taken as a fair estimate of the lag-time. This approach is similar to the previously reported procedure (Kao et al., 1997).

The $f2$ bootstrap method, which can better handle dissolution data variability, was applied to various drug release profiles within the groups of cases A, C, and E, as per previously reported protocols (Mendyk et al., 2013; Paixão et al., 2017) (see Section A.1 of Appendix A for the details).

2.2.3.7 Visualization of Swelling/Eroding for Wetted Tablets. The swelling and eroding behaviors undergone by the tablets with 5 and 30 wt% drug were visualized via capturing digital photographs. The tablets represented the cases C1 and C4, respectively; however, the larger size tablets (model dimensions: ø: 6.6 mm, H: 2.7 mm) were printed for better delineation. A flat disk was printed using PLA filament. The circles on the disk and thickness of the disk served as a marker to observe the changes in the tablet size in the axial and radial direction,

respectively (Sujja-Areevath et al., 1998). The calculations of changes in the tablet size are in Appendix A (Equations A1 and A2). The positioned tablet on the disk was placed into a glass beaker. Thereafter, the beaker was filled with 500 ml DI maintained at room temperature. The digital photographs of the tablets were taken at successive time intervals. The aqueous medium was kept unstirred to prevent the tablet from floating around.

2.3 Results and discussion

2.3.1 Mechanical properties of filaments

The tensile strength (TS) and modulus of elasticity (ME), of the filaments at varying drug concentrations ranging 0–30 wt% were obtained from stress-strain curves using the texture analyzer. Although there are no established standards for these properties to assure printability, it has been suggested that a printable filament should possess simultaneously high breaking stress, high stiffness, and long breaking distance (Zhang et al., 2017a). The mechanical properties of the filaments, Figure 2.1, were found satisfactory in terms of filament printability. Filaments containing MC-GF particles from 5 to 25 wt% exhibited similar tensile strength (TS: 56.0–63.8 MPa) and modulus of elasticity (ME: 316.8–358.5 MPa). The placebo filament had similar TS as those with 5–25 wt% drug; whereas, its modulus of elasticity (ME: 241.4 MPa) was lower and increased in the presence of drug particles. Since ME is directly obtained from the slope of the initial linear portion of stress-strain curves, lower ME indicates higher elastic strain, and thus lower material stiffness (Callister, 2007). On a macroscopic scale, the magnitude

of ME is an expression of resistance to separation of adjacent atoms, related to interatomic bonding forces (Callister, 2007). Therefore, the increased stiffness of the filaments with 5–25 wt% could be an indication of the polymer network being disrupted by the drug particles. A similar impact due to incorporation of the API particles on mechanical properties has been previously reported, where the drug-loaded filaments generally exhibited a higher stiffness (Verstraete et al., 2018).

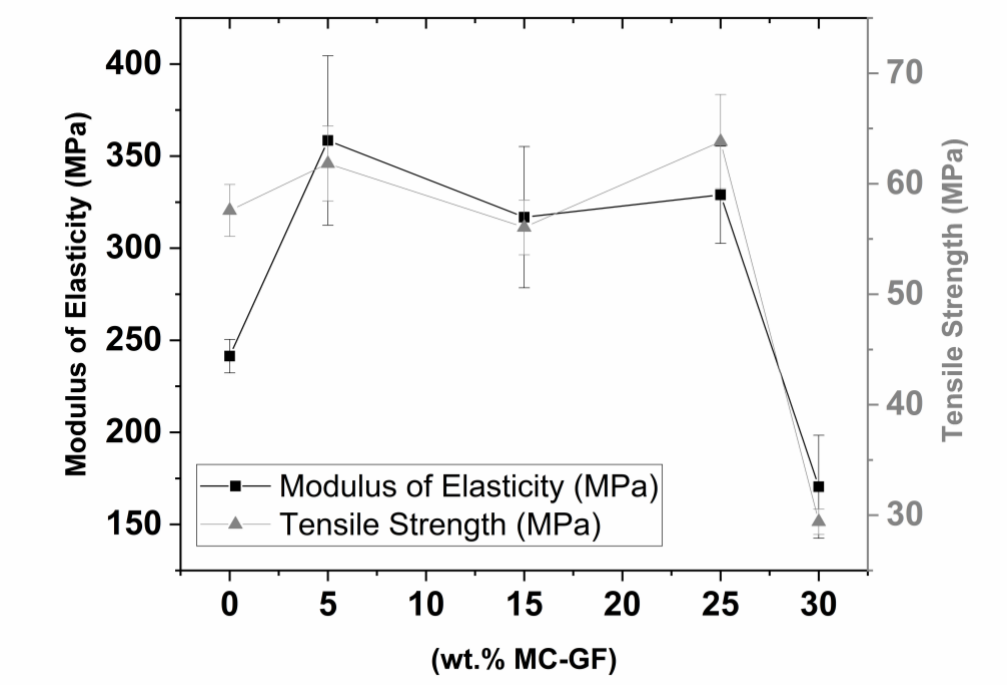

Figure 2.1 Mechanical properties of the feed materials (filaments) with varying drug concentrations, ranging 0–30 wt%.

It was previously reported that TS was not mainly dependent on drug content in the formulation but on additives (Laukamp et al., 2014). In contrast, TS & ME of the filament containing 30 wt% drug remarkably decreased to 29.4 and 170.4 MPa, respectively. This may suggest that the decreased polymer amount in the matrix may not provide sufficient polymer networks around the drug

particles for printing. This is in line with the previous finding of reduced integrity of the polymer film matrix containing GF concentration above ~40 wt% (Krull et al., 2017). The decreased values of mechanical properties indicated that more than 30 wt% drug concentration might not be favorable in terms of printability; yet, all the filaments could be used successfully in the FDM printer to prepare the tablets.

2.3.2 Characterization of FDM 3D printed tablets

2.3.2.1 FDM 3D printing and structure of printed tablets. Tablets of all the designs shown in Figure 2.2a were successfully printed using an FDM 3D printer, see Figure 2.2b for their digital images. The dimensions of printed tablets are presented in Table 2.2. It is noted that in an effort to fix the aspect ratios for all designs and other printing constraints, it was not possible to either attain exactly the same drug amount for case B or varying the drug amounts for cases A, C, D, and E in the same ratios.

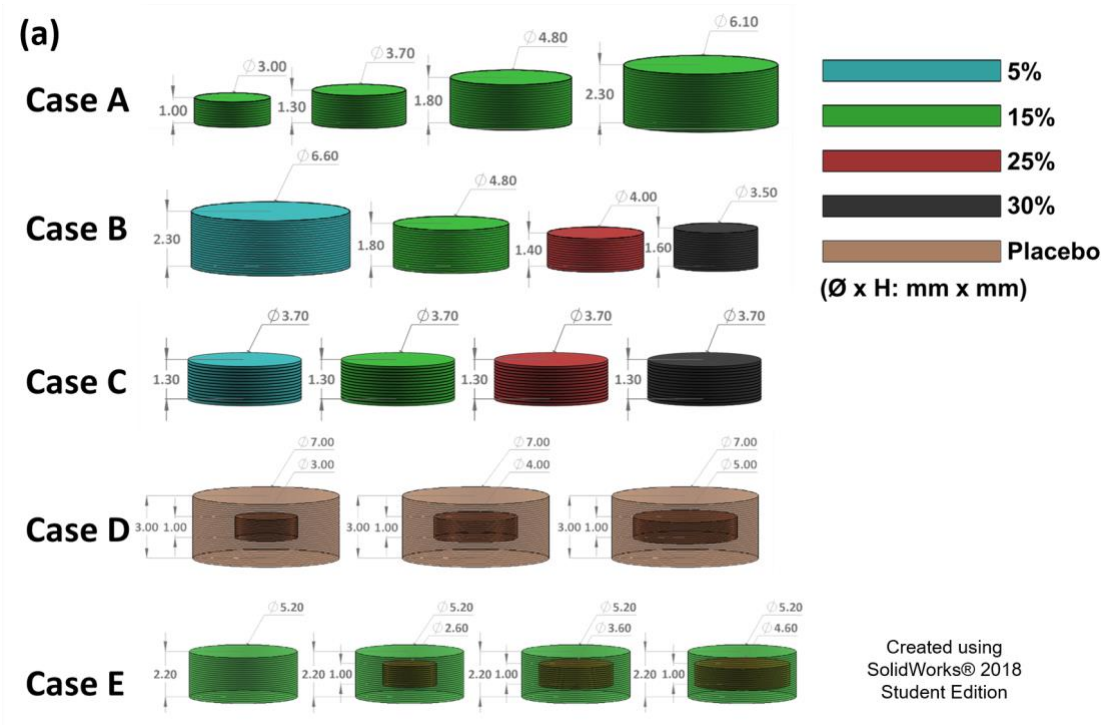

Figure 2.2 (a) Graphical depiction of the tablet design options. (b) Digital images of FDM 3D printed tablets for cases A through E.

In general, the colors of the printed tablets varied largely depending on the drug concentration and not because of any thermal degradation. As drug

concentration increased, the tablet color became lighter, as the tablet became more opaque. There were no black or dark brown colors present, which the occurrence of those would imply thermal degradation (Zhang et al., 2017a). Overall, the color changes are not expected to have any direct impact on subsequent assessments. The relative standard deviations (RSDs) in drug amounts, Table 2.2, for all the cases with the exception of case D were less than 6% indicating acceptable uniformity in drug content. The high RSDs for the cases D1 and D2 could be attributed to the printing constraints, where dispensing imprecision was evident during printing of internal drug-rich regions, particularly for the tablets with smaller sizes (Govender et al., 2020).

Table 2.2 Dimensions of 3D Printed Tablets for Various Designs, and Drug Concentration (DC) of the Filament Used

Case	Filament DC (wt.%)	Tablet size (mm x mm)	SA/V (mm^{-1})	Drug amount (mg)	RSD%
A1	15%	3.3 x 1.2	2.9	1.69	2.1
A2	15%	4.0 x 1.6	2.3	3.12	3.5
A3	15%	5.1 x 2.0	1.8	7.08	0.9
A4	15%	6.3 x 2.5	1.4	13.65	1.0
B1	5%	6.9 x 2.8	1.3	6.66	2.1
B2	15%	5.1x 2.0	1.8	7.08	0.9
B3	25%	4.3 x 1.7	2.1	7.07	4.4
B4	30%	3.8 x 1.5	2.4	6.71	2.1
C1	5%	3.9 x 1.5	2.4	1.24	5.9
C2	15%	4.0 x 1.6	2.3	3.12	3.5
C3	25%	4.0 x 1.5	2.3	5.49	3.2
C4	30%	4.0 x 1.6	2.3	6.92	1.2
D1	15%	3 by 1 within 7.4 x 3.0	1.2	0.93	17.4
D2	15%	4 by 1 within 7.5 x 2.9	1.2	1.97	12.9
D3	15%	5 by 1 within 7.4 x 2.8	1.3	3.55	5.31
E1	15%	5.9 x 2.2	1.6	10.26	0.3
E2	15%	2.6 by 1 within 5.8 x 2.3	1.6	9.38	1.9
E3	15%	3.6 by 1 within 5.8 x 2.3	1.6	8.50	2.9
E4	15%	4.6 by 1 within 5.8 x 2.2	1.6	7.02	0.7

2.3.2.2 Crystallinity. The XRD analysis was conducted to show the crystalline state of the drug in filaments and 3D printed tablets after the thermal processing in HME and FDM, respectively. The results are presented in Figure 2.3. The polymer HPC did not show any peaks apart from the amorphous halo diffraction pattern. The characteristic peaks of GF powder (Li et al., 2017a) were observed at the main diffraction angles (2θ) 10.0°–35.0°, indicating the crystalline structure of the particles. Similarly, the physical mixture, the filament, and the 3D printed disk followed the same characteristic peaks. This outcome suggested that the crystalline structure of GF was maintained after both HME and 3D printing processing. This is expected because both the processing and printing temperatures were well below the melting point of GF, and sufficiently low to allow any dissolving of GF particles in the polymer matrix.

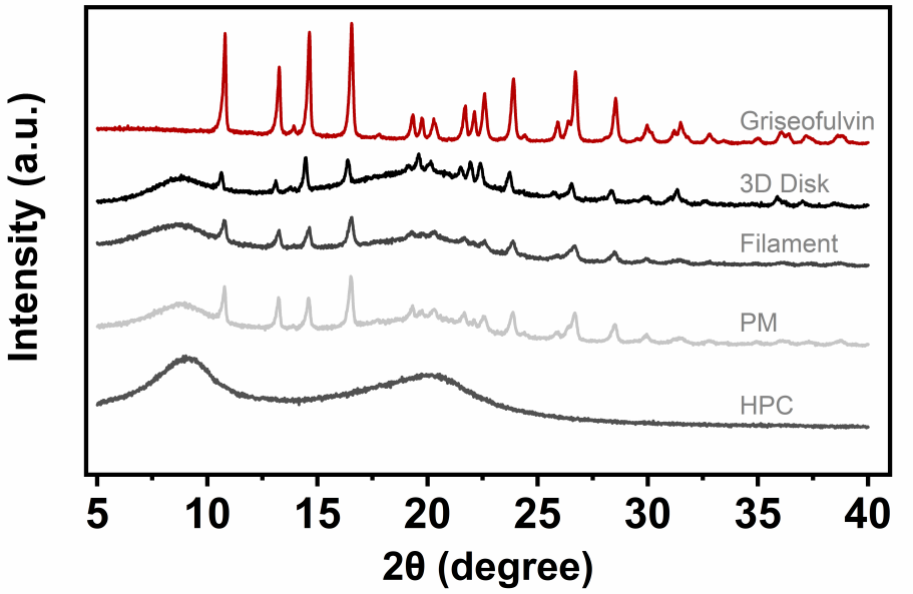

Figure 2.3 XRD patterns of pure GF, dry HPC along with physical mixture (PM), filament, and representing the printed tablets, a 3D printed disk loaded with 25 wt% drug.

2.3.2.3 Thermo-gravimetric analysis of filaments and printed tablets. The results for the thermo-gravimetric analysis (TGA), Figure 2.4, indicate that all the tested filaments and printed tablets have low moisture contents at 100 ºC. The highest weight loss at 100 ºC, which indicates the amount of free or bound water, was just under 1.6%. At temperature corresponding to the HME processing temperature, the filament weight loss remained less than about ~1.8% (see Figure 2.4). Since the weight loss for either GF or HPC powders was much lower at higher temperatures, the weight loss from the filaments and tablets could be attributed to the free or bound water (Ahmad et al., 2011; Tidau et al., 2019) rather than thermal degradation. This is also in line with (Goyanes et al., 2019), where HPC was found stable up to 250 ºC with less than 3% weight loss. At the higher 3D printing temperature, the weight loss for the 3D printed tablets was in the range 0.3–0.4%, and less than that of filaments, likely due to the loss of water during thermal processing for 3D printing at 170 ºC. Overall, these results indicate lack of thermal degradation (Goyanes et al., 2015b; Goyanes et al., 2015d) for both filaments and printed tablets and it is unlikely that the moisture amounts would have a substantial impact on the mechanical properties of the filaments or their dissolution behavior. It has been reported that storage conditions may have an impact on the mechanical properties of filaments (Tan et al., 2020), investigation of which could be considered for future studies.

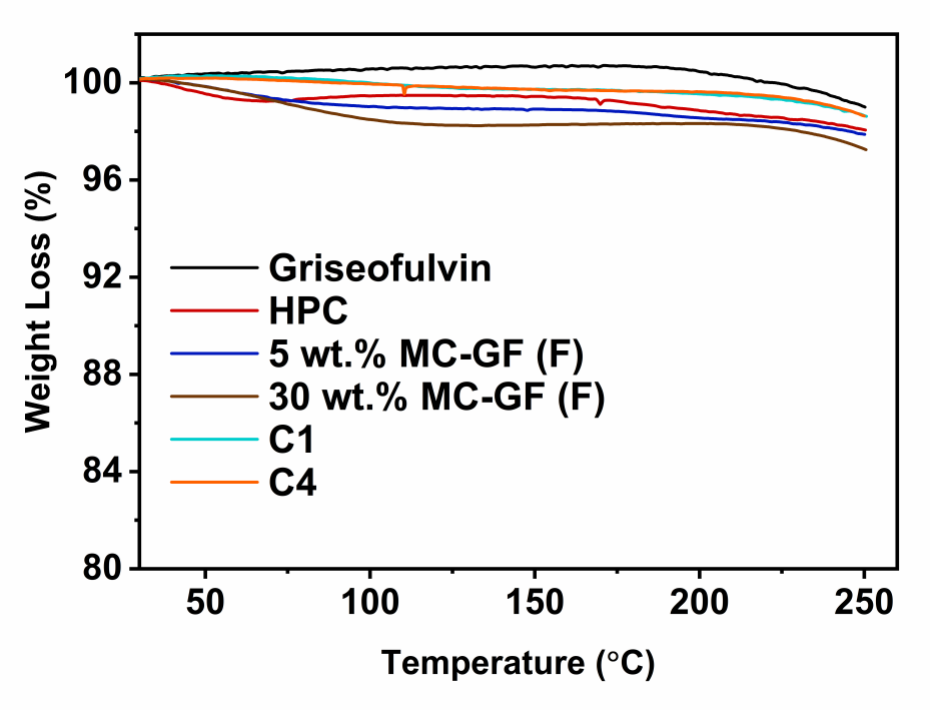

Figure 2.4 TGA thermograms for dry GF, HPC powder, as well as filaments and printed tablets at 5 and 30 wt% GF concentrations.

2.3.2.4 Drug release and dissolution kinetics. Dissolution profiles for each case are presented in Figure 2.5, the time required to dissolve 50% and 75% drug amount is presented in Table 2.3, and the dissolution kinetics constants for four different cases are presented in Table 2.4. In addition, visualization of swelling and erosion is presented in the next section. The analysis of the release kinetics would allow determination of which phenomena, such as Fickian transport, anomalous transport, or polymer erosion/relaxational, are prevalent during drug dissolution for better understanding the key features of various tablet designs.

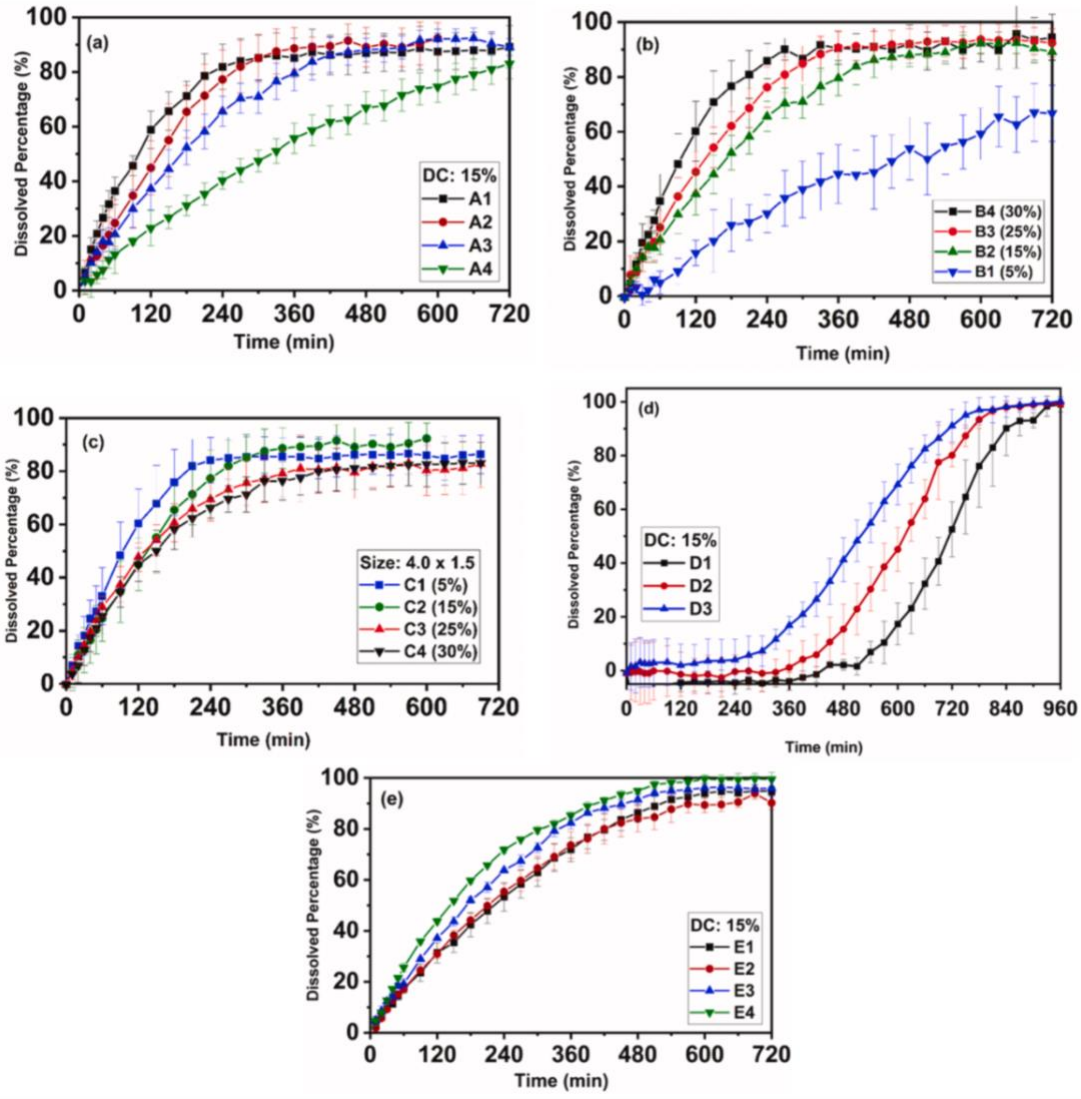

Figure 2.5 Dissolution profiles of 3D printed tablets for; (a) case A, (b) case B, (c) case C, (d) case D, and, (e) case E. For cases B and C, varying drug concentration (DC) filaments are used for each sub-case.

Table 2.3 The Time Required To Dissolve the Drug at the Percentage of 50 and 75

Case	$t_{50\%}$ (min)	$t_{75\%}$ (min)
A1	105±14	211±78
A2	136±33	232±49
A3	162±26	311±39
A4	315±56	588±90
B1	438±147	667 ±49
B2	162±26	311±39
B3	138±23	236.7±39
B4	99±23	171±44
C1	100±27	179.2±45
C2	136±33	232±49
C3	128±26	281±93
C4	146±29	396.7±184
D1	721±28	781±43
D2	610±29	698±19
D3	520±34	621±31
E1	223±31	379±35
E2	209±14	380±47
E3	173±6	308±8
E4	141±3	261±6

Table 2.4 Fitting Parameters of the Fitting Dissolution Curves from the 3D Printed Tablets with Varying Tablet Designs

Case	Korsmeyer-Peppas			Zero-order	
	k (%/min^n)	n	R^2	k_0 (%/min)	R^2
A1	1.52	0.76	0.992	0.55	0.934
A2	0.67	0.88	0.996	0.39	0.985
A3	0.89	0.79	0.992	0.31	0.956
A4	0.40	0.84	0.997	0.16	0.985
B1	0.26	0.86	0.982	0.11	0.973
B2	0.89	0.79	0.992	0.31	0.956
B3	0.79	0.85	0.995	0.39	0.975
B4	0.89	0.89	0.992	0.56	0.983
C1	1.10	0.84	0.996	0.56	0.974
C2	0.67	0.88	0.996	0.39	0.985
C3	1.02	0.80	0.990	0.40	0.954
C4	0.88	0.81	0.990	0.36	0.962
E1	0.51	0.85	0.998	0.23	0.985
E2	0.50	0.86	0.997	0.24	0.986
E3	0.72	0.82	0.998	0.30	0.975
E4	0.80	0.84	0.995	0.37	0.973

Case A

The dissolution profiles for this case, considered as the control design being the most common approach to tailor the drug amount (Pietrzak et al., 2015; Skowyra et al., 2015), are presented in Figure 2.5a. As the tablet size increased, the percentage drug release rate decreased, and the release profiles became statistically different from each other (see Table A.1, Appendix A) as per the bootstrap $f2$ similarity test (Mendyk et al., 2013; Paixão et al., 2017). The rate of percentage drug release appeared to be well correlated with the surface area to volume ratio (SA/V) of the printed tablet, see Tables 2.2 and 2.3. As tablet size

increased, SA/V value decreased, and the release times got longer. Specifically, the release times $t_{50\%}$ and $t_{75\%}$ in Table 2.3 were proportional to SA/V. These results are in line with the trend of faster percentage drug release rate for higher SA/V of 3D printed tablets (Pietrzak et al., 2015; Skowyra et al., 2015). The trends with respect to SA/V are similar even when previous studies utilized water-soluble drugs (BCS Class I) (Pietrzak et al., 2015; Skowyra et al., 2015; Tidau et al., 2019), whereas the current results are for the poorly water-soluble drug (BCS Class II). That suggested that the drug release is predominantly controlled by the polymeric matrix.

The drug release rates were analyzed through Korsmeyer-Peppas model. The exponent *n* in Korsmeyer-Peppas model, Equation (2.2), was found to be in the range 0.76–0.88, Table 2.4. Therefore, it appears that the system showed combined drug diffusion and polymer relaxation mechanisms (anomalous transport). The fact that the *n* values are close to the zero-order limit (0.89), it is likely that the drug release was almost zero-order (Case II transport). High R^2 (0.934–0.985) values for the zero-order model, Table 2.4, confirmed this assessment. The release rate constants (k_0) from zero-order model exhibited a decreasing trend with decreasing tablet SA/V values. Case II transport describes that the diffusion contribution is faster than the relaxation contribution, suggesting that the release rate is limited by the relaxation process (Baggi et al., 2016). Generally, the swelling causes an increase in size while tablet decreases in size by erosion (Siepmann et al., 2013). The higher the swelling the longer the drug diffusion path length and the slower the release rate (Sujja-Areevath et al., 1998).

Therefore, increases in tablet size could negatively contribute to drug diffusion from the swellable polymeric matrix. Siepmann et al. (Siepmann et al., 2012) observed a similar decrease in drug release rate with increasing tablet height, referring to increasing diffusion path length with decreasing relative surface area.

The drug release kinetics may be affected by the properties of HPC, which has been identified as a polymer that undergoes swelling as well as erosion (Borujeni et al., 2020; Gazzaniga et al., 2011; Macchi et al., 2015). Hence, the release of poorly water-soluble drugs would be controlled by polymer relaxation and erosion (Borujeni et al., 2020; Ford et al., 1985). Drug release is also affected by inherently dense structure of FDM 3D printed tablets (Borujeni et al., 2020; Zhang et al., 2017a), leading to slower water imbibition and ultimately higher potential for zero-order release. This is in line with previous observations where denser tablets achieved zero-order release (Zhang et al., 2017b). Thus, the combination of HPC being a swelling/erodible polymer, the drug having poor water solubility, and inherently dense tablets, may explain the resulting drug transport controlled by polymer relaxation. Since the release is strongly affected by SA/V values, the effect of polymer and highly dense tablets may be the dominating factors, which was also the case for a water-soluble drug (Pietrzak et al., 2015; Skowyra et al., 2015).

Case B

Case B allowed for examining the impact of tablet surface area and volume ratios without changing the total drug amount (6.9 ± 0.2 mg) in each tablet. The drug release profiles are presented in Figure 2.5b. These had similar trends as

case A in the sense that increased tablet size, which means decreased SA/V ratio, resulted in decreased drug release rate. However, the effect of slowing down the drug release rate was stronger for the largest tablet that contained the same amount of the drug as the smaller tablets. Overall, this case demonstrated that the SA/V ratio of the tablet dominates the drug release rate, which was largely independent of the total drug amount. This case reinforced that the release is dominated by the polymer and dense tablet structure, resulting in a near zero-order release with high R^2 values shown in Table 2.4. The table also presents release constant k_0 values, which exhibited a strongly linear trend with increasing SA/V ratio of the tablets.

Case C

Case C was intended to support the hypothesis that by using different drug-concentration filaments, nearly similar drug release profiles would be attained even when the drug dose is varied, while the tablet size and SA/V ratios were held constant. Drug release profiles, presented in Figure 2.5c, were similar except that case C1 (5 wt%) had a slightly faster release rate attributed to lower drug concentration and amount. The bootstrap $f2$ similarity test (Mendyk et al., 2013; Paixão et al., 2017) confirmed this observation, see Table A.1, Appendix A.

For compressed tablets, varying the drug concentration could cause substantial changes in drug release profile, e.g., increased drug amount within polymeric matrix increased the release rate significantly (Siepmann et al., 2002; Xu et al., 1995). In contrast, for the release profiles of case C, the differences were not significant even when there was a wide range of drug concentration, 15–30

wt%. This is most likely since FDM 3D printed tablets have an inherently dense matrix (Borujeni et al., 2020; Yang et al., 2018; Zhang et al., 2017a), and solidified HPC offers prolonged-release (Chai et al., 2017; Loreti et al., 2014). Thus, the dense matrix of 3D printed tablets negates the expected difference in drug release rate when drug concentration is changed (Goyanes et al., 2015a; Zhang et al., 2017b). Even a minor exception where the printed tablet containing the lowest drug concentration (16 wt.%) dissolved more slowly, the range of drug concentration was limited (~8 wt.%) (Yang et al., 2018).

The release profiles were fitted to Korsmeyer-Peppas model for which the exponent n was in the range 0.80–0.88, Table 2.4, indicating nearly zero-order (Case II transport) release. As per zero-order model, as expected, the lowest drug concentration case, C1 (5 wt%) exhibited the highest k0 value of 0.56. However, C2, C3, and C4 had lower and comparable k_0 values, with C4 being the lowest. Based on these release constants, C1 was different from C2–C4, which also supports the bootstrap $f2$ similarity test results (Table A.1, Appendix A). Since the SA/V ratio was kept constant, the different behavior of C1 is likely due to its different polymer network properties which affect water penetration (Siepmann et al., 2000). Further, as the drug concentration increases, the hydrophobic nature of the drug impacts the polymer network resulting in slower drug diffusion. If the drug diffusion outwards is slower than the imbibition of water, the swelling mechanism would have a more pronounced effect on the drug release (Sujja-Areevath et al., 1998). That was evident through the visualization of wetted tablets for cases C1 and C4, discussed in the next section. Thus for drug concentrations at or above a

certain limit, which for GF could be 15 wt%, the effect of slowing down of the drug release may remain constant, in line with previous observations (Yang et al., 2018). Therefore, the GF concentration within the range 15–30 wt% may help achieve similar release profiles while varying the tablet drug concentration, offering a pragmatic pathway to design personalized dosages using filaments with varying drug concentrations.

Case D

Case D design was expected to allow testing the effect of shell thickness and interior tablet size in reservoir systems on drug release. Due to the printing resolution limitations and for the sake of maintaining the sink conditions, only three duo-tablet configurations were printed, presented in Figure 2.2a and, Table 2.2. The drug release profiles for the cases D1, D2, and D3 are presented in Figure. 6d. The most prominent feature of this design was the presence of lag times. As per the procedure discussed before (Kao et al., 1997), the slope and time axis intercept were estimated to obtain the lag times and the release rate constants, as shown in Table 2.5. Here, very high R^2 values confirm the goodness of linear fit, which was also visually verified in the plot of the data from 20% through 80% drug release. The lag times proportionally increased with the shell thickness and exhibited a linear correlation with a high R^2 value of 0.9996 with the theoretical radial shell thickness (plot not shown for the sake of brevity). It is noted that the axial shell thickness was invariant for these cases. These rather long lag times were likely due to the swelling nature of HPC. It led to significantly higher delay times for slightly lower thickness values, as compared to the lag time of 85 min for

a shell thickness of 2.25 mm when polyvinyl alcohol was the polymer (Li et al., 2017b). The slopes for the linear drug release portion are the release rate constants of the respective drug release profiles, and increased SA/V ratio values of the interior tablets resulted in increased slope values, hence the higher drug release rates. Even with significantly long lag periods, the release rates of the inner drug-loaded tablets followed a similar trend as before where higher SA/V ratios led to faster drug release.

Table 2.5 Time Axis Intercept, Slopes of Constant Rate Release Portion and Corresponding R^2 Values for the Cases D1, D2, D3 along with Their Theoretical Radial Shell Thickness Values

Case	Intercept (min)	Slope (%/min)	R^2	Shell Thickness (mm)
D1	566.5	0.3496	0.988	2.0
D2	433.1	0.2805	0.994	1.5
D3	305.8	0.2350	0.999	1.0

These results show how the shell thickness and interior tablet size along with the polymer being used could be used to tailor the drug release profiles and add value to a growing body of literature in reservoir systems, where the studies on reservoir printed tablets are scant (Goyanes et al., 2015d; Okwuosa et al., 2017). Unfortunately, this design was found to be unsuitable for providing nearly similar release profiles while varying the drug dose. Instead, it would be suitable for adjusting the release lag times while attaining a drug release rate that is dependent on the SA/V ratio of the interior tablet.

Case E

This case, similar to case D except that drug-rich regions were printed peripherally instead of internally, is useful for testing the hypothesis that similar drug release profiles would be attained even with varying drug dose. The drug release profiles, Figure 2.5e, confirmed they were similar although E4 was slightly faster, attributed to the much decreased drug-rich shell thickness. However, according to the bootstrap $f2$ similarity test (Mendyk et al., 2013; Paixão et al., 2017), the other three cases, E1, E2, and E3, were statistically the same, Table A.1, Appendix A. These results proved the hypothesis that similar drug release profiles can be attained with constant tablet size with constant initial, external SA/V ratio values while varying the drug amounts. Case E4, although an exception, was an artifact of the design constraint leading to the smallest shell thickness of 0.3 mm, as compared to E1 through E3 of 2.6, 1.3, and 0.8 mm, respectively. Interestingly, when the dissolution was plotted as the amount of drug dissolved, all four cases were nearly identical for the first 240 minutes (plot not shown for the sake of brevity). Regardless, for limited thickness (0.3 mm) of drug-rich material for E4, polymer swelling and consequent retardation of drug release would not be prominent (Sujja-Areevath et al., 1998). This is in line with the faster percentage of drug release rate for the thinner outside shell thickness (0.4 mm) (Zhang et al., 2017b), although those tablets did not have a placebo inner core.

The fitted drug release profiles indicated almost zero-order transport with the n values of 0.82–0.86. The higher k_0 value (0.37) of case E4 was in line with its faster drug release seen in Figure 2.5e. The cases E1 and E2 had similar k_0

values of 0.23 and 0.24, respectively, in line with the bootstrap $f2$ similarity test (Table A.1, Appendix A). Overall, it would be necessary to design tablets by avoiding very thin drug-rich shells for obtaining similar drug release rates, and case E appears to be the best suited for achieving similar drug release profiles while achieving different drug doses without the need to use filaments with varying drug concentrations as in case C.

Incomplete release profiles were observed for the sub-cases of case A–C and E, attributed to the use of DI water as the dissolution medium and the structure of 3D printed tablets, which are inherently dense and require a longer time for complete drug release. Several other studies have reported similar results for FDM-based 3D tablets (Goyanes et al., 2015a; Ilyés et al., 2019a; Zhang et al., 2017a). Further, the importance of the dissolution method has been emphasized to demonstrate that inconsistencies in the agitation and the exposure of the dissolution buffer experienced by the tablets gave rise to incomplete drug release in a given time period (Ilyés et al., 2019a; Smirnova et al., 2004). To further add to these factors, the tablets having higher drug concentrations tend to dissolve slowly, most likely stemming from increased hydrophobicity by GF, possibly requiring additional dissolution time (Jambhrunkar et al., 2014). For the dissolution profiles of case D, the drug dissolved at 24h was considered as the total drug amount in those tablets due to the high RSDs in their drug contents, Table 2.2.

2.3.2.5 Visualization of swelling/eroding for wetted tablets. In order to visualize the aforementioned swelling and eroding mechanism based on varying drug concentrations, the digital images of the wetted tablets from case C were

captured. Cases C1 (5 wt%) and C4 (30 wt%) were visualized since their drug release profiles were significantly different from each other (Table A.1, Appendix A). Besides, these two values covered the range of the examined drug concentrations. The digital images in Figure 2.6 qualitatively indicate swelling and erosion and, Table A.2, Appendix A, quantitatively assesses swelling and eroding phenomena. For both cases, the swelling and eroding mechanisms in the radial direction were much smaller, estimated to be less than 10%, implying a lesser impact on release kinetics for these formulations containing HPC and hydrophobic GF. This corroborates previous observations of only small contractions (Ilyés et al., 2019a).

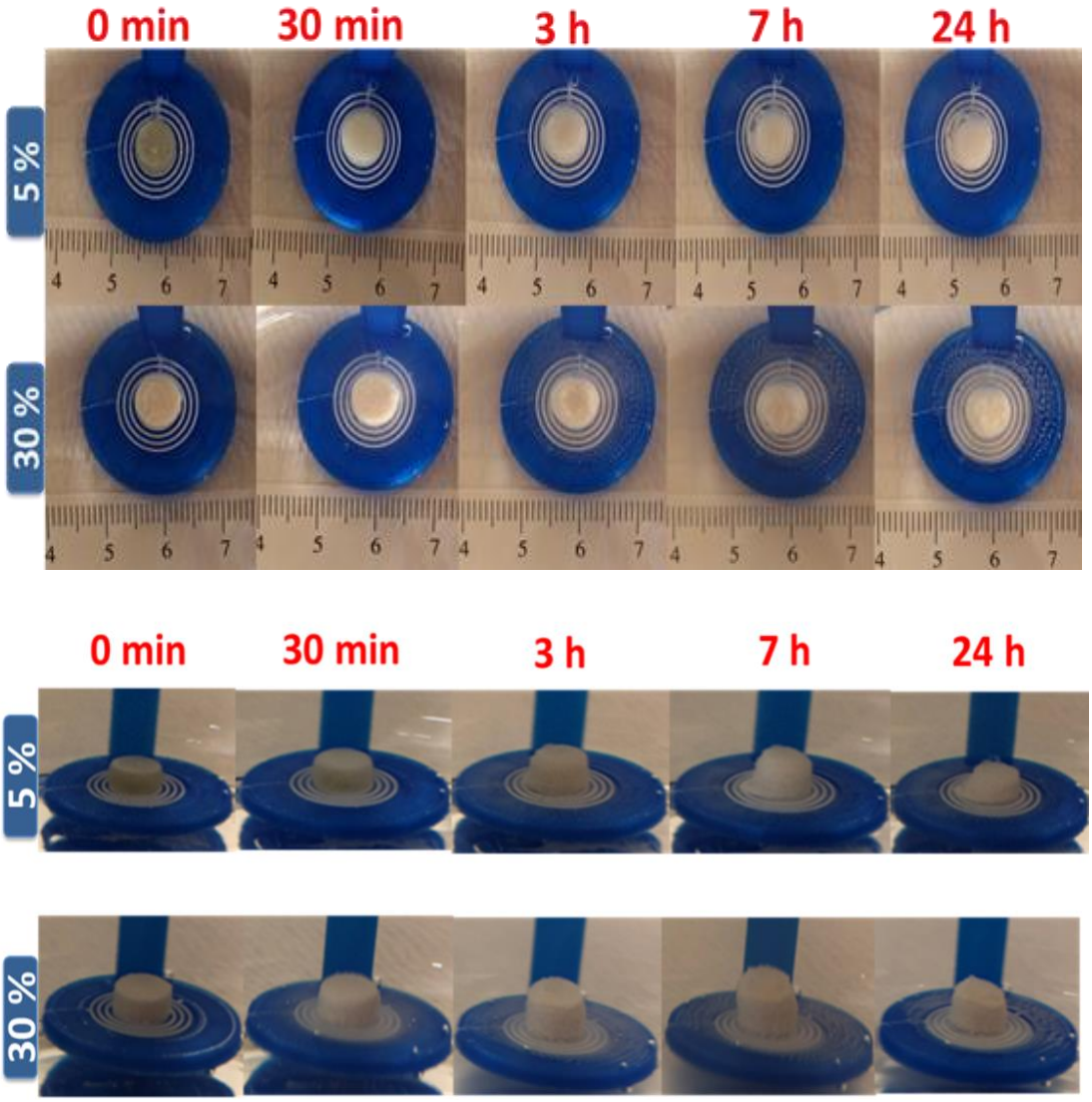

Figure 2.6 Digital photographs of the top and side views of the printed tablets printed at 5 and 30 wt.% drug concentrations with a constant SA/V ratio, representative of the designs C1 and C4, respectively.

For case C1, the maximum swelling of 17.48% in the axial direction was observed when the tablets were exposed to DI water after 7h. However, as an important outcome for case C1, erosion (-33.12%) was much higher than that of swelling. The eroded tablet layers indicate that the tablet size gets smaller, which leads to the SA/V ratio getting larger. The resistance to water penetration inwards,

caused by swelling, would also be expected to decrease due to erosion. Therefore, higher available SA/V for drug release due to the higher extent of erosion could be the reason for the resulting faster drug release rate in case C1.

For case C4 printed using the highest drug concentration of 30 wt.%, swelling of 112% within 7h in the axial direction was considerably greater than that for case C1 (also see Figure 2.6). Further, the eroding mechanism was seen to be less prevalent. Such outcomes suggest that outward drug diffusion was slower than the imbibition of water (Sujja-Areevath et al., 1998), likely due to the higher concentration of GF, which is very hydrophobic. Higher amounts of the poorly soluble drug resulted in slower water penetration, implying slower polymer relaxation and retarded erosion due to the altered polymer network properties (Siepmann et al., 2000). These observations are in line with the release kinetics of case C4 having the smallest k_0 and slower drug release rate than for case C1.

2.4 Conclusion

For dense solid tablets printed via the FDM method, tablet SA/V ratio was shown to be the main driver for the drug release rate, which was also near zero-order in most cases due to the use of HPC that provides swellable and erodible matrix. Thus, to assure the same release rate while varying the drug dose, the tablet designs had to have the same SA/V ratio. Two options could meet that requirement, being case C, which required using filaments with different drug concentrations, and case E, which offered the ability to use a combination of single drug-concentration filament and a placebo filament. These options may offer the

required flexibility in producing tablets having a desirable amount of drug for the purpose of personalized medicine, without significantly altering the drug release profiles. Amongst other tablet designs, the standard option, case A, was the simplest way to achieve a desirable dose. However, owing to their different SA/V ratios, the drug release profiles from those tablets would be different since higher dose tablets having higher SA/V ratios take longer time to attain full drug release. Case B was the control option to test the impact of SA/V ratios with the same total drug amount in each tablet, unlike case A. The dissolution profiles of case B indicated that the impact of SA/V ratio on the dissolution rate was largely independent of the total drug amount. The outcomes from case D indicated that it is an attractive approach to achieve desired lag times by adjusting the placebo shell-thickness.

CHAPTER 3

DOSE TITRATION VIA THREE-DIMENSIONAL PRINTED MINI-TABLETS

3.1 Introduction

Many pediatric formulations require manipulation (Breitkreutz et al., 2007; Ernest et al., 2012; Ranmal et al., 2016; Richey et al., 2017; Salunke et al., 2016; Strickley, 2019) for either administering the prescribed dose per age/body weight or minimizing the swallowing issue. Splitting a large tablet into small pieces (Cohen, 2002; Fawell et al., 1999; McDevitt et al., 1998; Quinzler et al., 2006; Teng et al., 2002) is the most prevalent and simplest practice for manipulating the dosage. However, the respective fragments formed may not meet the intended dose owing to the possible variation in weight and content uniformity (Boggie et al., 2004; McDevitt et al., 1998; Shah et al., 2010; Teng et al., 2002; van Riet-Nales et al., 2014). That may also lead to an uncontrollable effect on drug metabolism (FDA, 2013; Shah et al., 2010). Such inconsistencies in drugs having a narrow therapeutic index could prove detrimental for patients who are at risk for administering under or excessive dosage (Collier et al., 2011; Shah et al., 2010). Alternatively, liquid dosage forms could be appropriate for pediatric patients. However, stability issues or the struggles arising from adhering to the dosing instructions and inadvertent negligence of caregiver may adversely affect the dose accuracy (Brown et al., 2004; Mitra et al., 2020; Preis, 2015; Rood et al., 2014; Wening et al., 2011). Clearly, relying on a single dosage form is less than ideal for age-specific formulations (Ranmal et al., 2016; Salunke et al., 2016) and is the motivation for developing patient-tailored medicines.

Mini-tablets have enormous potential as age-specific drug therapy (Aleksovski et al., 2015; Klingmann, 2017; Mitra et al., 2017; Mitra et al., 2020; Strickley, 2019; Thomson et al., 2009). Their size generally defined in diameter of 3–5 mm (Goh et al., 2017; Lennartz et al., 1998; Palekar et al., 2019; Sujja-Areevath et al., 1998; Terán et al., 2016) offers high level of patient compliance, which could mitigate swallowing issues, and promotes administering of single or composite (multi-unit) tablet (Aleksovski et al., 2015; Bayan et al., 2021; Klingmann et al., 2015; Lennartz et al., 1998; Mitra et al., 2020). Particularly, multi-unit mini-tablets loaded with low drug concentration enable high flexibility for manipulating low-dose therapy (Mitra et al., 2020). Moreover, the size benefit overcomes the excipient burden (Mitra et al., 2020) for the formulations containing a large amount of excipient yet low drug concentration. Besides, mini-tablets retain the benefit of intact tablets, which means they are less sensitive to the external factors unlike liquid forms, and hold the advantage of dose accuracy over fragmented tablets (Aleksovski et al., 2015; Preis, 2015; Shah et al., 2010). That would potentially prevent the failure in attaining therapeutic concentration associated with subdividing adult tablets. Therefore, examining these distinct advantages of mini-tablets to provide dose flexibility for age-specific patients will be the focus of this study.

Traditionally, the manufacturing steps of mini-tablets are similar to that of standard size tablets, which involve mixing followed by compression using conventional tablet presses equipped with multiple punches (Gaber et al., 2015; Priyanka et al., 2018). However, ensuring uniformity and consistency in such

small-sized products naturally requires further effort in the formulation preparation and processing such as an upper limit particle size to avoid clogging of the die opening (Zhao et al., 2018), excellent flow properties to meet the consistency in die fill (Chen et al., 2020; Gaber et al., 2015; Priyanka et al., 2018), strict control of the tablet tool alignment against the high die-wall friction (Lennartz et al., 1998; Priyanka et al., 2018). In response to the challenges associated with the traditional manufacturing of mini-tablets, fused deposition modeling (FDM) 3D printing shows promise owing to its intrinsic advantages. The most prominent advantage is the starting material used, which is thermoplastic solid filament (Melocchi et al., 2016; Wang et al., 2018; Wei et al., 2020; Zhang et al., 2017a) rather than a powder blend. That may tackle some, but not all, the challenges in traditional manufacturing associated with die fill, equipment changeover, and particle size limit. Seemingly, the manufacturing of filaments through hot-melt extrusion (HME) adds an additional step to the production line. However, intense mixing through the processing potentially offers enhanced content uniformity (Maniruzzaman et al., 2012; Pawar et al., 2017; Sadia et al., 2018b). Bridging the HME process with 3D printing highly likely promotes dosing reliability. Indeed, several examples reporting 3D printed final products being contently uniform corroborate these observations (Okwuosa et al., 2016; Pietrzak et al., 2015; Scoutaris et al., 2018; Solanki et al., 2018b). In addition to that, regardless of the complexity and size of the given device, the 3D design of the intended dose is precisely deposited with successive layers of thermoplastic filaments (Goyanes et al., 2015c; Pietrzak et al., 2015). That digitally controls the prescribed dose with high precision.

Due to its potential for flexible dosing, FDM 3D printing platform is actively researched for dose titration (Arafat et al., 2018a; Rycerz et al., 2019; Sadia et al., 2016), child-appealing designs (Scoutaris et al., 2018), and low-dose formulations i.e., <5.0 mg (Sadia et al., 2016; Skowyra et al., 2015). Although, these options could ultimately extend the availability of precise, effective, and safe formulation for pediatric patients, interestingly, mini-sized tablets, which are significantly smaller than the regular tablets, have yet to be addressed in those reports. In the limited examples of FDM 3D printed mini-tablets, the required size was obtained as one of the consequences of size configuration (Tagami et al., 2017). However, the products did not serve the purpose of dose titration, which is one of the primary reasons for manufacturing the mini-tablets. This renders the need for 3D printed mini-tablets capable of delivering the intended varying doses for pediatric patients.

The primary objective of this study is to fabricate 3D printed mini-sized tablets with a set diameter of 3.0 mm containing low drug concentration, which may allow sensitive dose titration, for administering the prescribed dose with single or multi-units. Having said that, a preliminary understanding of layer resolution is sought since the structural variability in 3D printed objects could influence the tablet characteristic (Ilyés et al., 2019a; Sadia et al., 2018a; Zhang et al., 2017b). Later, achieving similar drug release profiles from multi-unit tablets used for dose titration, in which the total drug amount varies as per tablet count, is deemed important for reliable flexible dosing. As previously reported, the incorporation of hydroxypropyl cellulose (HPC) polymer into the formulation could advance achieving similar release profiles for varying drug concentrations, where the drug

is poorly water-soluble and the tablet surface area to volume ratio (SA/V) is kept constant (Buyukgoz et al., 2020). Moreover, HPC has been widely used in FDM 3D printing owing to its printability (Chai et al., 2017; Öblom et al., 2019). Thus, it may be a logical choice to incorporate HPC into the formulation along with a poorly soluble drug to assure reliable dissolution profiles from titrated doses. Although higher drug concentrations somewhat limit the flexibility in dose titration, it could alleviate the excipient burden. Thus, higher drug concentrations loaded mini-tablets are also examined. Finally, to gain insight into the robustness of the 3D printed mini dosage forms printed multi-unit tablets and split tablets are compared, where both contain similar target doses. Toward this end, HPC polymer and a model BSC class II drug, griseofulvin, are selected as the main components of the formulation. The design options described below are examined.

A. Single and multi-unit mini-tablets i.e., 1, 5, 10, 15, 20 count(s) to test content uniformity of the tablets with low-dose, 1 wt%, and to evaluate the corresponding dissolution profiles in the sense of similarity.

B. Varying resolutions of tablet layers i.e., 0.1, 0.15, 0.2, 0.25, and 0.3 to gain a preliminary understanding of layer resolution into the tablet characteristic.

C. Split tablets i.e., full, half, and quart size, to compare with the multi-units mini-sized tablets employing content uniformity and dissolution tests.

D. Single unit mini-tablets loaded with 10 and 20 wt% drug concentration to mitigate excipient burden.

3.2 Materials and methods

3.2.1 Materials

As-received griseofulvin (GF) (Letco Medical, Decatur, AL, USA) with a primary particle size of 11 µm was selected as a model Biopharmaceutics Classification

System (BCS) class II drug. Hydroxypropyl cellulose (HPC, SL grade) was donated by Nisso America Inc. (New York, NY). It has been widely used as a printing polymer of FDM 3D printing since it offers mechanical resilience for the filaments to be printed (Borujeni et al., 2020; Öblom et al., 2019; Pietrzak et al., 2015; Zhang et al., 2017a). The fact that HPC has been identified swellable/erodible polymer may control the release of poorly water-soluble drugs (Borujeni et al., 2020; Ford et al., 1985; Gazzaniga et al., 2011; Macchi et al., 2015). This may mitigate the variations stemming from intrinsic tablet properties to a certain extent and facilitate achieving similar release profiles from multi-unit mini tablets. Kollicoat® Protect (KP) was donated by BASF (Tarrytown, NY, USA). KP composes of polyvinyl alcohol-polyethylene glycol graft copolymer, polyvinyl alcohol, and fumed silica. It is a readily soluble polymer in water and is known to improve protection against moisture (Kolter et al., 2012). Sodium dodecyl sulfate (SDS) (Sigma-Aldrich, Saint Louis, MO, USA) was used as a solvent.

3.2.2 Preparation methods

3.2.2.1 Manufacturing of filaments. Table 3.1 presents the composition of the powder blends used for manufacturing the filaments. To mix the powder blends, a high-intensity vibrational mixer (LabRAM, Resodyn Acoustic Mixers, Inc., Butte, MT, USA) was used at a frequency of 61 Hz with an acceleration of 75 G for 5 min. The powder blend was extruded through an 11 mm diameter co-rotating twin-screw extruder (Thermo Fisher Scientific Inc., MA, USA) with the processing temperatures and screw speed presented in Table 3.1. A round-shaped die with a 2 mm opening was used to extrude the molten blend. The processing temperature

was optimized, where the instrument-safety and filament quality were simultaneously considered.

Table 3.1 Composition of the Formulations

Run #	Formulation	HME Processing Temperature (°C)	HME Screw Speed (rpm)
F1	1 wt% GF + 84 wt% HPC + 15 wt% KP	150	40
F10	10 wt% GF + 75 wt% HPC + 15 KP	150	40
F20	20 wt% GF + 65 wt% HPC + 15 wt% KP	155	40

3.2.2.2 Printing via FDM. The impact of the structural variability on the tablet characteristic has been widely reported for regular size 3D printed tablets (Ilyés et al., 2019a; Sadia et al., 2018a; Zhang et al., 2017b). In this study, varying layer resolutions are examined for mini-tablets to gain a preliminary understanding. The resolution of mini-tablet layers (Ilyés et al., 2019a) was adjusted by keeping the height of the final product constant while altering the thickness of each layer and the total number of layers. The details of the designs for a single-unit mini-tablet are presented in Table 3.2. It is hypothesized that varying resolution could affect the mechanical strength and available surface area of the tablet, which may eventually influence the drug release profile. In addition, layer resolution could affect the printing quality, in turn, the weight of the finished product. This was evaluated with the content uniformity test.

Table 3.2 Mini-tablet Design with Varying Layer Resolution along with the Corresponding Number of Tablet Layers

Formulation	Layer Resolution (mm)	Total Number of Tablet Layers
F1	0.10	20
F1	0.15	13
F1	0.20	10
F1	0.25	8
F1	0.30	7
F10	0.20	10
F20	0.20	10

Apart from layer height (resolution), the intended dose was printed via varying design options such as mini-tablets containing varying drug concentrations, split tablets, and multi-unit mini-tablets. The tablets printed with the filament containing 1 wt% drug concentration were used for micro-dosing, which means the dose was titrated with small increments, i.e., <1.0 mg. The tablets containing higher drug concentrations served the purpose of reducing excipient burden while printed subdivided tablets were examined to compare multi-unit tablets containing similar drug amounts. The details of tablet properties, dimensions, and count(s) are shown in Table 3.3. All the tablet designs were created using Autodesk® Fusion 360 Ultimate (Autodesk 3D design software) and recorded as an STL file. The designs were sliced using FlashPrint software (Version 3.18.0; Jinhua, China) and printed with FDM 3D printer (Flashforge®, Creator Pro 3D, 2016, China). The printer nozzle having a 4 mm opening was used. For all the print designs, the printing temperature of 180 ºC, the print speed of 35 mm/s, the traveling speed of 80 mm/s, and 100% infill were applied. The

temperature used met the general guideline of the printing temperature that FDM processing requires a higher processing temperature than that of HME owing to lacking high shear (Pietrzak et al., 2015)

Table 3.3 Tablet Size and Number of Units of the Printed Tablets

Run	Formulation	*Theoretical Tablet size		Number of unit (s)
		Diameter (mm)	Height (mm)	
M1	F1	3	2	1
M2		3	2	5
M3		3	2	10
M4		3	2	15
M5		3	2	20
M6	F10	3	2	1
M7	F20	3	2	1
F1	F1	13	2.2	1
H1		6.5	2.2	1
Q1		3.3	2.2	1

*All the tablets were printed with 0.2 mm layer resolution. M: mini-tablet, F: Full-size H: Half-size Q: Quart-size tablet.

3.2.3 Characterization methods

3.2.3.1 Thermo-gravimetric analysis. To examine any thermal degradation event stemming from thermal processing in FDM 3D printing, HPC, KP, and as-received GF powders, physical mixtures (PM), and the printed tablets were tested by thermo-gravimetric analysis (TGA) (TGA/DSC1/SF STARe system, Mettler Toledo Inc., OH, USA). In a standard ceramic crucible, the samples were heated from 25 to 240 ºC at a rate of 10 ºC/min and cooled back to 25 ºC under a nitrogen flow.

3.2.3.2 Solid-state characterization. X-ray diffraction was performed to analyze the solid-state of GF after the processing of FDM 3D printing. To fit the printed tablets on an XRD sample holder, the tablets were reprinted following the method in (Buyukgoz et al., 2020). Diffraction patterns were acquired for the samples using PANalytical (Westborough, MA, USA), scanning for 2 theta angle within the range of 5–30º (0.01° step).

3.2.3.3 Scanning electron microscopy (SEM). A scanning electron microscopy (JSM-7900F, JEOL Ltd, MA, USA) was performed to illustrate the resolutions of individual layers for the printed mini-tablets. The half-cut mini-tablets were perpendicularly placed on an aluminum stub using carbon tape and coated with golden via a sputter coater (Q150T 16017, Quorum Technologies Ltd, Laughton, East Sussex, England).

3.2.3.4 Mechanical properties. Due to the inherent high mechanical strength of FDM 3D printed objects, determining the influence of design on the mechanical properties is not easy (Borujeni et al., 2020; Nukala et al., 2019). In addition, cracks may occur at multiple locations of the printed structure, which is also fundamentally different than the compressed tablets (Arafat et al., 2018b). That may misguide determining the maximum load. In our example, the tested objects are cylindrical mini-sized tablets constructed with horizontal layers, where the calculation errors may arise from separating multilayers under the force applied. In addition, the size itself may pose difficulties in testing. Considering these challenges and our ultimate goal being to evaluate the impact of layer resolutions on mechanical resilience, a simpler method has been developed by printing a rectangular solid shape (slab) at

varying layer resolution. The slabs with the dimension of Length: 16 x Height: 1 x Width: 2 mm were designed using Autodesk® Fusion 360 Ultimate (Autodesk 3D design software). The procedures in Subsection 2.2.2.3 of Chapter 2 were followed for printing the designs with varying layer resolutions (0.1–0.3 mm). Next, the samples were tested using a 3-point bender tester (Instron, Norwood, MA), where the external force is applied with a loading pin at one location. That may break the layers alternately rather than simultaneously, which may allow determining the difference in layer resolution. For testing, the samples were horizontally placed on the probe having a 16 mm gap. The force was applied with a constant speed at 0.5 mm/min until the samples break. The influence of layer resolution was evaluated by calculating the tensile strength (TS) for the slabs using Equation (3.1) (Callister, 2007).

$$\sigma_{fs} = \frac{3FL}{2bd^2} \tag{3.1}$$

Here, the flexural strength (σ_{fs}) is defined for a sample having a rectangular cross-section, where *F* is the load at fracture, *L* is the distance between support points, *b* is the length and *d* is the thickness of the sample. The gap on the probe was set up as 16 mm. Later, each sample was positioned on the sample holder, and the force was applied at a constant speed at 0.5 mm/min until the breaking point. The average values and standard deviation of TS were computed over the 3-4 samples.

3.2.3.5 Content uniformity. The variations in tablet size, tablet weight, and drug mass were measured from randomly collected printed mini-tablets. The sample size for the single unit mini-tablets containing low drug concentration, 1.0 wt%, was n = 30 (FDA et al., 2014; Mitra et al., 2020). However, the sample size was kept as n = 3 for the tablets containing higher drug concentrations, 10 and 20 wt%, and for the multi-unit (composite) tablets comprised of 5, 10, 15, and 20 counts per sample. Content uniformity in multi-unit mini tablets was assessed to determine the critical number of mini-tablets having the acceptable dose variability. The tablet weights and dimensions were recorded. Each sample was dissolved in 7.2 g/L SDS solution and stirred via magnetic bars overnight. The dissolved samples were filtered with a 0.45 µm nylon membrane-type syringe filter (Celltreat scientific products, Pepperell, MA, USA), and analyzed for GF content and uniformity at 297 nm UV absorbance wavelength using a Thermo Scientific Evolution 300 UV–vis spectrophotometer (Thermo Fisher Scientific Inc., MA). The acceptance criteria given in USP <905> (FDA et al., 2014) were also applied for the assessment of content uniformity testing.

3.2.3.6 Dissolution. The release behaviors of printed tablets in Tables 3.2 and 3.3 were examined. First, the impact of layer resolution on drug release behavior of the single unit mini-tablets was assessed. Later, the proposed approach of achieving similar drug release profiles from multi-unit tablets, where the total drug amount varies as per tablet count(s), was examined with 1–20 unit(s) mini-tablets. The resulting release profiles were also compared with single unit mini-tablets containing higher drug concentrations as well as split tablets. To prevent any bias

on the dissolution performance of the tablets arising from differences in their drug content, the samples to be compared were designed such that they contain similar drug amounts. For example, the total drug amount in 10 unit mini-tablets containing 1 wt% drug was attempted to be kept similar to the drug amount of a single mini-tablet with 10 wt% drug or of a half-split large tablet containing 1 wt%. The dissolution paddle apparatus (USP II, Sotax, Switzerland) was used for testing the release profiles of the individual and multi-unit mini tablets. The sinkers were used for the multi-units to prevent the tablets from floating around. Deionized water (DI) was used as a dissolution medium (Bhakay et al., 2014; Li et al., 2017a). The samples were added to 500 ml dissolution medium, where the sink conditions were maintained, at 37 ºC with a paddle speed of 100 rpm. However, the paddle speed was decreased down to 50 rpm to better discriminate the differences in drug release arising from micron-level changes in layer resolution. Aliquots were withdrawn at certain time intervals over 24h, filtered through a 0.45 µm nylon membrane-type syringe filter (Celltreat scientific products, Pepperell, MA, USA). The filtrate was analyzed for the average percentage of the dissolved GF at 297 nm UV absorbance wavelength using a Thermo Scientific Evolution 300 UV–vis spectrophotometer (Thermo Fisher Scientific Inc., MA). The average percentage of the dissolved drug was plotted as a function of time. Each test was replicated minimum of three times.

3.3 Results and discussion

3.3.1 Mini-tablet printing

The mini-sized tablets with cylindrical shapes were successfully printed via FDM 3D printer. Their small size allowed printing multiple tablets at a time. That potentially improved the consistency between printed objects since the material changeover and tablet collection were mitigated. The digital photographs of the single mini-tablets at varying layer resolutions are presented in Figure 3.1. There was no visual difference in the quality of printed layers based on layer resolutions ranging 0.1–0.3 mm, except that the higher resolutions, exhibited tighter structure.

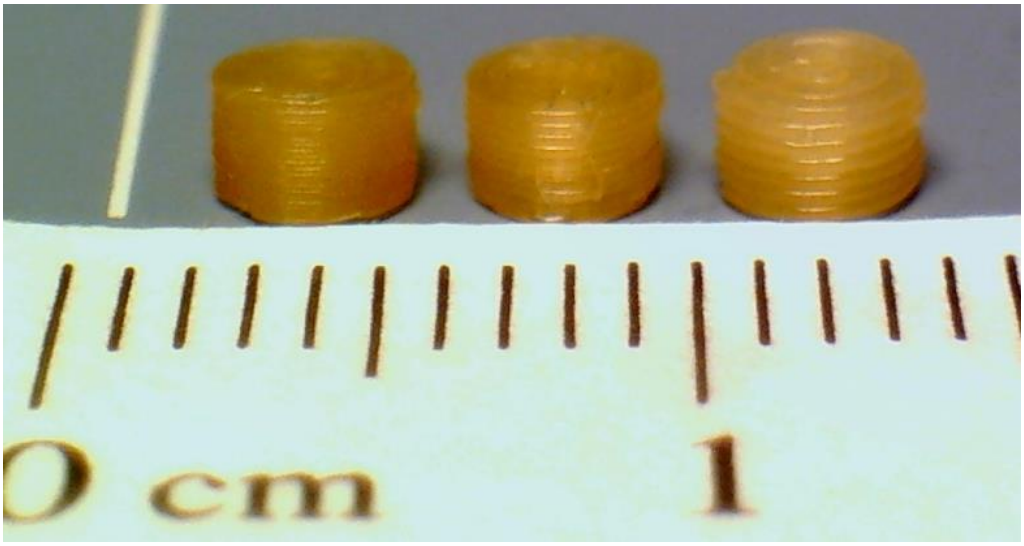

Figure 3.1 Digital photographs of the printed mini-tablets at varying layer resolutions; from left to right 0.1, 0.2, and 0.3 mm.

3.3.2 Thermo-gravimetric analysis

The outcomes of the thermo-gravimetric analysis (TGA) are presented in Figure 3.2. The highest weight loss was observed for KP powder, which was less than

2.3% at 100 ºC, which could be attributed to the free or bound water (Tidau et al., 2019). Increasing the temperature up to 180 °C did not increase the weight loss much (2.4%), indicating no thermal degradation at the printing temperature. The weight loss for all other powder materials and 3D tablets was below that, which indicates that they are thermally stable throughout the mini-tablet printing processing.

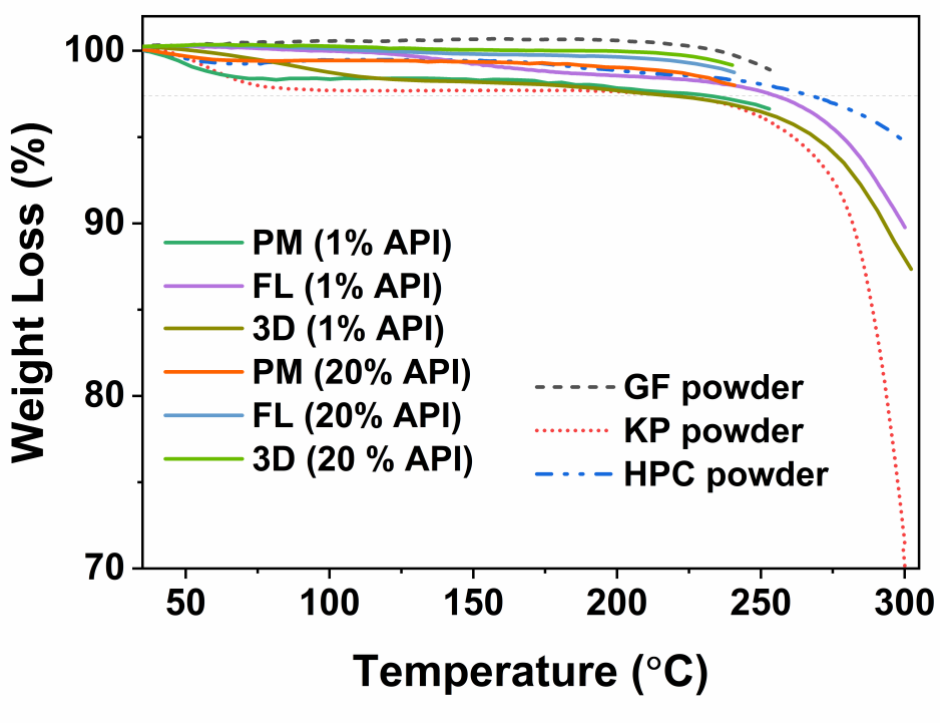

Figure 3.2 TGA thermograms for GF, HPC, and KP powders, physical mixtures (PM), filaments, and printed tablets at 1 and 20 wt% drug concentrations.

3.3.3 X-ray diffraction (XRD)

To assess the crystalline state of GF after FDM 3D printing process, as-received GF, HPC, and KP powders, the PMs, and the printed tablets were examined using XRD. The XRD diffractograms were presented in Figure 3.3. The halo patterns for

the polymers, indicating their amorphous nature, and the characteristic peaks of GF (Rahman et al., 2019) were observed. The diffractogram of PM for 1 wt% GF lacked characteristic peaks of GF and exhibited a halo pattern. This is most likely the consequence of low drug concentrations being below the limit of detection for determining GF crystallinity (Siddiqui et al., 2014). Further, the PMs with the drug concentration of 10 and 20 wt% showed similar characteristic peaks that of GF. Their lower intensity could be attributed to the surface coverage and dilution of GF particles with polymers (Li et al., 2017a; Rahman et al., 2019). In the diffractograms of printed tablets containing 20 and 10 wt% GF concentration, the disappearing characteristic peaks of GF at 13.2º and 16.5º (Rahman et al., 2019) indicated partial miscibility of GF with polymers after heat treatment by 3D printing. This is in line with (Rahman et al., 2020c), where the partial miscibility for GF-HPC formulation was reported.

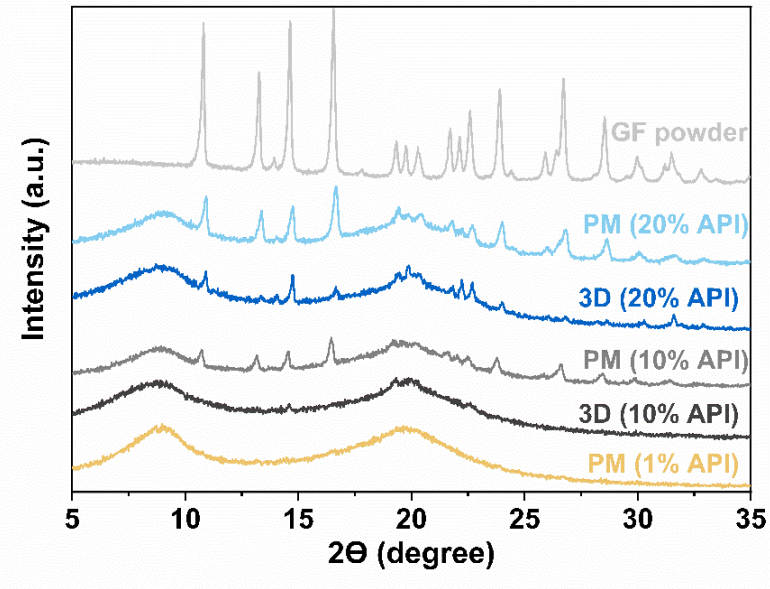

Figure 3.3 XRD diffractogram of GF powder, physical mixtures (PMs), and printed tablets.

3.3.4 Scanning electron microscopy (SEM)

The SEM images for the layer resolutions of the mini-tablets were demonstrated in Figure 3.4. All the layer resolutions up to 250 µm were found mostly uniform between consecutive layers. The further decreases in layer resolution caused inconsistencies in layer thicknesses. That suggested reduced reliability of the design with 300 µm. It is useful to note that this problem could be printer or software related rather than the capability of the formulation to print a high-resolution object since the performance of the printer used in this study was limited.

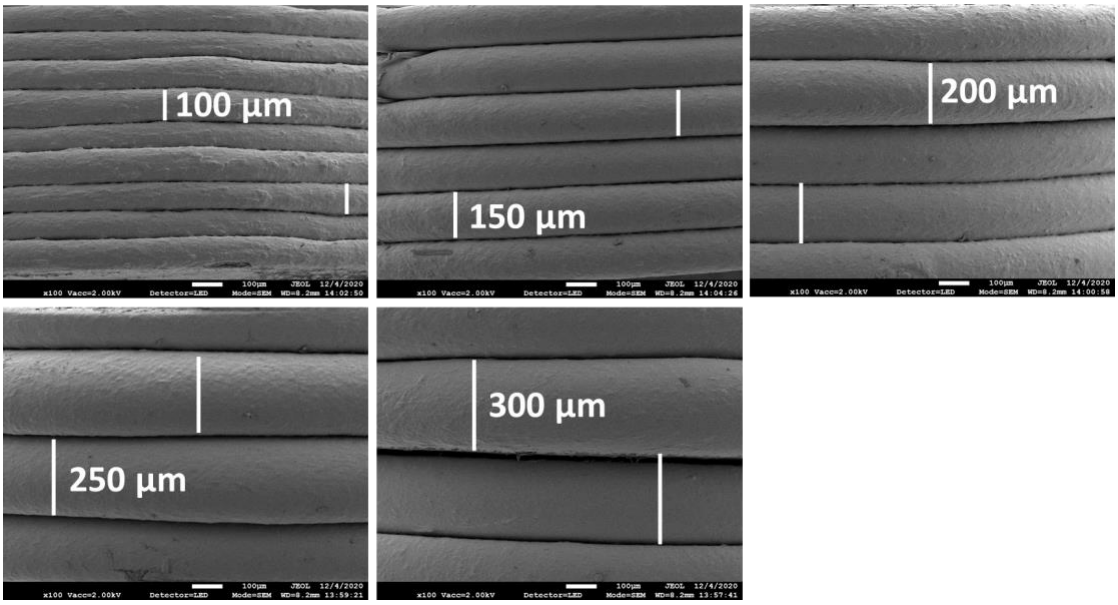

Figure 3.4 SEM images of the printed mini-tablets at varying layer resolutions.

3.3.5 Mechanical properties

The tensile strength (TS) of the printed slabs having varying layer resolutions were obtained from stress-strain curves and the results are presented in Figure 3.5. Decreasing the layer resolution from 0.1 to 0.3 mm proportionally decreased the TS. Since the final height was constant for all the samples, the tablets with thicker

layer configurations had fewer total layers, see Table 3.2. The increasing thickness between the consecutive layers decreased the mechanical strength of the structure with 0.3 being the lowest, which could be mainly driven by the resulting fewer adherent layers. This is in line with (Ilyés et al., 2019a), reporting the decreasing tablet hardness with decreasing layer resolution. Although our main purpose was to understand the impact of layer resolution on mechanical strength, it is useful to mention that there are no established standards for acceptable values of the tablet mechanical properties to assure the tablet quality. However, 3D printed solid structures are inherently strong, thus, conformance of mechanical properties to handling and packing have been widely documented (Borujeni et al., 2020; Ilyés et al., 2019a; Nukala et al., 2019; Sadia et al., 2018b). Therefore, it is considered that the printed tablets only with a resolution of 0.3 mm may not have appropriate mechanical properties.

As opposed to the influence of layer resolution, no significant difference in mechanical properties was realized when the drug concentration varied. This is expected since the difference between the drug concentrations was not significant.

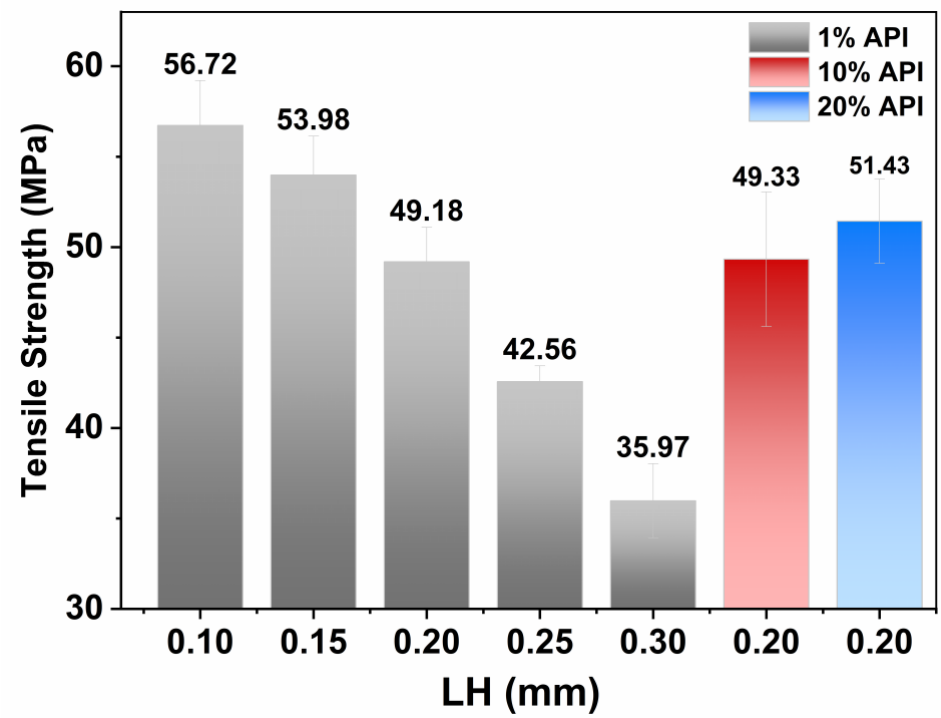

Figure 3.5 Mechanical properties of the mini-tablets at varying layer resolutions and drug concentrations.

3.3.6 Content uniformity and morphological properties of mini-tablets

3.3.6.1 Individual mini-tablets with varying layer resolutions. For individual mini-tablets, the variations in drug mass, tablet weight, and dimensions are shown in Table 3.4. The weight and dimensions of the mini-tablets for each resolution configuration had minor standard deviations. Although no discernible trend in tablet properties was realized with respect to the layer resolution, the lower resolutions had somewhat higher weight and dimensions. This could be linked with the swelling properties of HPC (Borujeni et al., 2020; Gazzaniga et al., 2011; Macchi et al., 2015). That implied that achieving the desired layer thickness using a swellable material in the formulation is likely more controllable at higher

resolutions. That also helps minimize the deviation from the target weight. Nevertheless, these negligible variations pointed out the capability of FDM 3D printing to produce any resolution in the range of 0.1–0.3 mm from HPC-based formulations even for small-sized tablets. That may also corroborate that the intrinsic advantages of FDM 3D printing could help minimize the challenges faced in conventional techniques for mini-tablet manufacturing.

As per USP <905> L2 criteria (FDA et al., 2014), the acceptance value (AV) for n = 30 units cannot exceed 25.0. According to that, all individual mini-tablets had excellent content uniformity with AV< 7.9, and their label claim (LC) values were within the acceptable range i.e., ±25% of the target dose, see Table 3.4. The enhanced content uniformity would not be surprising considering the fact that an intense mixer of HME could potentially produce contently uniform products (Maniruzzaman et al., 2012; Pawar et al., 2017; Sadia et al., 2018b). In addition to that, the even-sized mini-tablets being the product of FDM 3D printing exhibited closely similar weights, which further promotes the resulting uniformity in drug content.

Table 3.4 Drug Content and Uniformity

LR (mm)	Tablet mass (mg)	Diameter (mm)	Thickness (mm)	Drug mass (mg)	LC%	AV
0.10	20.38±0.21	3.30±0.03	2.06±0.03	0.21±0.00	101.09±0.90	1.81
0.15	20.42±0.24	3.41±0.02	2.02±0.01	0.21±0.01	101.39±2.72	5.44
0.20	19.18±0.32	3.38±0.05	1.97±0.03	0.19±0.01	99.67±3.92	7.83
0.25	20.15±0.30	3.51±0.03	2.01±0.02	0.20±0.00	99.62±0.93	1.85
0.30	21.03±0.34	3.55±0.07	2.16±0.05	0.21±0.00	99.33±0.83	1.67

LR: Layer resolution

3.3.6.2 Dose titration. All the tables aimed for use in dose titration were printed at 0.2 mm resolution. The drug amount from a single mini-tablet enabled titrate the dose with 0.19 mg escalations. Using 1–20 counts of mini-tablets covered the dispensed dose in the range of 0.19–3.91 mg, see Table 3.5, for the corresponding drug amounts per tablet count(s). To evaluate the robustness of the dose titration, tablet count(s) versus drug amounts was plotted with the upper confidence limit of 95%. In Figure 3.6, high accuracy with R^2 of 0.9996 was achieved. Generally, the uniformity of the composite dosages is the parameter for determining the minimum count(s) of mini-tablets for an acceptable dose variability (Mitra et al., 2020). In our case, however, the single unit mini-tablets exhibited excellent content uniformity. The linear trend achieved (R^2 of 0.9996) with increasing tablet count(s) confirmed the reliability of a single unit mini-tablet. That eliminated the need for minimum multi-dose for titrating the reliable dose.

Table 3.5 Dose Titration with Varying Tablet Counts and Drug Concentration (DC)

DC (wt%)	# of Tablet Unit	Tablet mass (mg)	Drug mass (mg)	LC%	AV
1	1	19.18±0.32	0.19±0.01	99.67±3.92	7.83
1	5	97.97±1.95	1.04±0.03	105.96±0.84	0.44
1	10	191.53±1.12	1.93±0.01	100.79±0.22	1.78
1	15	279.77±3.84	2.85±0.06	101.97±0.66	2.39
1	20	379.13±2.15	3.91±0.02	103.17±0.36	6.49
1	1	312.23±11.11	2.93±0.07	93.92±1.04	6.67
1	0.5	201.97±2.73	1.95±0.02	96.73±0.50	2.77
1	0.25	104.63±0.73	1.00±0.00	95.92±0.08	2.75
10	1	20.03±0.39	1.95±0.04	97.25±0.52	2.30
20	1	19.6±0.32	3.76±0.06	96.00±0.35	3.19

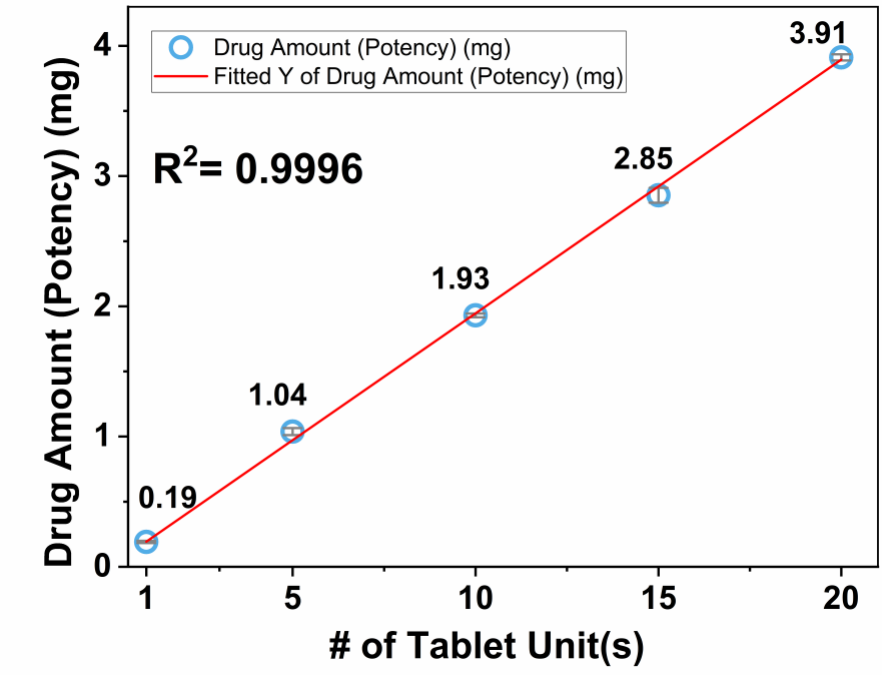

Figure 3.6 Dose titration via multi-unit mini-tablets at 1 wt% drug concentration.

To compare the split tablets with multi-unit tablets, their drug amounts were kept similar. The details of the corresponding doses are presented in Table 3.5.and visual demonstrations of the split tablets and multi-unit mini-tablets are presented in Figure B.1, Appendix B. To evaluate the performance of the split tablet for dose titration, tablet count(s); i.e., full, half, quart, versus drug amounts were plotted with the upper confidence limit of 95%. The plot is shown in Figure 3.7. The split tablets were found contently uniform and their LC% values were in the acceptable range. This level of uniformity was expected for the printed split tablets since they printed as designed and fragmentation became out of concern. However, this did not translate into enhanced linearity in dose titration, where R^2 was found 0.936. This could be again attributed to the swelling properties of HPC. That implied the impact of swelling to the tablet weight, which in turn to the drug amount, became more prominent in larger size tablets.

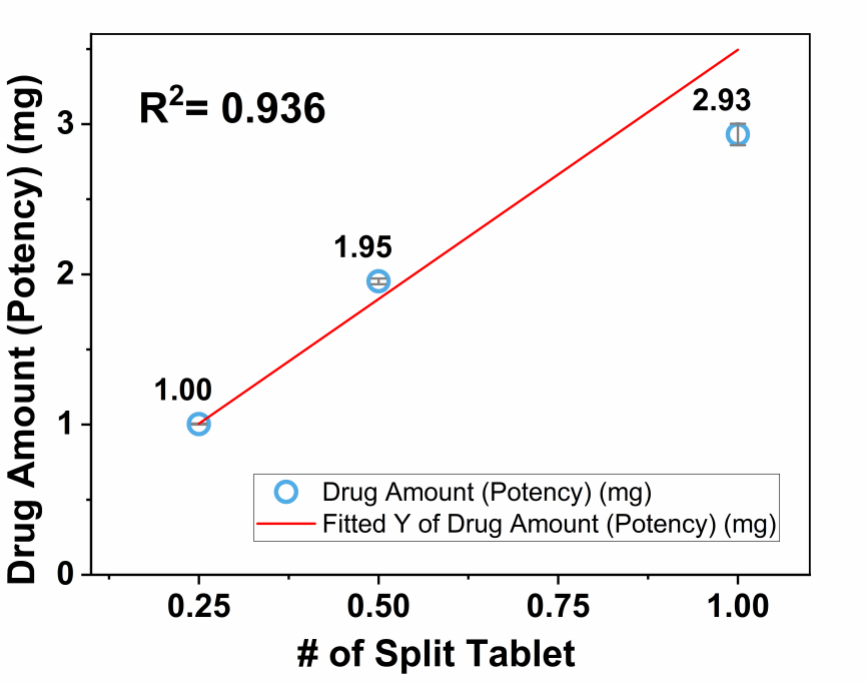

Figure 3.7 Dose titration via split tablets at 1 wt% drug concentration.

In an attempt to reduce the excipient burden (Mitra et al., 2020), single-unit mini-tablets containing higher drug concentrations, see Table 3.3, were examined. They showed enhanced content uniformity with acceptable LC% values. As previously reported, using filaments at varying drug concentrations is a safe practice for dose adjustment (Buyukgoz et al., 2020). Thus, the resulting uniformity at higher concentrations was deemed reasonable. Indeed, the performance in dose titration for the tablets at higher drug concentrations showed high linearity with R^2 of 0.9997, see Figure 3.8. It is useful to highlight that the drug amounts in twenty single mini-tablets containing 1 wt% drug concentration, (3.91 ± 0.02 mg), and one single mini-tablet containing 20 wt% drug concentration, (3.76 ± 0.06), are similar, Table 3.5. Although using higher drug concentration limits the increment in dose titration yet significantly reduces the excipient burden. Therefore, those tablets containing higher drug concentrations could be suggested for use in age-specific formulations not requiring close dose titration.

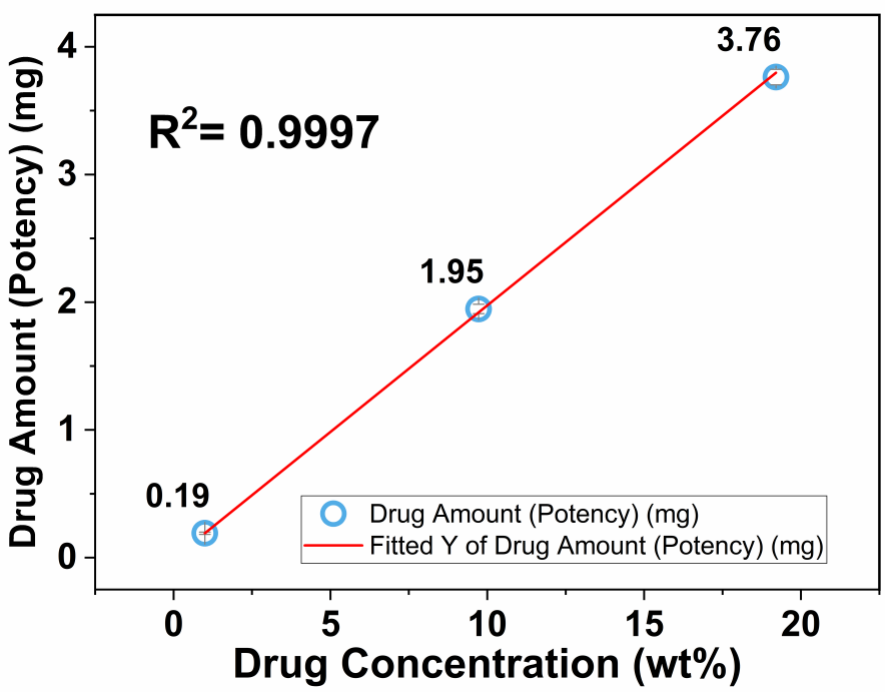

Figure 3.8 Dose titration with mini-tablet at 1–20 wt% drug concentrations.

3.3.7 Drug dissolution

The dissolution profiles of the mini-tablets with varying layer resolutions are examined. In Figure 3.9, surprisingly, no direct correlation was noticed between the resolution and drug dissolution. Drug release rate increased proportionally with decreasing layer resolution from 0.1 to 0.2 mm. The resolution at 0.2 mm exhibited the fastest drug release, $t_{75\%}$: 92 min. Further decreases in layer resolution decreased the release rate, with 0.3 mm being the slowest i.e., $t_{75\%}$: 247 min, amongst all the resolutions. Decreasing the total number of tablet layers with decreasing the layer resolution, see Table 3.2, decreased the external surface area available for water penetration. Indeed, Ilyes et al. (Ilyés et al., 2019a) has been reported a higher rate of water uptake for the thin resolution, 0.1 mm,

compared to that of the thicker one, 0.3 mm. However, they did not examine the intermediate resolution of 0.2 mm, which is where the difference was revealed in this study. That implied the presence of another factor affecting the drug release besides the layer resolution. As mentioned earlier, increasing the layer resolution increased the mechanical strength of the tablet (refer to Subsection 3.3.5). One might expect an inverse correlation between tablet mechanical strength and drug dissolution owing to the ease of water penetration into the structure (Kitazawa et al., 1975). This correlation was valid for the thinner resolutions i.e., 0.1–0.2 mm yet became reverse after 0.2 mm resolution. Although determining the dominating factor for the drug release requires more extensive investigation, it is clear that the differences in mechanical strength and external surface area of the tablet arising from varying tablet resolution play an important role in drug release behavior. Considering the fact that printing of the higher resolutions naturally requires the longer printing times as well as the resulting faster drug release for 0.2 mm resolution, we preferred 0.2 mm resolution for printing all the tablets in this study unless otherwise indicated.

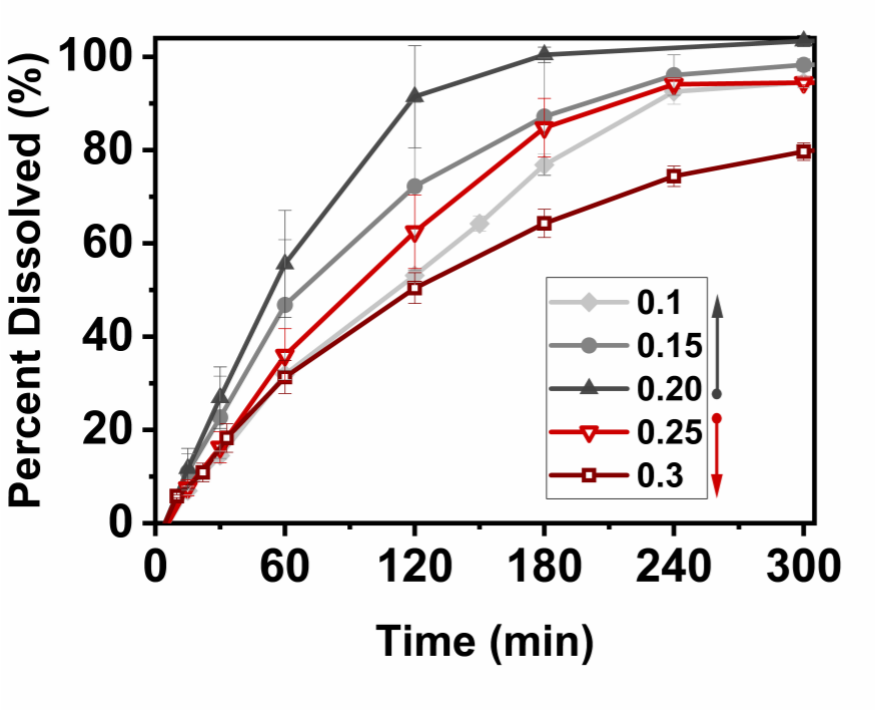

Figure 3.9 Drug release profiles of the mini-tablets at varying layer resolutions.

The release profiles of the 1–20 unit(s) mini-tablets are presented in Figure 3.10. The release profiles of the composite units i.e., 5–20 counts were found statistically similar with each other as per the bootstrap $f2$ similarity test (see Table B.1, Appendix B). Besides, the release profile of the single unit mini-tablets showed a slight difference from that of multi-units. This could be the result of the low drug amount being around 190 µg in a single tablet, which possibly caused relatively large standard deviations in the individual release profiles, see Figure 3.9. Similarly, Mitra et al. (Mitra et al., 2020) suggested the need for additional method development for testing the dissolution profile of a single mini-tablet at low drug concentration. Nevertheless, these outcomes reinforced that using solidified HPC and inherently dense matrix of FDM 3D printed tablets (Borujeni et al., 2020; Yang

et al., 2018; Zhang et al., 2017b) facilitated achieving similar release profiles from composite unit mini-tablets. It is worth mentioning that the high consistency in tablet size might have further contributed to the similarity in release profiles, where the minor standard deviations in the individual drug release profiles corroborated this observation (refer to Figure 3.10).

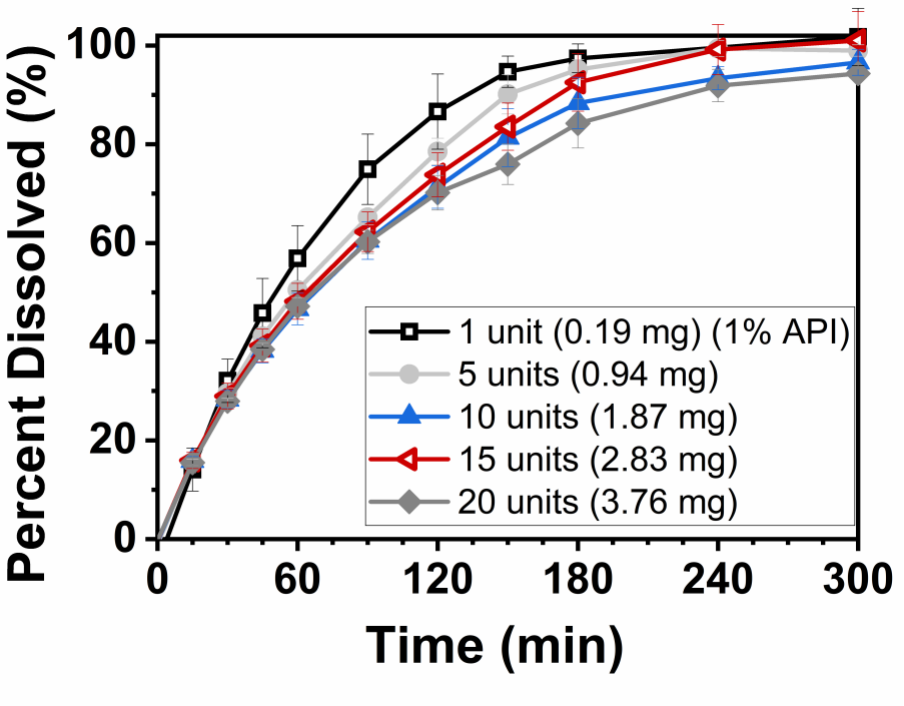

Figure 3.10 Drug release profiles of single and multi-unit mini-tablets.

In Figure 3.11, the drug release profiles from printed split tablets are presented. The full and half-split size tablets exhibited seemingly similar release profiles. However, large standard deviations appeared in the release curve of the half-split tablets. Thus, the release profiles of full, half-split, and quartered tablets became statistically different according to the bootstrap $f2$ similarity test, (Table B.1, Appendix B). In comparison to the release profiles of multi mini-tablets, they

exhibited slower drug release owing to their size being significantly larger than mini-tablets. Therefore, the split-tablets could not compete with the performance of mini-tablets in the sense of drug release rate and consistency.

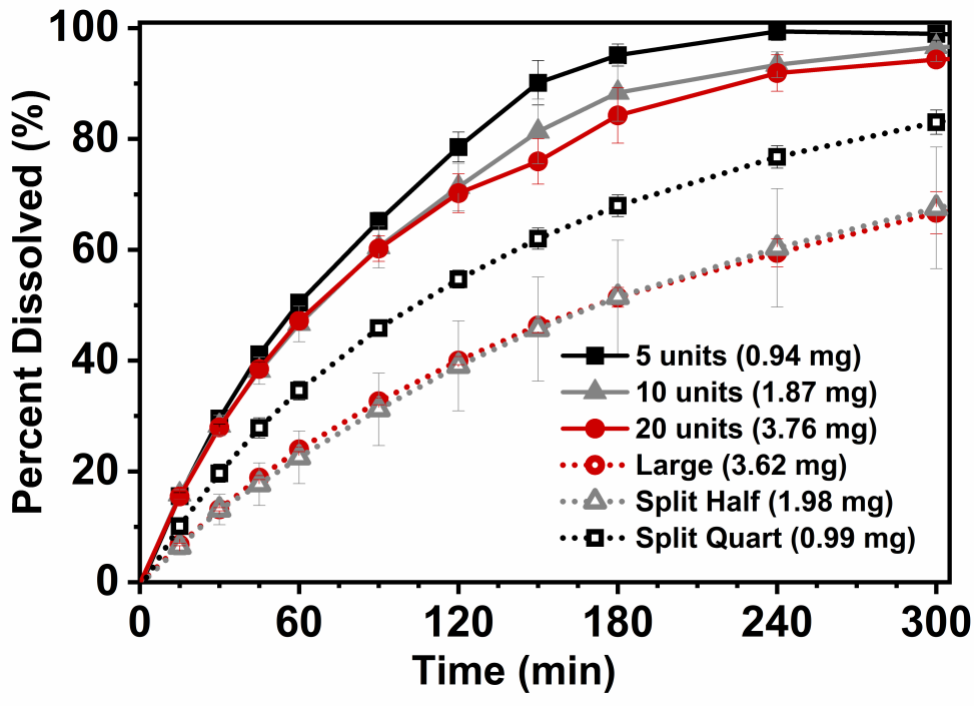

Figure 3.11 Drug release profiles of multi-unit mini-tablets and split tablets.

In Figure 3.12, the release profiles of the mini-tablets at higher drug concentrations are presented. The mini-tablets at 10 and 20 wt% drug concentrations showed statistically similar drug release profiles with each other yet different release profiles with the mini-tablets at 1% drug concentration. This was expected since the large difference in the drug concentration range could change the drug release characteristic even for inherently dense FDM 3D printed tablets (Buyukgoz et al., 2020; Yang et al., 2018). Nevertheless, GF concentration within

the range of 10–20 wt% could help reduce the excipient burden while providing similar release profiles.

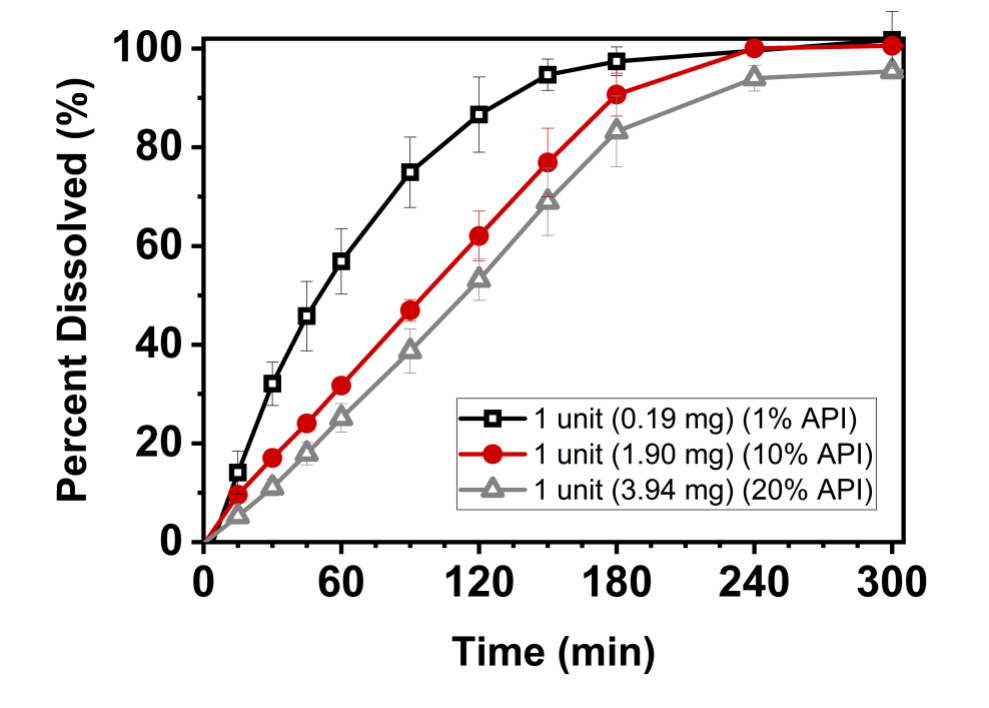

Figure 3.12 Drug release profiles of single unit mini-tablets at 1–20 wt% drug concentrations.

3.4 Conclusions

For specific patient population who needs manipulations in administering the prescribed dose, tailored dosages were achieved via FDM 3D printed mini-tablets. It was found that HME processing followed by FDM 3D printing promotes content uniformity even for miniature tablets containing micro-dose. That offered desired flexibility with high accuracy for close dose titration (micro-dosing) through multi-unit mini-tablets. Further, reliable dosing was reinforced with similar drug release profiles from multi-unit mini-tablets afforded by the similarity in size and inherent dense structure. Naturally, size and shape differences in split tablets demonstrated

different release behavior. Besides, the tablet structure i.e., layer resolution was found to be an important factor affecting the release behavior, suggesting careful consideration in design for achieving desired drug release. Another important outcome is that the tablets at higher drug concentrations demonstrated similar release behavior with each other. Thus, formulating the mini-tablets at higher drug concentrations offered reduced excipient burden.

CHAPTER 4

THREE-DIMENSIONAL PRINTED TABLETS LOADED WITH FUSION-ASSISTED AMORPHOUS SOLID DISPERSIONS

4.1 Introduction

Approximately 40% of drug entities being discovered are poorly water-soluble (Lipinski, 2002). The fact that these active pharmaceutical ingredients (APIs) exhibit poor solubility in the aqueous environment (Amidon et al., 1995) leads to low absorption in the gastrointestinal tract, which results in poor bioavailability. The technology of forming amorphous solid dispersions (ASDs) is one of the most successful and common strategies to enhance the bioavailability of poorly soluble drugs, which relies on dispersion of a drug into the hydrophilic carriers resulting in an amorphous mixture (Chiou et al., 1971; Hancock et al., 1997; Lakshman et al., 2008; Leuner et al., 2000; Moseson et al., 2020; Rumondor et al., 2009a; Sun et al., 2012; Van den Mooter, 2012; Vasconcelos et al., 2007). Since the kinetic solubility of an amorphous drug is greater than its crystalline counterpart, ASDs potentially enhance the dissolution rate and eventually bioavailability of the poorly soluble drug (Newman et al., 2012; Serajuddin, 1999). Amongst several preparation technologies to produce ASDs (Janssens et al., 2009; Rahman et al., 2020b; Serajuddin, 1999; Zheng et al., 2019), hot-melt extrusion (HME) is a widely used method as it offers one-step, continuous, and solvent-free manufacturing (Baghel et al., 2016; Mendonsa et al., 2020; Moseson et al., 2020; Sarode et al., 2013b; Solanki et al., 2018a).

Recently, Fused Deposition Modeling (FDM) based three-dimensional (3D) printing has become a popular drug delivery platform owing to its ability for on-demand production and flexible dosing. In this technique, a feed-material (filament) produced by HME is fed into a heated nozzle and deposited layer by layer to form 3D printed dosage or device. The coupling of FDM 3D printing with HME compounded filament led to creating a new applicable dosage form, which is ASDs loaded 3D printed device. This is typically achieved by producing ASDs loaded filaments through HME processing (Arafat et al., 2018a; Gioumouxouzis et al., 2018; Ilyés et al., 2019a; Jamróz et al., 2017; Kempin et al., 2018; Palekar et al., 2019; Scoutaris et al., 2018; Solanki et al., 2018b; Wei et al., 2020). In some cases, even when the filament containing crystalline drug was used for 3D printing, the amorphous form of the drug formed in the printed device owing to the transient heat transfer generated during the printing processing (Chai et al., 2017; Jamróz et al., 2018). In such studies producing ASDs loaded 3D printed tablets, the influence of tablet design, tablet size, infill density, and polymer type on the drug dissolution rate were examined (Arafat et al., 2018a; Kempin et al., 2018; Palekar et al., 2019; Solanki et al., 2018b; Wei et al., 2020; Zhang et al., 2017a; Zhang et al., 2017b). Briefly, 3D structure design, i.e., infill density and shell thickness, were found efficient for controlling the drug release rates (Solanki et al., 2018b; Wei et al., 2020; Zhang et al., 2017b), where thick and tight structure led to slower drug release, while the direct conclusion was not possible for the polymer effect due to their system-specific properties such as pH-dependent solubility, concentration in the composition and interactions with APIs (Solanki et al., 2018b; Wei et al., 2020;

Zhang et al., 2017a). However, those studies have yet to test the solubility advantage of the amorphous drug by examining the generation and maintenance of drug supersaturation (Moseson et al., 2020; Ozaki et al., 2012; Price et al., 2019; Sun et al., 2013; Sun et al., 2016). Therefore, the majority of this study is focused to examine generating and maintaining the drug supersaturation produced by ASDs loaded 3D printed tablets. To this end, the factors affecting the dissolution performance such as tablet surface area (Buyukgoz et al., 2020; Goyanes et al., 2015c), tablet design (Sadia et al., 2018a; Zhang et al., 2017b), and dissolution testing conditions (Newman et al., 2012; Price et al., 2019; Sun et al., 2012) were considered as the important factors that might influence the degree of drug supersaturation.

Apart from the final product properties, filament quality is the prerequisite criteria to be compatible with FDM 3D printing. Hence, approaches aiming to produce ASDs loaded filaments have to primarily meet the acceptable filament quality. The acceptable filament quality has been described with the characteristics of uniform diameter, sufficient mechanical resilience, lack of voids and bubbles throughout the filament as well as thermal stability (Govender et al., 2020; Isreb et al., 2019; Kempin et al., 2017; Nasereddin et al., 2018; Yang et al., 2016; Zhang et al., 2017a). All of these aspects are greatly impacted by the melt rheology, HME processing temperature, and individual properties of drug and polymer (Sarode et al., 2013a; Solanki et al., 2018a; Solanki et al., 2019b), which are also crucial factors for the approaches producing ASDs. That renders the mutual satisfaction of both ASDs and filament quality is difficult. Thus, the formulation development

being the most prevalent approach, where polymers and drugs are screened to generate and maintain the ASDs (Solanki et al., 2018b) may not guarantee acceptable filament quality. For instance, Govender et al. (Govender et al., 2020) manufactured filaments using a miscible drug-polymer formulation, offering amorphous molecular level solid dispersion. Whilst they indeed produced the filament containing amorphous API, filament brittleness prevented the automatic feeding, which failed the 3D printing process. Manually feeding the filament resulted in a dispensing imprecision at all the print volumes (Govender et al., 2020). Another approach, the fusion-assisted technique, is that operating the HME at relatively high temperatures, where API could melt and form an amorphous phase, even not being completely miscible with the polymer (Aho et al., 2017). However, several studies reported the adverse effect of the high processing temperature on filament quality (Aho et al., 2017; Censi et al., 2018; Kempin et al., 2017; Yang et al., 2016). These seemingly unconnected approaches pointed out that producing ASDs loaded filament being compatible with FDM 3D printing could be challenging, in some cases not possible.

Maintaining the physical stability of ASDs loaded filaments for the duration of product shelf life is equally important as generating the ASDs. Over storage, the amorphous drug being thermodynamically unstable is prone to revert back to the crystalline form that is so-called recrystallization (Baird et al., 2010; Newman et al., 2012; Uekama et al., 1992). That is strongly undesired because it could reduce the solubility advantages of ASDs (Censi et al., 2018; Moseson et al., 2020; Wei et al., 2020). Due to the novelty of the FDM 3D printing platform, scant information exists

on stability assessment for ASDs loaded filaments to be used in 3D printing (Govender et al., 2020; Solanki et al., 2018b; Wei et al., 2020). Such studies intended to produce ASDs loaded filaments have been pointed out the recrystallization issue and put an appreciable effort into developing the stable formulations. As one example, Wei et al. (2020) develop formulations using different APIs either haloperidol or carvedilol to produce ASDs loaded feed materials. However, incorporation of plasticizer into the formulation with intent to improve the melt extrusion caused recrystallizations of the APIs under accelerated conditions. When drug concentration was reduced to half, the physical stability was ensured for only carvedilol. Another interesting point of view, some research groups (Chai et al., 2017; Jamróz et al., 2018) reported that transient heat energy generated during 3D printing could transfer the residual crystals in the filaments to amorphous form. Although this fusion-assisted approach may tackle the stability problem of amorphous drug in the filament, unfortunately, the crystal growth is not a uniformly occurring process and causes differences in crystal sizes throughout the product (Cetindag et al., 2020). Thus the efficiency of transferring heat for melting those non-uniform particles (Brenken et al., 2016) becomes confounded, which was also previously emphasized by (Buyukgoz et al., 2020).

These studies have been played a key role in fabricating pharmaceutically favored ASDs via FDM 3D printing. However, the integral parts of the fabrication reveal that maintaining the physical stability of ASDs over the shelf life along with satisfactory filament quality requires appreciable exertion (Govender et al., 2020; Wei et al., 2020). The approach of transferring residual drug crystals to amorphous

form during the 3D printing process applied by those studies (Chai et al., 2017; Jamróz et al., 2018) appears to be able to circumvent the stability problem. However, it remained unclear that the fusion-assisted approach could be applicable to what extent of residual crystals. Particularly, this concern becomes more prominent over storage owing to the non-uniform particle growth (Cetindag et al., 2020). By the motivation of crystalline drug being thermodynamically stable, this study postulates that if the filament is manufactured by retaining the drug in largely crystalline form, and subsequently ASDs are produced at the point of tablet printing rather than at the beginning of filament preparation, it would be more likely to minimize the confounding effects arising from drug recrystallization. Because, the filament containing largely crystalline fraction would potentially refer to the lesser amount of amorphous form to be recrystallized, indicating higher uniformity in particle size (Thommes et al., 2011). That could offer uniform distribution in heat transferring at the point of converting those drug particles to the amorphous form. The fact that this approach requires the drug to have adequately high melting temperature and minimal miscibility with the polymers at the low processing temperatures through HME operation could help tolerate some but not all the aforementioned disadvantages of high processing temperatures on the filament quality. In addition, this could be useful for the drugs being difficult to stabilize in amorphous form (Thommes et al., 2011). However, to generate fusion-assisted ASDs at the point of FDM 3D printing from those filaments, the FDM processing temperature is desired to be sufficiently high to soften the drug-polymer mixture for the extrusion process (Aho et al., 2017; Govender et al., 2020; Solanki et al.,

2018a). On one hand, thermally labile compounds could be the shortcoming of the approach owing to their propensity to thermal degradation at the high printing temperatures. In fact, those are also a limitation for most HME compounded formulations (Shah et al., 2013). On the other hand, relatively lower residence time of the FDM processing compared to that of HME (Govender et al., 2020) could compensate for the potential compound degradation during 3D printing.

Towards those objectives, griseofulvin (GF) is selected as a model BCS class II and a fast-crystallizing drug (Baird et al., 2010). Since GF has a high melting point, it may better serve to retain the drug in crystalline form and allows flexibility with setting the printing temperatures. Hydroxypropyl cellulose (HPC) is used as the matrix-forming polymer while Kollicoat® Protect (KP) is used to promote drug-polymer interactions at high processing temperatures**.** Drug supersaturation under extreme non-sink conditions is examined by considering the factors affecting dissolution performance such as FDM processing temperatures, tablet design options with varying surface areas including cylindrical tablets, square-pattern perforated tablets, mini-sized tablets, and agitator speed. Ultimately, drug supersaturation behaviors during dissolution are mechanistically differentiated using Korsmeyer-Peppas model. That may allow designing the 3D tablets loaded with pharmaceutically favored ASDs. To the best of the author's knowledge, evaluation of those aspects from FDM 3D printed tablets is missing in the current literature.

4.2 Materials and methods

4.2.1 Materials

Griseofulvin (GF; Letco Medical, Decatur, AL, USA) was used as the model Biopharmaceutics Classification System (BCS) class II drug. GF is a crystalline drug with a melting point T_m of 220 ºC (Rahman et al., 2020c). It is considered a challenging drug for the development of ASDs given the fact that it rapidly crystalizes (Baird et al., 2010). Hydroxypropyl cellulose (HPC, SL grade, Nisso America Inc., New York, NY) is a semi-crystalline polymer with the glass transition temperature (T_g) of in range -25–0 ºC and T_m of around 170–200 ºC (Rahman et al., 2020c; Sarode et al., 2013a). Due to its ability to produce filaments with satisfactory mechanical properties, it has been reported as a suitable polymer for FDM 3D printing (Öblom et al., 2019; Pietrzak et al., 2015; Zhang et al., 2017a). Besides, it helps in enhancing the wettability of hydrophobic GF particles (Li et al., 2017a). Kollicoat® Protect (KP, BASF, Tarrytown, NY, USA) is readily soluble in water and composed of polyvinyl alcohol-polyethylene glycol graft copolymer, polyvinyl alcohol, and fumed silica. It has a T_m of 205 ºC and a T_g of 45 ºC, and is known to improve protection against moisture (Bühler, 2007). Further, Kollicoat® Protect lowers the surface tension of water i.e., surface tension is 61.6 for 0% solution and 42.3 mN/m for 15% solution (Bühler, 2007). Sodium dodecyl sulfate (SDS) (Sigma-Aldrich, Saint Louis, MO, USA) was used as a solvent.

4.2.2 Preparation methods

4.2.2.1 Preparation of feed materials (filaments). The compositions of the powder blends and HME processing parameters are shown in Table 4.1. The blends were mixed by a high-intensity vibrational mixer (LabRAM, Resodyn Acoustic Mixers, Inc., Butte, MT, USA) at a frequency of 61 Hz with an acceleration of 75 G for 5 min. HME processing was operated with an 11 mm diameter co-rotating twin-screw extruder (Thermo Fisher Scientific Inc., MA, USA) with a round-shaped die having a 2 mm opening. As similar to the procedure applied by (Moseson et al., 2020), the HME processing temperatures were gradually elevated, Table 4.1, in an attempt to prepare filaments with varying fractions of crystalline/amorphous GF. The largely crystalline fraction is considered that high physical stability of GF in filaments could be assured since the higher crystalline fraction refers to the lesser amount of amorphous formed. That potentially reduces the adverse effect arising from recrystallization of an amorphous drug, e.g. incoherent particle growth (Cetindag et al., 2020). This becomes important in the sense that fusion-assisted ASDs, where transient conductive heat is used to melt the suspended drug particles (Gogos et al., 2012). Non-uniform particles in the filament may lead to obtaining the last product containing unmelted drug particles, which represents the residual crystallinity and reduces product reliability. Moseson et al. reported that the presence of residual crystallinity in the product caused loss of the solubility advantage of ASD (Moseson et al., 2020). Possibly, the higher crystalline fraction could mitigate this deleterious effect. This approach requires the HME processing temperature to be lower than T_m of GF and poor drug-polymer

miscibility at those processing temperatures for avoiding the temperature-induced drug-dissolve. It has to be noted that the formulation retaining the drug completely crystalline may not be desired for affording the drug-polymer interactions, which are necessary for producing and maintaining the ASDs (Rahman et al., 2020c; Rumondor et al., 2009b). The varying amorphous fractions serve to confirm that the fusion method is suitable for the GF-HPC-KP formulation, where the HME processing temperatures are gradually elevated to form an increasing fraction of amorphous GF in presence of HPC-KP, eventually GF ASDs.

Table 4.1 Composition of Powder Blends and Their Processing

Run	**Blend Composition**		**Processing Parameters in HME**			**Final Product**
	Drug (wt%)	Polymer(s) (wt%)	Temperature (ºC)	Screw Speed (rpm)	Feed Rate (g/min)	
H160	-	Placebo	160	30	0.7	Filament
H165	15% GF	75% HPC + 10% KP	165	35	1.1	
H180			180	50	1.8	
H190			190	60	2.4	

"H" implies HME processing
Placebo composed of 7.5:1.0 HPC: KP

4.2.2.2 Printing dosage forms. The filament H160, Table 4.1, was used for printing placebo tablets, while H165, Table 4.2, was used for printing all the tablets loaded with GF, (see Tables 4.2 and 4.3). It was aimed to produce fusion-assisted ASDs using FDM 3D printing at varying processing temperatures. The rationale of fusion-assisted ASDs (Moseson et al., 2020) is that the transient heat energy generating during the FDM 3D printing process is used for transferring the crystalline GF particles to their amorphous form. On a macroscopic scale, as the

temperature rises, the mobility of the chains in the molten drug-polymer mixture increases (Kempin et al., 2017). That promotes the drug-polymer interactions and leads to forge hydrogen bonds between GF and HPC-KP, which is the sign for the formation of ASDs (Rumondor et al., 2009b). Hence, to test the efficiency of processing temperature on the formation of ASDs, the temperatures above or below the melting point of the GF were determined as the processing temperatures for FDM 3D printing, Table 4.2. All the tablets in Table 4.2 were printed with cylindrical geometry.

Table 4.2 3D Printing Processing Temperatures for GF-loaded and Placebo Tablets

Run	Filament Used For Printing	FDM Printing Temperature (ºC)	Final Product
F165	H165	165	FDM 3D Printed Tablet
F210		210	
F230		230	
F240		240	
P165	H160	165	
P240		240	

"F" implies FDM 3D processing, "P" implies FDM 3D printed placebo tablets
The set tablet dimensions for all the printed tablets: ø: 16 mm x H: 2 mm

It is helpful to mention that to conduct the characterizations with freshly prepared samples, F165 was printed as representative of H165 since the printing process is time-saving and requires less material for the final product compared to the HME process. However, %crystallinity was estimated with H165 to eliminate any bias that may arise from different processing. Later, to test the influence of tablet surface area on the supersaturating performance of GF during dissolution, two design options with enhanced surface area, multi-mini tablets, and square-

pattern perforated tablets, Table 4.3, were created. The details of the tablet designs are shown in Table 4.3. The tablet designs were created using Autodesk Fusion 360 Ultimate (Autodesk 3D design software), exported as STL files and, converted to X3G files using FlashPrint software (Version 4.3.0; Jinhua, China) as the slicer. FDM 3D printer (Flashforge, Creator Pro 3D, 2016, China) with the nozzle having a 0.4 mm opening was used for printing of the tablets. The following operating parameters (Buyukgoz et al., 2020) were kept constant for all the tablets in Tables 2 and 3; printing speed, 35 mm/s; nozzle traveling speed, 80 mm/s; layer height, 0.20 mm; infill percentage, 100%.

Table 4.3 Dimensions and Relative Surface Areas for Various 3D Tablet Designs, Number of Samples per Dissolution Vessel along with the Agitator Speed

Run	3D Printed Tablets				Agitator Speed
	Design	Size	*Relative SA	Quantity	(Rpm)
F240	Cylinder	16 by 2	1.0	1	50
F240a	Cylinder	16 by 2	1.0	1	250
F240b	Multi-mini	3 by 2	2.2	33	50
F240c	Structured w sinker	16x16x4.2	7.9	1	50
F240d	Structured w/o sinker	16x16x4.2	7.9	1	50

*The tablet surface areas are relative to that of F240

4.2.3 Characterization methods

4.2.3.1 Mechanical properties of filaments. To assess the impact of varying HME processing temperatures on the filament quality, the mechanical properties were determined via a Texture Analyzer (3-point bender tester, Instron,

Norwood, MA). Randomly selected five to six filaments were cut into 1 cm segments. Diameters of the filaments were recorded using a digital caliper. The samples were placed on the probe having a gap with 4 mm. With a constant speed at 0.5 mm/min, the force was applied until the filament breaks. Stiffness and breaking force are the common parameters to evaluate filament printability (Zhang et al., 2017a). In this study, modulus of elasticity (ME) and tensile strength (TS) were considered as the stiffness and the breaking force, respectively. From the stress-strain plot, the slope of the initial linear segment was used to calculate ME. TS was calculated using Equation (2.1) of Chapter 2 (Callister, 2007).

4.2.3.2 Fourier transform infrared spectroscopy (FT-IR). To determine the drug-polymer interactions, FT-IR analysis was performed with as-received GF powder, physical mixture (PM), and the printed tablets. An attenuated total reflectance (ATR) infrared spectra were collected using Agilent Cary 620 FT-IR equipped with single bounce diamond crystal and Golden Gate type ATR unit. Each spectrum was acquired with 32 scans with a resolution of 4 cm^{-1}. The spectral data was reported in the range 1550–1750 cm^{-1} wavenumber.

4.2.3.3 Solid-state characterization. To analyze the crystalline state of GF after thermal processing in HME and FDM 3D printing, as-received GF, HPC, and KP powders, the filaments, and the printed tablets were examined via X-ray diffraction (PANalytical, Westborough, MA, USA). In an attempt to fit the filaments on an XRD sample holder, the filaments were milled via LabRAM, where the extruded filaments along with six metal beads were placed in a metal jar and shake at a frequency of 61 Hz with an acceleration of 100 G for 5 min. For the same

reason, the tablets were printed with the set dimensions of ø: 15.5 mm x H: 1.7 mm. The printing parameters described in Subsection 4.2.2.2 were kept the same. The samples were scanned for 2θ angle ranging from 5º to 35º (0.01° step). To determine the %crystallinity of GF in the samples, OriginPro (Version 2020b) software was used following the previously established method in (Rahman et al., 2019).

4.2.3.4 Morphology. To determine the morphology of the particles, as-received GF and KP powders, filament (H165, Table 4.1), and the printed tablets (F240 and P240, Table 4.2) were tested via a scanning electron microscopy (JSM-7900F, JEOL Ltd, MA, USA). The samples were placed on an aluminum stub using carbon tape and coated with golden via a sputter coater (Q150T 16017, Quorum Technologies Ltd, Laughton, East Sussex, England). The images from each sample were recorded. To further examine the morphology of the GF particles in the filament (H165, Table 4.1) and printed tablet (F240, Table 4.2), polarized light microscopy (PLM, Axio Scope.A1, Carl Zeiss Microscopy GmbH, Göttingen, Germany) was used. In an attempt to obtain a better visualization, the tablets, F165 and F240, with a thinner layer of approximately 0.1 mm were printed. The samples were imaged with 10X resolution.

4.2.3.5 Thermal analysis. To determine the thermal degradation of the compounds, if any, at the high processing temperatures, as-received GF, HPC, and KP powders, PM, and the printed tablet, F240, were tested by thermo-gravimetric analysis (TGA) using a TGA/DSC1/SF STARe system (Mettler Toledo Inc., OH, USA). 5–8 mg sample was placed in a standard ceramic crucible, heated

from 25 ºC to 300 ºC at a rate of 10 ºC/min, and cooled back to 25 ºC under a nitrogen flow.

4.2.3.6 Determination of drug concentration. Since the tablets were designed for testing the supersaturating performance of GF, the tablets with a high dose of GF (~100 mg) (Rahman et al., 2020a) were printed with the tablet size of ø: 16 mm x H: 2 mm. However, for the sake of less solvent consumption to test the drug concentration and for better elucidating the differences in content uniformity, smaller size tablets with the set dimensions of ø: 5 mm x H: 1 mm were printed with the same printing parameters described in Subsection 4.2.2.2. The samples were dissolved in 150 ml of 7.2 g/L SDS solution and stirred via magnetic bars overnight. A Thermo Scientific Evolution 300 UV–vis spectrophotometer (Thermo Fisher Scientific Inc., MA) was used to measure the UV absorbance at a wavelength of 297 nm for the dissolved samples. The tablet mass and dimensions were recorded. The relative standard deviations (RSDs) in the drug concentrations were calculated for each set of 3-5 samples.

4.2.3.7 GF supersaturation, *in-vitro* dissolution test, and release kinetics. The degree of GF supersaturation was determined under non-sink dissolution conditions. It has been previously emphasized that the extent of deviation from sink condition, in other words, the extent of non-sinkness, could characterize the drug dissolution behavior (Sun et al., 2012; Sun et al., 2013; Sun et al., 2016). To quantitatively describe the extent of non-sinkness, Sun et al. (2012) introduced the dimensionless sink index (SI) = C_sV/(dose), where C_s is the equilibrium solubility of crystalline drug, V is the volume of dissolution medium, and “dose” is the total

amount of drug in the test sample. According to (Sun et al., 2012; Sun et al., 2016), SI = 0.1 indicates extreme non-sink conditions which allow observing the drug precipitation. In this study, extreme non-sink conditions with SI = ~0.1, were applied to explore the supersaturating performance of GF generated by ASDs loaded printed tablets in Tables 4.2 and 4.3. The supersaturaing performance of PM and H165 were examined as the control options since they are not meant to produce ASDs. DI water was selected as a dissolution medium as it better discriminates the GF formulation (Bhakay et al., 2014; Li et al., 2017a; Thommes et al., 2011) and is a second commonly used dissolution medium for ASDs (Newman et al., 2012). The dissolution paddle apparatus (USP II, Sotax, Switzerland) was used. The samples containing high dose of GF, equivalent to ~90 mg, were added to 1000 mL of DI at 37 ºC, which referred to SI = ~0.1. The paddle speed of 50 rpm was used for testing all the printed tablets in Tables 4.2 and 4.3, except F240a in Table 4.3, which was tested at 250 rpm (Tagami et al., 2018; Wei et al., 2020). It was considered that the higher agitator speed could give rise to a faster disintegration of the printed tablets. Hence, that served another control option that allows testing the effect of faster rise of drug dissolution on supersauration behavior. Similarly, supersaturation behaviors of the tablets having enhanced tablet surface areas were tested. Although utilizing the sinkers to prevent tablet floating during the dissolution testing is debatable (Ilyés et al., 2019a), floating is also considered as bio-relevant. Thus, the square-pattern perforated tablet design was tested with (F240c) and without (F240d) basket sinkers while testing the multi-mini tablet design (F240b) without the sinkers was

found impractical owing to their smallness. Aliquots were withdrawn over 24h and filtered with a 0.45 µm nylon membrane-type syringe filter (Celltreat scientific products, Pepperell, MA, USA). The filtrates were diluted with the dissolution medium. The 3-4 replicates were performed for each sample. The average amount of drug dissolved was plotted as a function of time (minute). As previously reported by (Rahman et al., 2020a), the relative %supersaturation was calculated based on thermodynamic solubility of as-received GF and the GF concentration at ~9-12h, unless otherwise indicated.

To mechanistically explain the supersaturating performance of GF, Korsmeyer–Peppas model, depicted in Equation (2.2) of Chapter 2, was employed for the dissolution data of the printed tablets in Table 4.3. This model is commonly applied for describing the drug release behavior from dense polymeric matrices, such as FDM 3D printed tablets (Buyukgoz et al., 2020; Ilyés et al., 2019a; Li et al., 2017b; Zhang et al., 2017b). The model was fitted for about the first 60% of fractional GF dissolution data.

In Equation (2.2), n is the release exponent, indicative of the drug release mechanism. The exponent represents Fickian diffusion for n = 0.45, Case II transport with n = 0.89 and, anomalous transport with $0.45 < n < 0.89$ for cylindrical geometry while the lower and the upper limits of n are 0.5 and 1 for the slab geometry, respectively (Ritger et al., 1987). The assessment of the release kinetics was made for the cylindrical geometry except for square-pattern perforated tablet designs, F240c and F240d, which were assumed as the geometry of a thick slab

(film). This assumption in line with (Alhijjaj et al., 2019), where a similar design option was defined as a film with grids.

4.2.3.8 Stability. The stability test was examined for F240. The printed tablet was stored in a plastic bag at the humidity of 35% ± 5% RH at the ambient temperature (20–25 ºC) over 1 month. The samples were analyzed through dissolution tests according to described procedures in Subsection 4.2.3.7.

4.3 Results and discussions

4.3.1 Manufacturing of filaments via HME

To produce filaments with varying fractions of crystalline GF, the processing parameters were adjusted, Table 4.1. In order to obtain a filament containing largely crystalline GF, the processing temperature was kept lower than T_m of GF (Moseson et al., 2020) without hampering the HME processing to carry on. Hence, the minimum operable temperature was achieved at 165 ºC (H165, Table 4.1), which was far below the T_m of GF. Further lowering the temperature detrimentally increased the torque value, which is not recommended for instrument safety (Wei et al., 2020; Yang et al., 2016). Later, to produce filament containing amorphous GF, the processing temperature was gradually elevated. The maximum processing temperature was reached at 210 ºC (H210, Table 4.1). The product was liquid-like at the point of extrusion from the die owing to the reduced viscosity by temperature. A substantially high rotation speed for the screws was required to properly convey the material through the barrel. Thus, increasing the temperature further was found ill-advised for conducting the processing. The appearance of the resulting products

was opaque at the temperature in range 165–190 ºC (H165–H190), while a more clear appearance was realized at 210 ºC (H210), which is an indication for the formation of the amorphous structure (Moseson et al., 2020). The degree of GF crystallinity in the filaments will be discussed in the following sections.

4.3.2 Filament quality

The effect of HME processing temperatures on filament quality was assessed with the focus of filament printability. The assessment included mechanical resilience of the filaments, i.e., tensile strength (TS) and modulus of elasticity (ME), and the uniformity of filament diameters. The outcomes are presented in Figure 4.1. The TS and ME were the lowest for the placebo filament, H160, and increased in the presence of drug particles. The higher ME, which means increased stiffness, for the drug-loaded filaments, H165–H210, could be attributed to the polymer network being disrupted in presence of the drug (Verstraete et al., 2018). As the processing temperature increased, the filaments, H165–H210, exhibited similar ME while increasing TS. That may indicate ME was influenced more by the existence of GF particles rather than the processing temperature. The increasing TS could be attributed to the drug-polymer interactions, where stronger interactions were expected at the higher processing temperatures due to the melting of the drug, which potentially forms an intact matrix. This outcome is in line with Yang et al (2016), where a similar trend of increasing TS with increasing temperature was reported. Further, as the processing temperature increased, the standard deviations in diameters of the filaments were considerably increased, with H210 being the largest, Figure 4.1.

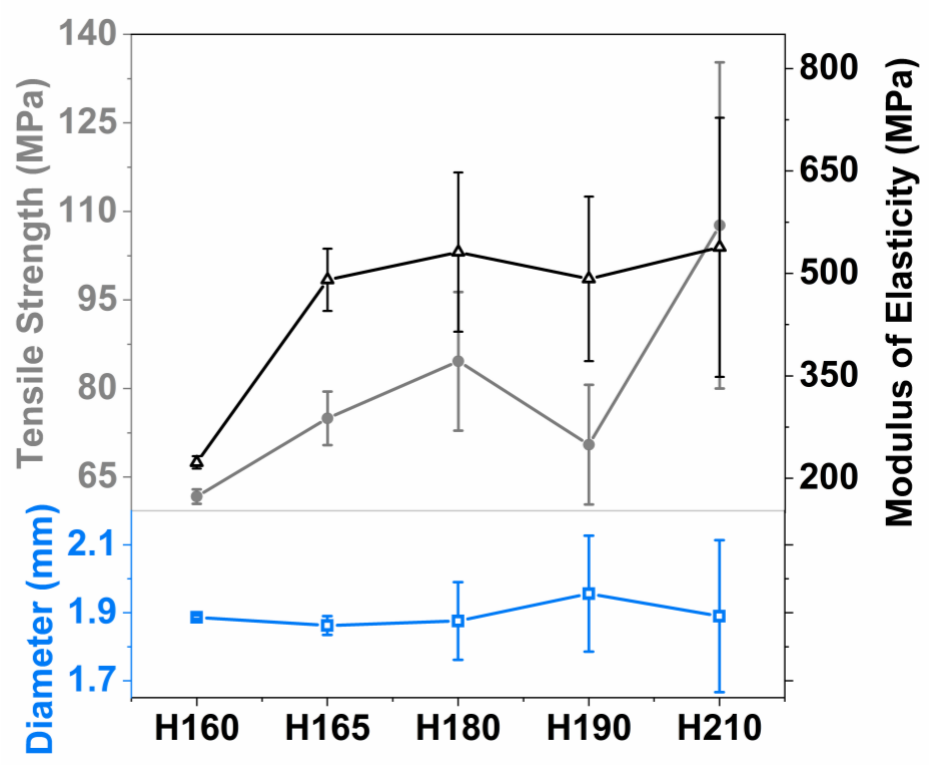

Figure 4.1 Mechanical properties and diameters of the filaments with varying HME processing temperatures, ranging 160–210 °C.

It is noted that there are no established standards for acceptable values of these properties to assure printability. However, simultaneously high breaking stress, high stiffness, long breaking distance, and a uniform diameter are the indicative properties for a printable filament (Korte et al., 2018; Zhang et al., 2017a). Although all the filaments possessed satisfactorily high mechanical properties, H210 was not printable. Its propensity to spread out at the point of the extrusion from the die made the filament diameter unreliable. It was either too thick for the transfer column through the heater or too thin for the conduction rolls inside the print head of the 3D printer. Such poor quality for the filaments associated with

high processing temperatures has been reported, which included dispensing imprecision, dosing inaccuracy, or poor mechanical resilience (Govender et al., 2020; Kempin et al., 2017; Yang et al., 2016). Therefore, H165 was found the most suitable filament for FDM 3D printing due to having satisfactory mechanical properties and a highly uniform diameter. Those results supported that producing ASDs loaded filament along with the satisfactory filament quality being necessary for printing is quite challenging. Although formulation development might avert such problems by screening the materials (Aho et al., 2017; Korte et al., 2018; Solanki et al., 2018a), processing at lower temperatures appears to control the filament properties with less exertion. This could be another advantage of retaining the drug in crystalline form.

4.3.3 Fourier-transform infrared spectroscopy (FT-IR)

To reveal molecular interactions, if any, between the drug and polymers, FT-IR spectra of as-received GF, PM, and printed tablets are presented in Figure 4.2. In FT-IR spectrum of as-received GF exhibited characteristic peaks in the region 1550–1800 cm^{-1} correspond to the C=O stretching vibrational frequencies, which are in line with (Bennett et al., 2015; Yadav et al., 2009). It is expected that the hydroxyl groups of HPC and KP can potentially form hydrogen bonds with the carbonyl groups of GF (Rahman et al., 2020c; Sarode et al., 2014). The IR spectra indicating hydrogen bonding often contain peaks that are shifted, broadened or had lower intensity, signaling the formation of amorphous structure and strong drug-polymer interactions (Rahman et al., 2020c; Rumondor et al., 2009b). As seen in Figure 4.2, the skeleton stretches of the PM and as-received

GF superimposed while the PM had inappreciably lower intensity, indicating no evidence of strong molecular interactions (Sathigari et al., 2012). In the spectrum of H165, the peak at 1606 cm^{-1} no longer existed, and the neighboring peaks broadened and shifted. In addition, the peak at 1658 cm^{-1}, C=O stretching, broadened and split into two sub-peaks of 1652 and 1662 cm^{-1}. The broadening refers to the distribution of free and bound carbonyl groups of GF (Al-Obaidi et al., 2009; Bennett et al., 2015). This may suggest a disruption in drug-drug interactions in favor of drug-polymer interactions, most likely due to the increased mobility in chains during melt extrusion (Kempin et al., 2017; Scoutaris et al., 2018). As the processing temperature increased through F210–F240, the peak intensities decreased. Particularly, the peak at 1652 cm^{-1} monotonically decreased, and eventually diminished in the spectrum of F240. That suggested hydrogen bonding occurred was proportional to the increasing processing temperatures through 210–240 ºC, with being strongest at 240 Cº. As hydrogen bonds refer to the amorphisation, these outcomes implies that the degree of amorphisation in the printed tablets was in the order of F240 > F230 > F210.

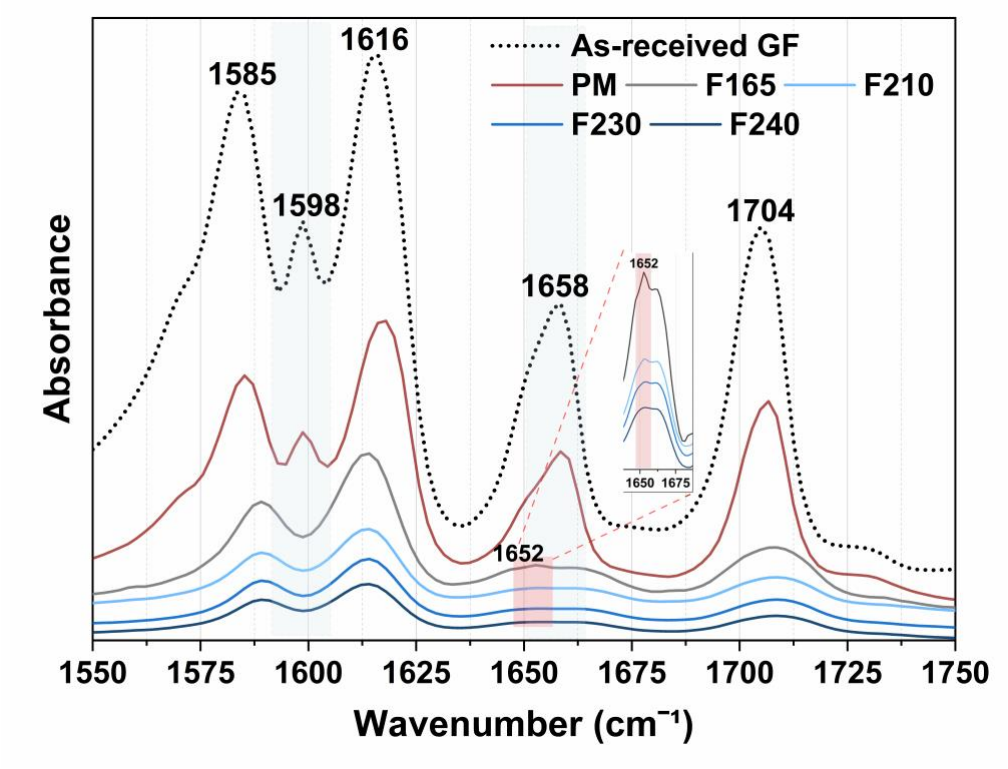

Figure 4.2 FT-IR spectra of as-received GF, physical mixture (PM) and 3D printed tablets through F165-F240.

4.3.4 Crystallinity

To reveal any solid-state changes to GF after heat processing in HME and FDM, as-received GF, HPC, and KP, the PM, filaments, and printed tablets were examined using XRD and DSC. The XRD diffractograms were presented in Figure 4.3. As-received GF showed characteristic peaks (Rahman et al., 2019), whereas polymers exhibited a halo pattern indicating their either amorphous nature or non-detectable amount of crystallinity, Figure 4.3a. The PM showed similar characteristic peaks yet with lower intensity. This is expected due to the surface coverage and dilution of GF particles with polymers (Li et al., 2017a; Rahman et al., 2020c). The diffractograms of H165 and PM resembled along with their

comparable peak intensities. The %crystallinity of GF in H165 was estimated to be 83.06%. That confirmed that GF particles were mostly distributed (Gogos et al., 2012) within the polymeric matrix and remained largely crystalline. The fact that the total %crystallinity of GF reduced approximately ~17% could be explained by the formation of amorphous GF stemming from temperature-induced drug-polymer miscibility (Gogos et al., 2012). That said, it is necessary to produce ASDs at higher processing temperatures. Indeed, increasing the processing temperature in HME further lowered the peak intensities of H180 and H190, indicating a further reduction in %crystallinity of GF. Eventually, H210 showed a halo pattern; the characteristic peaks of GF disappeared. Therefore, ASDs loaded filament was produced at 210 ºC. A similar observation was valid for FDM printed tablets, F210–F240, as all showed a halo pattern (see Figure 4.3b). These halo patterns confirmed that largely crystalline GF in the filament was successfully transferred to ASDs by melting via FDM 3D printing at the temperature range of 210–240 ºC.

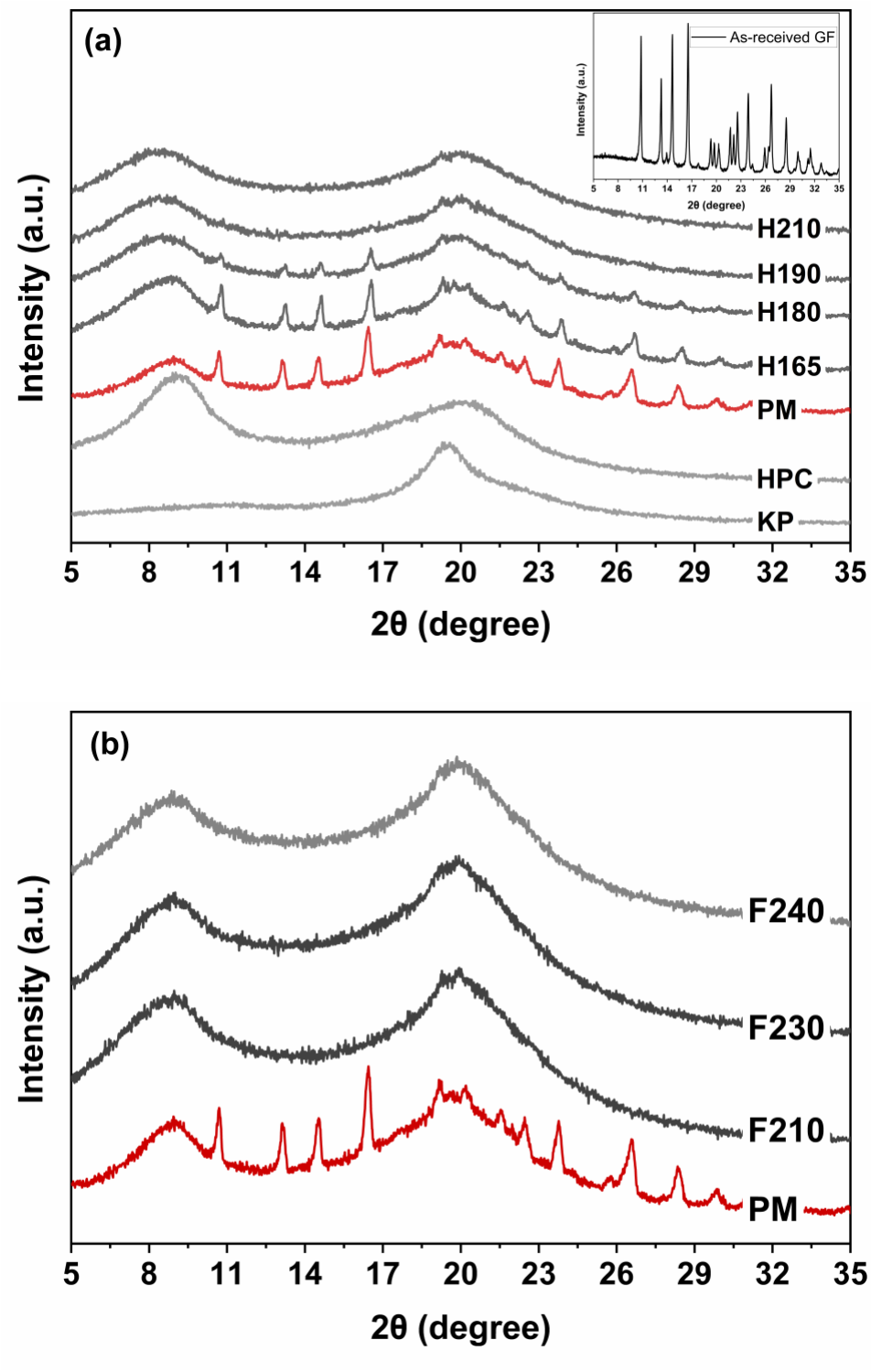

Figure 4.3 XRD pattern of (a) as-received GF, physical mixture (PM), filaments through H165-210, and (b) printed tablets, F210-F240.

4.3.5 Visual characterization

To assess the morphology of the particles after heat processing in HME and FDM, the SEM images of as-received GF and KP powders, the filament (H165), and printed tablets (P240 and F240) are presented in Figure 4.4. The as-received GF had an irregular shape while KP exhibited a spherical particle shape. This is expected as the surface morphology of what appears to be in H165. As depicted in Figure 4.4, embedded particles appeared in the matrix of H165.

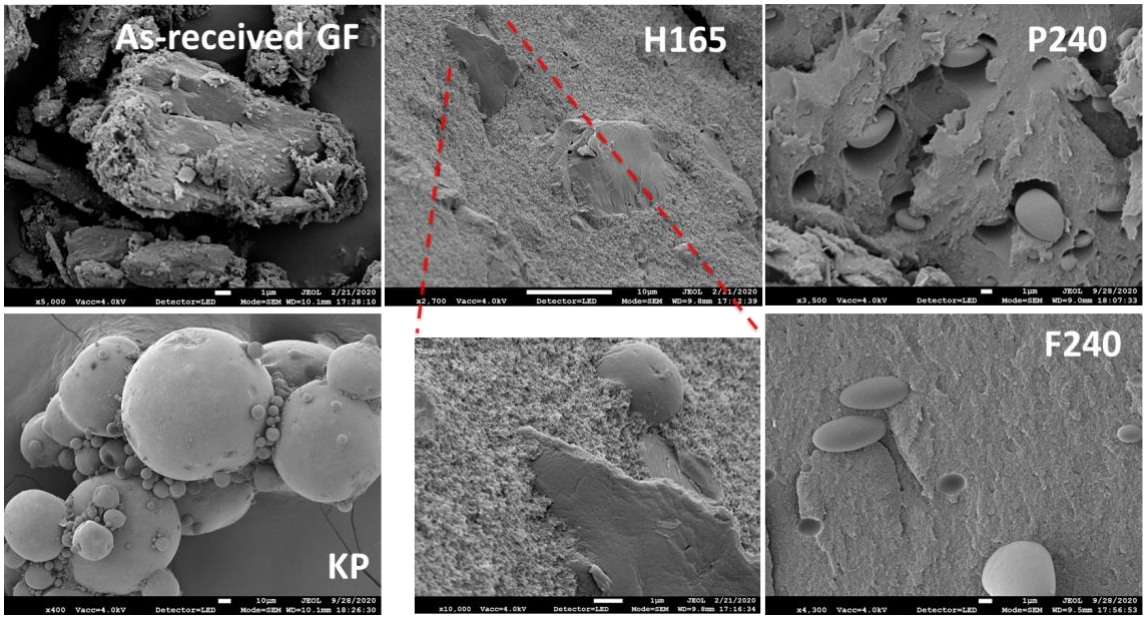

Figure 4.4 SEM images of as-received GF, KP powders, filament (H165), and 3D printed tablet (F240) along with 3D printed placebo tablet (P240).

The spherical particles were considered as KP owing to their similar surface morphology to dry KP particles. Since HPC was considered to be molten due to its lowest melting point amongst other compounds, the particles with irregular shapes were attributed to the GF particles. That suggested presence of un-melted GF and KP particles in H165. Besides, the particles with irregular shapes did not appear in

the cross-sections of printed tablets, P240 and F240, while spherical particles were observed in both, referring KP particles were remained un-melted to some extent while GF particles dispersed at the processing temperature of 240 ºC during 3D printing. The microscopy images, Figure 4.5, were supported by the outcomes for H165 and F240.

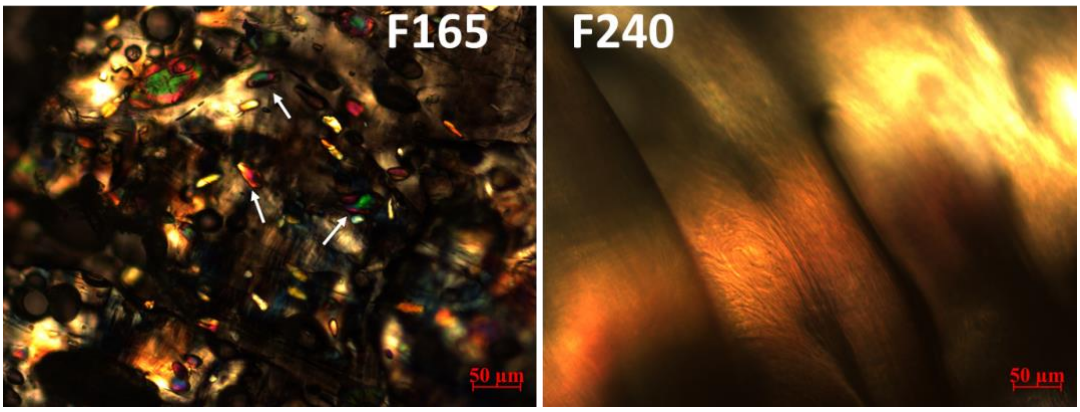

Figure 4.5 Microscopy images of 3D tablets printed at 165 °C and 240 °C.

4.3.6 Thermal stability

The results for the thermo-gravimetric analysis (TGA) were presented in Figure 4.6. The weight loss for all the tested samples was less than 2.8% at 100 ºC, which could be attributed to the free or bound water (Tidau et al., 2019; Wei et al., 2020). Similarly, Wei et al. (2020) reported that 2–5% weight loss referred to the loosely bound moisture at temperatures up to 100 ºC. At the FDM processing temperature, 240 ºC, the highest weight loss, approximately 3.8%, was realized for the PM. Since no additional weight loss was observed for the printed tablets, F240, the weight loss could be attributed to the loss of loosely bound moisture during thermal processing rather than thermal degradation, which is in line with (Goyanes et al.,

2019; Wei et al., 2020). Since FDM 3D printing processing was conducted at 240 ºC or lower temperatures, and no significant weight loss was realized up to 240 ºC, all the printed tablets were found thermally stable in the present study.

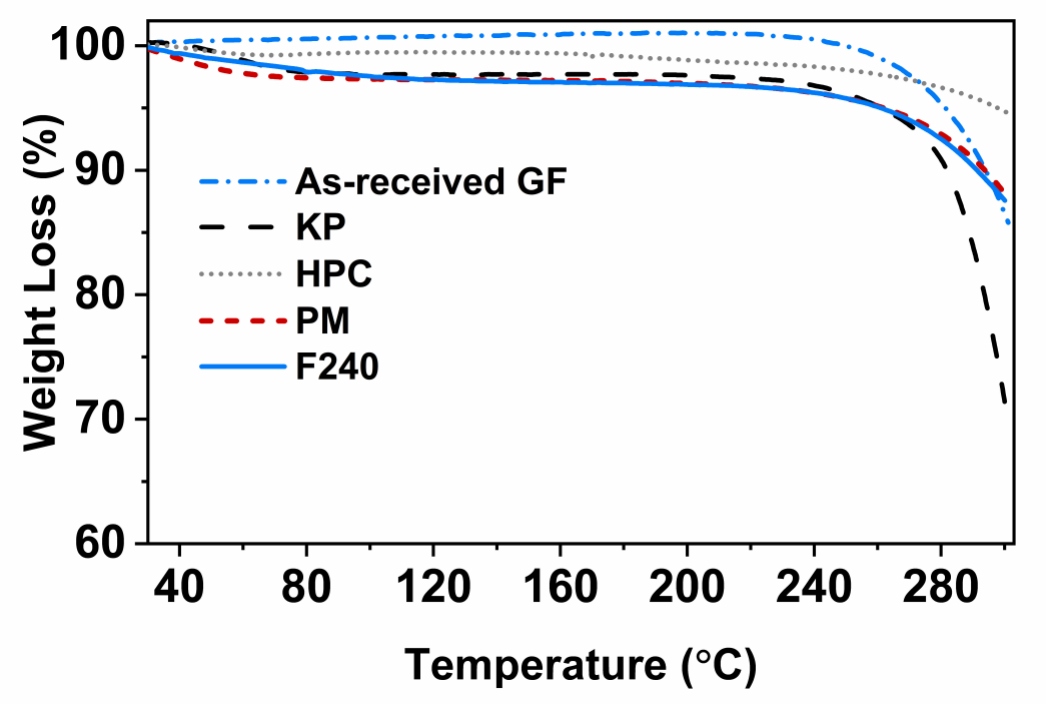

Figure 4.6 TGA thermograms of as-received GF, KP, and HPC powders along with 3D printed tablet (F240).

4.3.7 Content uniformity of printed tablets

The variation (RSDs) in the tablet mass, thickness, diameter, and drug concentration for the printed tablets are presented in Table 4.4. The RSD values in drug concentrations for all the tablets (F210–F240) were less than 1%, which referred to pharmaceutically acceptable content uniformity. Further, the tablet mass and dimensions had small RSD values, indicating printing processing was successfully conducted at the printing temperatures through 210–240 ºC.

Table 4.4 Post-printing Dimensions and Drug Content Uniformity of the FDM 3D Printed Tablets

Run #	Diameter (mm)	RSD	Height (mm)	RSD	Tablet Weight (mg)	RSD	DC (%)	RSD
F165	5.57	1.11	1.29	3.31	26.46	1.33	15.79	0.33
F210	5.68	1.07	1.21	2.66	30.33	3.43	15.98	0.32
F230	5.47	0.95	1.60	1.44	34.73	1.09	15.66	0.64
F240	5.47	2.25	1.56	5.42	33.86	5.36	15.81	0.32

DC: Drug Concentration

4.3.8 Drug supersaturation and dissolution kinetics

The drug dissolution profiles of the printed tablets were tested under supersaturated conditions, SI= 0.1, and are presented in Figure 4.7a. The mere presence of HPC-KP polymers in the physical mixture (PM) were enhanced the extent of GF release compared to the thermodynamic solubility of GF (14.2 mg/L) (Rahman et al., 2020a). This is likely due to the dissolution of the water-soluble polymers in the dissolution medium, which is in line with the previous reports (Loftsson et al., 1996; Rahman et al., 2020a). The H165 and PM showed comparable dissolution rates and extent of GF release, with H165 being slightly higher. This could be explained partly by the presence of a small fraction of amorphous GF in H165 (see Subsections 4.3.3 and 4.3.4 for the amorphous GF content), which has higher kinetic solubility than its crystalline counterpart, and partly by deagglomeration of as-received GF particles into polymer matrix through HME. The content uniformity test results, Table 4.4, supported this observation. Besides, noticeable dissolution trends were realized for 3D printed tablets, Figure 4.7a: (i) Slower GF release was obtained for all the cases, F210–F240, compared

to GF release from PM and H165. This is typical for most FDM 3D printed tablets, which are inherently dense and require longer time for drug dissolution (Goyanes et al., 2015a; Ilyés et al., 2019a; Zhang et al., 2017a). (ii) Unlike PM, no de-supersaturation of GF was realized for the printed tablets, which also includes H165. On one hand, the dense structure of the 3D tablets allowed a gradual GF release and sufficiently available water-soluble polymers in the dissolution medium. The presence of the polymers acted as a crystallization inhibitor, which afforded a sustained drug supersaturation. On the other hand, that caused slowing down the GF release by preventing the fast GF release from dense polymer structure. (iii) As the FDM processing temperature increased the extent of GF supersaturation increased through F210–F240, where all the printed tablets generated a higher extent of GF supersaturation compared to H165 and PM (see Table C.1, Appendix C for the values of GF supersaturations). Within ~12h, F230 and F240 generated 96 and 153% GF supersaturation, respectively, while F210 had a lower extent (62%). Through F210–F240, the increasing degree of drug-polymer interactions (refer to Subsection 4.3.3), which implies an increasing amount of amorphization (amorphous fraction of GF), could be mainly responsible for monotonically increasing GF supersaturation by increasing temperature. Further, it was postulated that the amorphization of GF in F210 is lower compared to that of F230 and F240 (refer to Subsection 4.3.4). The trend of higher GF supersaturations at higher processing temperatures through F210–F240 supported the postulate. In this study, the resulting 153% enhancement by F240 could be attributed to fusion-assisted ASDs, which created a high fraction of

amorphous GF, and incorporation of 10 wt% KP into the formulation, which forged strong bonds via drug-polymer interactions, afforded high miscibility with GF-HPC and reduced surface tension between drug and polymers. To further add to these, F240 being stored over one month at the ambient conditions showed similar drug release performance to the freshly prepared F240 (see Figure 4.7a). That corroborated that F240 maintained the ASDs formed due to both the presence of strong drug-polymer interactions via heat treatment and dense tablet structure.

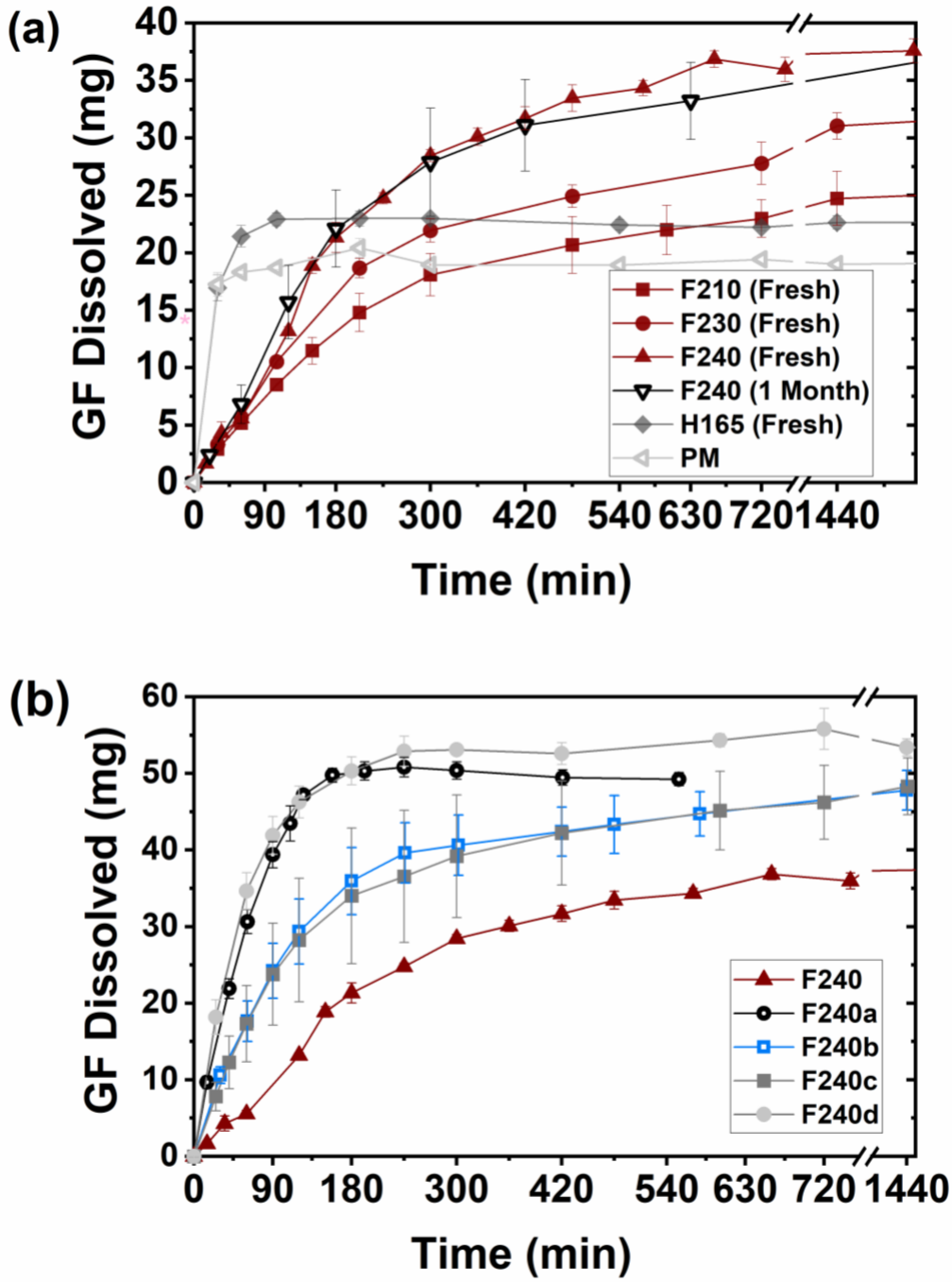

Figure 4.7 Dissolution profiles of (a) physical mixture (PM), filament (H165), and 3D printed tablets with varying FDM processing temperatures (F210–F240), and (b) 3D printed tablets with varying tablet surface area (F240b–d) as well as the control options (F240 and F240a).

To understand the effect of the dissolution rate on GF supersaturation performance, various tablet design options were tested. Prior to the assessment of tablet design, the agitator speed of 250 rpm, affording a rapid disintegration from 3D printed tablets, (F240a, Table 4.3), was assessed as the control option. As seen in Figure 4.7b, F240a enhanced the GF supersaturation by approximately ~250%. However, a small extent of GF de-supersaturation has started within 4h. Although modifying the agitation rate is found impractical based on *in vitro* assessment and undesired due to the recrystallization concern (Sun et al., 2016), it elucidated the effect of faster rise of dissolution and set the attainable extent of GF supersaturation. Thus, promoting the faster rise of dissolution without modifying the agitation rate, the tablets with higher surface areas were designed, Table 4.3. The rationale is that water imbibition into ASDs could be advanced with a higher available surface area that reduces to time for water absorption and eventually accelerates the drug release from the matrix. F240b and F240c generated GF supersaturation up to ~225%, which was comparable with F240a. However, the presence of sinkers was slowed down the circulation of water for imbibition into those tablets. Thus, F240b and F240c exhibited slowly increasing GF supersaturation and similar dissolution profiles despite their different tablet surface areas. By conducting the dissolution test without sinkers (F240d), a further increase in GF supersaturation was achieved. The resulting GF supersaturation (293%) was found higher than that of F240a. Further, F240d sustained the supersaturation over 12h, unlike F240a. That much of GF supersaturation was found comparable with the literature, where the GF supersaturation (300%) was

achieved by implementing simultaneous nano milling and spray drying methodologies in presence of a surfactant (Rahman et al., 2020a). Further, in this study, GF supersaturations were achieved from the final product, not requiring additional manufacturing steps for administration.

Overall, these findings emphasized that higher available surface area from printed tablets could afford a gradual drug release that leads to enhance and sustain the GF supersaturation, which is in line with (Sun et al., 2015). It is helpful to mention that the common consensus on the attainable drug supersaturation is that a slower dissolution rate avoids a sudden surge of supersaturation resulting in slower recrystallization but lower maximum supersaturation, while a faster rise of dissolution of an amorphous drug will inevitably lead to a higher maximum supersaturation but a sharper drop in the de-supersaturation phase (Augustijns et al., 2012; Sun et al., 2015). This was supported by the dissolution results from F240.–d. In light of these, it is considered that mechanistically configuring the extent of slow or rapid drug dissolution behavior helps identify pharmaceutically favored drug supersaturation, which is a high extent of supersaturation being sustainable, from FDM 3D printed tablets. Accordingly, tablets could be designed to tune by the desired control of release mechanism.

In Figure 4.8, the fitting results revealed three different release mechanisms: (i) F240 showed zero-order, (ii) F240a–c showed anomalous release transport, and (iii) F240d showed Fickian diffusion. Considering the fitting results in conjunction with GF supersaturations, Fickian transport appeared to meet the criteria of pharmaceutically favored ASDs; sustainable high extent of

supersaturation. The anomalous transport accounts for both drug diffusion and polymer relaxation/erosion (Sujja-Areevath et al., 1998), while zero-order release translates the constant drug release over time. These two models refer that dissolved polymers, which act as a crystallization inhibitor or surfactant, would be available in the dissolution medium as the polymer erodes or dissolves over time, respectively. Since the resulting transports from F240b and c; lower extent of GF supersaturation, and from F240a; minor de-supersaturation, could be associated with the lack of sufficient dissolved polymer in the dissolution medium when GF releases. In contrast, since the Fickian transport is a diffusion-controlled mechanism, a sufficient amount of dissolved polymers most likely existed in the dissolution medium and enabled higher and sustained GF supersaturation. In addition, the tablets with higher surface area and the polymers being water-soluble appeared to contribute further. These outcomes are in line with Sun et al. (2015), where the dissolution-controlled release mechanism was linked with the rapid surge of supersaturation following by de-supersaturation while diffusion-controlled release mechanism represented the gradually increasing yet sustained supersaturation. It should be highlighted that resulting dissolution behaviors are highly dependent on the apparatus type and speed, dissolution pH, and medium (Augustijns et al., 2012; Sun et al., 2016) as well as the extent of printed tablet density, investigation of which could be considered for future studies.

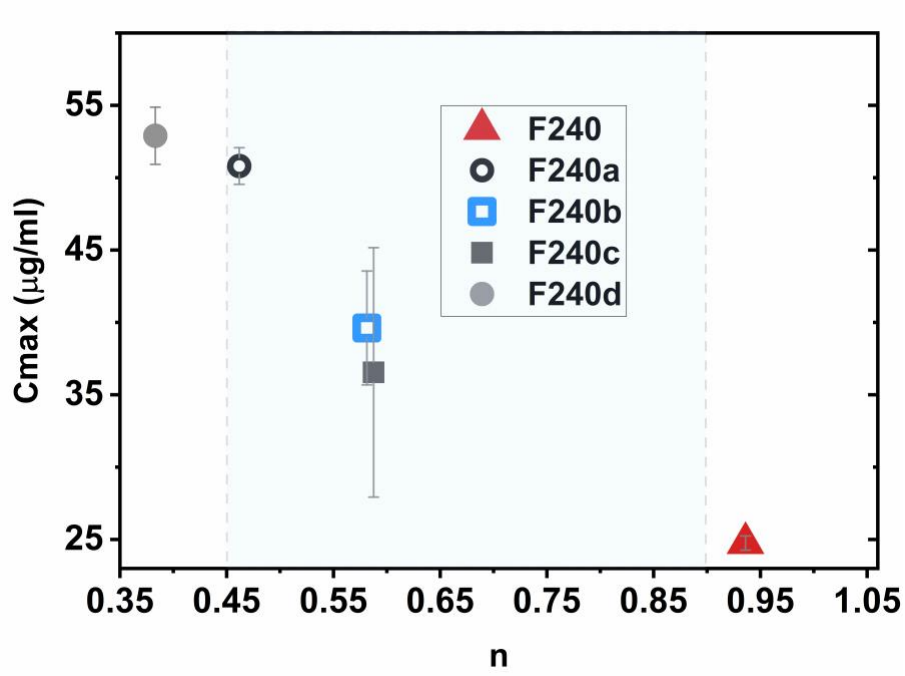

Figure 4.8 The maximum GF supersaturating concentration for the drug release from FDM 3D tablets within 12h, as a function of the release exponent, *n*, of Equation (2.2).

4.4 Conclusions

Processing the HME at lower temperatures reduced the disadvantages of high processing temperatures on filament quality and allowed producing the filaments containing largely crystalline GF. The crystalline amount (~83%) within the filament, H165, was found significant in the sense of reducing the confounding effects arising from particle recrystallization. The proof of the concept was demonstrated, where fusion-assisted ASDs were successfully achieved via FDM 3D printing. The higher amorphization of GF was attained by increasing the printing temperature above Tm of GF. It is worth highlighting that 153% enhancement of GF supersaturation was generated under non-sink dissolution conditions via a single-step printing process, which does not require additional manufacturing

steps for the administration. Further, the product design with a higher surface area i.e., multi mini-tablets, significantly enhanced the attainable GF supersaturation (~293). The GF supersaturation achieved by FDM 3D printing was found comparable with the literature implementing simultaneous nano milling and spray drying methodologies in presence of a surfactant [65]. In addition to these, fitting results in conjunction with GF supersaturations indicated that Fickian transport appeared to meet the criteria of pharmaceutically favored ASDs.

CHAPTER 5

IMPLEMENTATION OF PROCESS ANALYTICAL TECHNOLOGY IN FEED MATERIALS OF FUSED DEPOSITION MODELING THREE-DIMENSIONAL PRINTING

5.1 Introduction

Fused Deposition Modeling (FDM) 3D printing is an upcoming and promising drug delivery platform since the intended dose and release pattern of the final product per differing needs of patients (Breitkreutz et al., 2007) are achievable (Buyukgoz et al., 2020; Gioumouxouzis et al., 2017; Kadry et al., 2018; Pietrzak et al., 2015; Skowyra et al., 2015; Zhang et al., 2017b), which is challenging by conventional techniques. It allows printing the prescribed dosage at the point of care i.e., in a pharmacy or ambulatory setting (Prasad et al., 2016). This means that the dose would be available immediately after it prints. However, the direct administration of the printed dose could disqualify the assessment of drug content and uniformity of the final product. Thus, it would be logical to determine the drug amount before the printing step rather than from the end product. Since the last products prior to FDM 3D printing are filaments (starting materials) (Melocchi et al., 2016), it is hypothesized that if the drug concentration in the filament is given at the point of printing step, it is expected to obtain a final product containing similar drug concentration to that of the filament. Moreover, determining the drug concentration in filaments just before the printing step would also help determine the changes in drug properties that occured during storage. Thus, determining the drug concentration from filaments will be the focus of this study. The fact that 3D printed devices generally show high product and content uniformity (Okwuosa et al., 2016;

Pietrzak et al., 2015; Scoutaris et al., 2018) might further support the hypothesis by reducing the difference in drug content between the printed samples and filaments. Indeed, the expected high uniformity would not be surprising since it would be the consequence of the contently uniform filaments produced through an intense mixing via hot-melt extrusion (HME) (Maniruzzaman et al., 2012; Pawar et al., 2017; Sadia et al., 2018b). However, it should be noted that enhanced powder flow properties, particularly for the formulations at high drug concentrations, are highly important to achieve contently uniform products (Kunnath et al., 2018). This becomes crucial during the continuous powder feeding in HME processing. Because cohesive drug particles tend to resist flowing during processing (Castellanos, 2005), which may give rise to deviation in the label claim. Previous studies have explored the use of surface modification via dry coating as a way to reduce particle cohesion, and improve powder properties (Capece et al., 2014; Chen et al., 2008; Han et al., 2011; Huang et al., 2017; Jallo et al., 2012). Since it is a simple yet effective way to improve powder flowing, dry-coating methodology will be used in this study (see Subsection 2.2.2.1 for the procedure details of dry coating).

Although the conventional testing procedures are well established, they are costly and required significant testing time (Knop et al., 2013). Alternatively, Process Analytical Technology (PAT) is described as “to be a system for designing, analyzing, and controlling manufacturing through timely measurements (i.e., during processing) of critical quality and performance attributes of raw and in-process materials and processes, with the goal of ensuring final product quality”

by FDA (FDA, 2009). In light of this guidance, PAT helps predefine the product quality in a non-destructive manner and reduce the testing time (FDA, 2009). Rapid spectroscopic techniques followed by chemometric methods are mostly preferred for implementing PAT in pharmaceutical applications (Sánchez-Paternina et al., 2019; Tumuluri et al., 2008; Zhang et al., 2014). Recent literature has demonstrated that Raman spectroscopy can be a promising tool for qualitative and quantitative determination of active substance from the product (Mazurek et al., 2006; Saerens et al., 2011; Tumuluri et al., 2008; Zhang et al., 2014). Tumuluri et al. demonstrated the feasibility of Raman spectroscopy for use in PAT applications, where the melt-extruded film product containing varying drug concentrations was accurately quantified (Tumuluri et al., 2008). Similarly, drug concentration from polymeric films was monitored with high accuracy of the prediction models using Raman spectroscopy (Zhang et al., 2014). Although such studies showed that Raman spectroscopy is a robust tool for PAT applications, to the best of the author's knowledge, such implementations for filaments compatible with FDM 3D printing have yet to be investigated.

The main objective of this study is to implement PAT for determining drug concentration from filaments before FDM 3D printing. Surface modification of the drug particles via dry coating is performed to assess the flowability of the drug-polymer blends to be extruded. The filaments containing varying drug concentrations in range 5–50 wt% are manufactured via HME. Raman spectroscopy is used as a PAT tool. It is useful to mention that Raman spectroscopy is sensitive to solid-state changes, where crystalline or amorphous

forms of a drug could exhibit spectral differences (Sievens-Figueroa et al., 2012; Żarów et al., 2011). The drug material and processing protocols are selected to avoid confounding effect stemming from changes in the solid-state of the drug during the preparation of the feed-material in HME, which typically produces amorphous solid dispersions (ASDs) (Hancock et al., 1997; Li et al., 2018; Thommes et al., 2011; Wei et al., 2020). Later, chemometric methods i.e., principal component analysis (PCA) and partial least square (PLS) regression are applied for analyzing the data achieved via Raman spectroscopy and eventually creating the prediction models. The models are assessed regarding accuracy, linearity, precision, and optimum latent variable (PLS Factor) with the ultimate goal of achieving a reliable prediction model. The model developed is validated with a different training set of drug concentrations. Finally, the prediction results from the filaments are compared with the reference drug concentration of the filaments and the actual drug concentration of FDM 3D printed tablets.

5.2 Materials and methods

5.2.1 Materials

Griseofulvin (GF; Letco Medical, Decatur, AL, USA) was used as a model Biopharmaceutics Classification System (BCS) class II drug. Pharmaceutical grade silica (M5P, Cabot Corporation, MA, USA) was used for the surface modification of micronized GF particles. Hydroxypropyl cellulose (HPC, SL grade, Nisso America Inc., New York, NY) is used as a printing polymer, due to its ability to produce filaments with appropriate mechanical properties for fused deposition

modeling (FDM) 3D printing (Öblom et al., 2019; Pietrzak et al., 2015; Zhang et al., 2017a). In addition, HPC is poorly miscible with GF and unlikely to form amorphous structure (Li et al., 2017a). Sodium dodecyl sulfate (SDS) (Sigma-Aldrich, Saint Louis, MO, USA) was used as a solvent.

5.2.2 Preparation methods

5.2.2.1 Preparation of engineered GF particles and feed material. Micronization and surface modification of the GF particles were performed by adapting the procedure from earlier studies (Buyukgoz et al., 2020; Davé et al., 2011; Han et al., 2011) (see Subsection 2.2.2.1 of Chapter 2 for the procedure details). The formulations to be extruded and the processing temperatures are shown in Table 5.1. The drug with (micronized coated, MC) and without (micronized uncoated, MUC) surface modification, and the polymer at given concentrations (see Table 5.1) were mixed using LabRAM at a frequency of 61 Hz with an acceleration of 75 G for 5 min. The blends with MUC-GF particles were only used to compare the powder properties with MC-GF particles. Later, the powder blends containing MC-GF particles were fed into the extruder via a volumetric feeder (Model 102 M, Schenck Accurate, WI, USA) at a feed rate of 0.6–0.7 g/min. Only the blends containing MC-GF particles were processed with hot-melt extrusion (HME) with an 11 mm diameter co-rotating twin-screw extruder (Thermo Fisher Scientific Inc., MA, USA) to produce filaments. The HME manufacturing process is demonstrated in Figure 5.1. The HME processing parameters were adapted from Buyukgoz et al. (Buyukgoz et al., 2020) to maintain GF particles in crystalline form. A drug having a higher softening value than that of

a polymer requires higher energy input to soften the material at higher drug concentrations. Thus, higher extrusion temperatures for the formulation at 30 and 50 wt% drug concentration were applied (see Table 5.1).

Table 5.1 Compositions of the Filaments along with HME Processing Temperatures

Run	Drug Sample	Drug Concentration (wt%)	Polymer Concentration (wt%)	HME Extrusion Temperature (°C)
1		5.0	95	140
2		10.0	90	140
3		15.0	85	140
4	*GF	20.0	80	140
5		25.0	75	140
6		30.0	70	145
7		50.0	30	160

*Powder blends were prepared using micronized GF with (MC-GF) and without (MUC-GF) surface modifications. Only MC-GF particles were processed with HME.

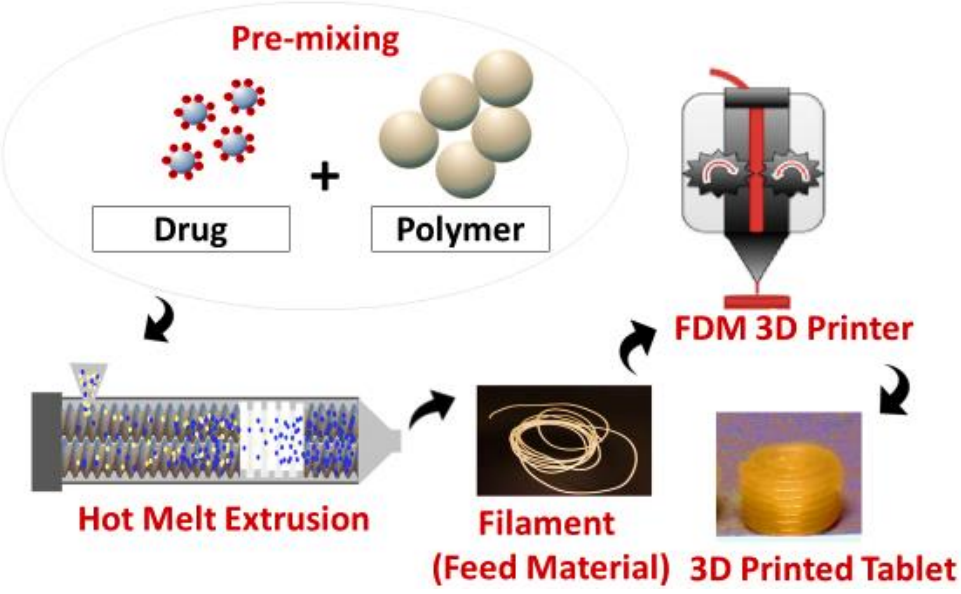

Figure 5.1 Manufacturing process of FDM 3D printed tablet including filament production through hot-melt extrusion.

5.2.2.2 Manufacturing of tablets via FDM 3D printing. To test the performance of the prediction models, which will be explained in the following sections, the tablets are manufactured using the GF-loaded filaments via FDM 3D printing (Flashforge®, Creator Pro 3D, 2016, China). The tablet dimensions were set as ø: 5.0 and H: 2.0 mm. The tablets were designed using Autodesk® Fusion 360 Ultimate (Autodesk 3D design software). The design was recorded as an STL file and was converted to an X3G file using FlashPrint software (Version 3.18.0; Jinhua, China) as the slicer. The tablets were printed with the following operating parameters; the printing temperature 170 ºC; printing speed, 35 mm/s; nozzle traveling speed, 80 mm/s; infill percentage, 100%.

5.2.3 Characterization methods

5.2.3.1 Blend characterization. The flow function coefficient (FFC) of the blends in Table 5.1 was measured using the Freeman Technology FT4 (Freeman Technology Ltd, UK). The previously established procedure was adapted from (Kunnath et al., 2018). The test applies 3 kPa consolidation normal stress and performs shear tests at 2.0–1.0 kPa normal stresses, where incipient failure shear stresses were recorded. FFC is a ratio of major principal stress (MPS) to unconfined yield strength (UYS) (Kunnath et al., 2018; Schulze, 2008), which were calculated with FT4 Data Analysis v4 software. The details of the physical interpretation of numerical FFC values are found in the literature (Kunnath et al., 2018; Schulze, 2008). The blends having the FFC value in range of 4–10 are indicative of easy-flowing powders.

5.2.3.2 X-ray diffraction (XRD). The solid state of the drug particles was tested via X-ray diffraction. Dry MC-GF particles, the physical mixture, the extruded filament at 15 wt% GF concentration were examined. The diffraction pattern was achieved using PANanalytical (West- borough, MA, USA) scanning for 2θ angle in the range 5–35° with 0.01º step.

5.2.3.3 Determination of drug content (assay) and uniformity. The drug content and uniformity of the filament and 3D printed samples were tested. The filaments containing varying GF concentrations were cut into 1 cm segments. The samples from segmented filaments and printed tablets were dissolved in 7.2 mg/ml SDS solution under continuous stirring for a minimum of 5h. A Thermo Scientific Evolution 300 UV–vis spectrophotometer (Thermo Fisher Scientific Inc., MA) was used to measure the UV absorbance at a wavelength of 297 nm of each dissolved sample. The average and standard deviation of drug concentrations were calculated for each sample. The reported drug concentrations for the filaments were used as the reference concentration for developing calibration models.

5.2.3.4 Spectral data acquisition by Raman spectroscopy. Raman spectra of the filaments were collected using a FergieTM Imaging Spectrograph System from Teledyne Princeton Instruments equipped with a fiber-coupled probe (105 µm FC/PC excitation fiber and 400 µm FC/PC collection fiber). The spectrometer has a 785 nm laser and maximum of 500 mW power. In this study, 60% of the power was utilized to prevent saturation of Raman signals. The spectral range used was 200–1800 cm^{-1}. The software powered by Lightfield was used for data acquisition. The acquisition time was set as 20 seconds.

5.2.3.5 Development of qualitative and quantitative models. To determine drug concentration from the filaments, qualitative and quantitative calibration models were developed with the aid of Unscrambler® X version 10.5.1 software from CAMO. This software includes commonly used chemometric methods, principal component analysis (PCA) and partial least squares (PLS) regression algorithms. PCA algorithm helps reduce the data dimensions and identify data patterns (Tatavarti et al., 2005; Tewari et al., 2010). PLS algorithm uses X and Y matrices to determine the relationship between the variables by generating orthogonal-based vectors (Cogdill et al., 2005; Kandpal et al., 2016; Workman, 1997). Accordingly, PCA algorithm was applied to qualitatively interpret the relationship among the variables such as drug concentration. PLS algorithm was applied to build prediction models for in-line quantification of the drug concentrations from filaments. Seven spectra collected from the filaments at 5, 10, 15, 25, 30, and 50 wt% drug concentration were used for developing PCA and PLS models. The filament at 20 wt% concentration was excluded from the calibration data and used as an independent drug concentration for validating the model. This independent sample was considered to help better evaluate the robustness of the developed models. The spectra in the prediction set were independent of those used in the calibration model yet were the same drug concentration levels, where five spectra were used for each drug concentration.

Three transformations, standard normal variate (SNV), de-trend, and baseline, were applied to the spectral data prior to PCA and PLS algorithms. Those pre-treatments help achieve scaling effect on the spectra, standardize the variation

in curvilinearity, and remove offset features of the baseline (Afseth et al., 2006; Barnes et al., 1989; Sánchez-Paternina et al., 2019). In addition, reducing the effect of scattering could prevent it to be modeled as one of the factor(s) in the model (Meza et al., 2006). The calibration models were first evaluated using leave-one-out cross-validation, also known as full cross-validation (Esbensen et al., 2010; Jouan-Rimbaud et al., 1995), which is a very common initial evaluation for quantification of the model (Popo et al., 2002). The linearity of the developed model was indicated by R^2 value. The first minimal value of prediction residual error sum of squares (PRESS), indicative of the optimum latent variable, was calculated (Jouan-Rimbaud et al., 1995; Popo et al., 2002). The accuracy of the model was assessed by root mean square error of prediction (RMSEP), root mean square error of calibration (RMSEC), and bias (average residual error) (Meza et al., 2006). RMSEP indicates the difference between the predicted and reference values and, is expected to be similar with RMSEC for accuracy of the prediction (Barimani et al., 2017; Blanco et al., 2001; Meza et al., 2006). The precision of the model was assessed with the standard deviation of the predicted data (Vargas et al., 2018). In addition to the statistical evaluation, the prediction capability of the quantitative models was evaluated with the limit of quantification (LOQ) of the model, referring to the quantitatively determinable lowest drug concentration on the calibration model.

5.3 Results and discussion

5.3.1 Flowability of the powder blends

To maintain the amount of material running in the HME barrel same, there should be adequate powder flowing from the powder feeder into the HME hopper. A consistent and adequate flow promotes product uniformity in size, shape, and weight. Figure 5.2 demonstrates the flow function coefficients (FFC) of the blends made with MC-GF and MUC-GF. The higher drug concentrations are prone to exhibit higher cohesiveness. Thus, for the sake of brevity, FFC values for the blends with drug concentration above 20 wt% were tested. FFC value above 10 has no physical differences (Kunnath et al., 2018). The blend with 25 wt% MC-GF showed an FFC value of 9.7 while its uncoated counterpart showed an FFC value of 7.5. Indeed, surface-modified particles enhanced the FFC values of the blends at each drug concentrations (see Figure 5.2), except the blend at the highest drug concentration, 50 wt%, which had an unacceptable FFC value (3.2) for easy-flowing. It was expected since the drug concentration was reasonably high. Inconsistency in powder flow may negate product uniformity. The flow improvement with the dry coating is in line with previous reports (Capece et al., 2017; Han et al., 2013; Huang et al., 2015), which might refer to the reduction in cohesive forces after surface modification (Chen et al., 2008).

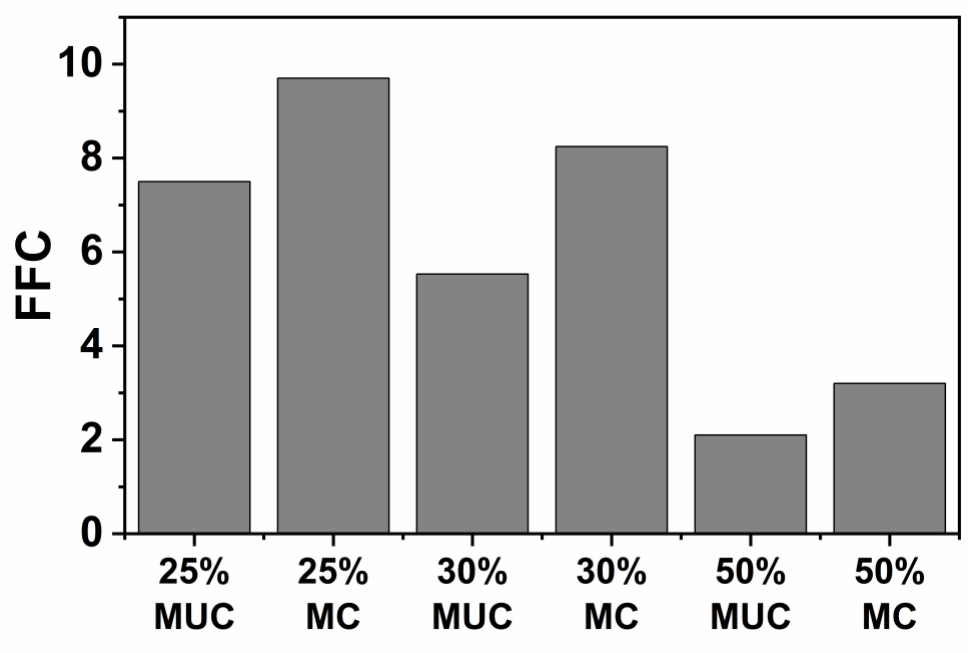

Figure 5.2 Flow Function Coefficient (FFC) values for blends made with MC-GF and MUC-GF.

5.3.2 Solid-state of the drug

The XRD pattern of as-received GF and HPC, physical mixture, and filament both at 25 wt% drug concentration are demonstrated in Figure 5.3. The characteristic peaks of as-received GF (Li et al., 2017a) were observed at the main diffraction angles (2θ) 10.0º–35.0º, indicating the crystalline form of particles. The polymer HPC showed an amorphous halo diffraction pattern while the physical mixture and the drug-loaded filament followed the characteristic peaks of GF. That outcome suggested that the crystallinity of GF was maintained during HME processing.

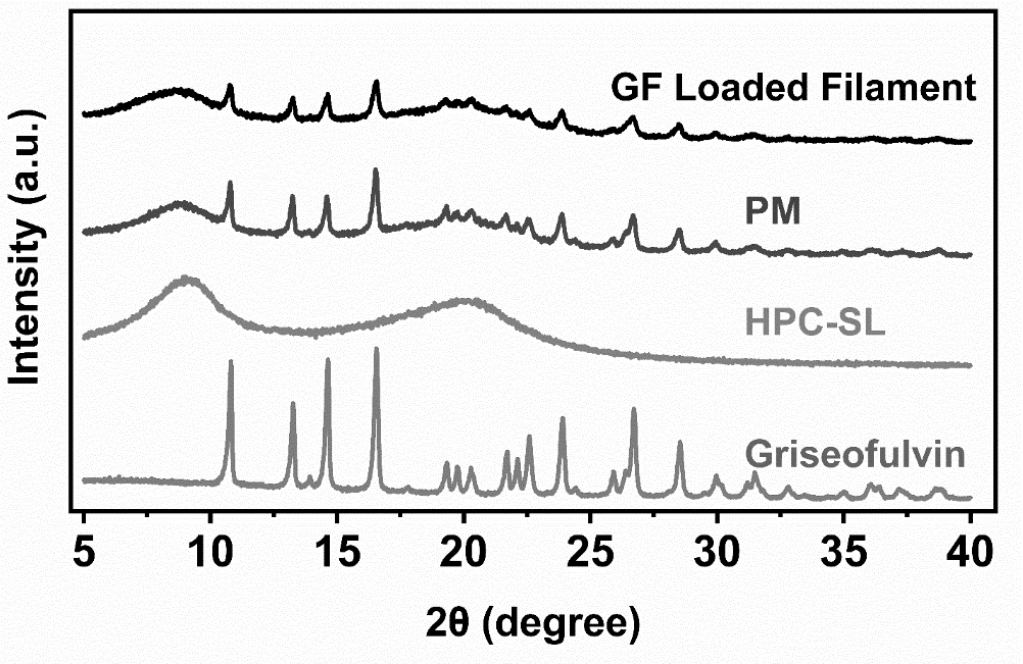

Figure 5.3 XRD pattern of as-received GF particles, as-received HPC-SL, physical mixture, and filament both at 25 wt% GF concentration.

5.3.3 Interpretation of Raman spectra

Raman spectra of as-received GF and HPC powders, placebo filament, and drug-loaded filament are presented in Figure 5.4, and the filaments at varying concentrations in range 5–50 wt% are presented in Figure 5.5. The strong Raman signals for as-received GF particles were observed in 1550–1750 cm^{-1} region. The band at 1712 cm^{-1} refers to C=O stretch in benzofuran, at 1665 cm^{-1} refers to C=C stretch in cyclohexanone, and at 1622 cm^{-1} refers to C=O mix with C=C stretch (Żarów et al., 2011). The GF-loaded filament followed a similar pattern while as-received HPC and placebo filament lacked those bands. The achieved Raman bands for the GF particles are agree with Raman spectra for crystalline GF in the studies of (Rahman et al., 2020a; Żarów et al., 2011). In Figure 5.5, increasing the

drug concentration increased the intensity of these Raman signals, which is desired to develop the prediction models based on varying drug concentrations. Therefore, the Raman spectra in 1550–1750 cm^{-1} region were analyzed in PCA and PLS algorithms.

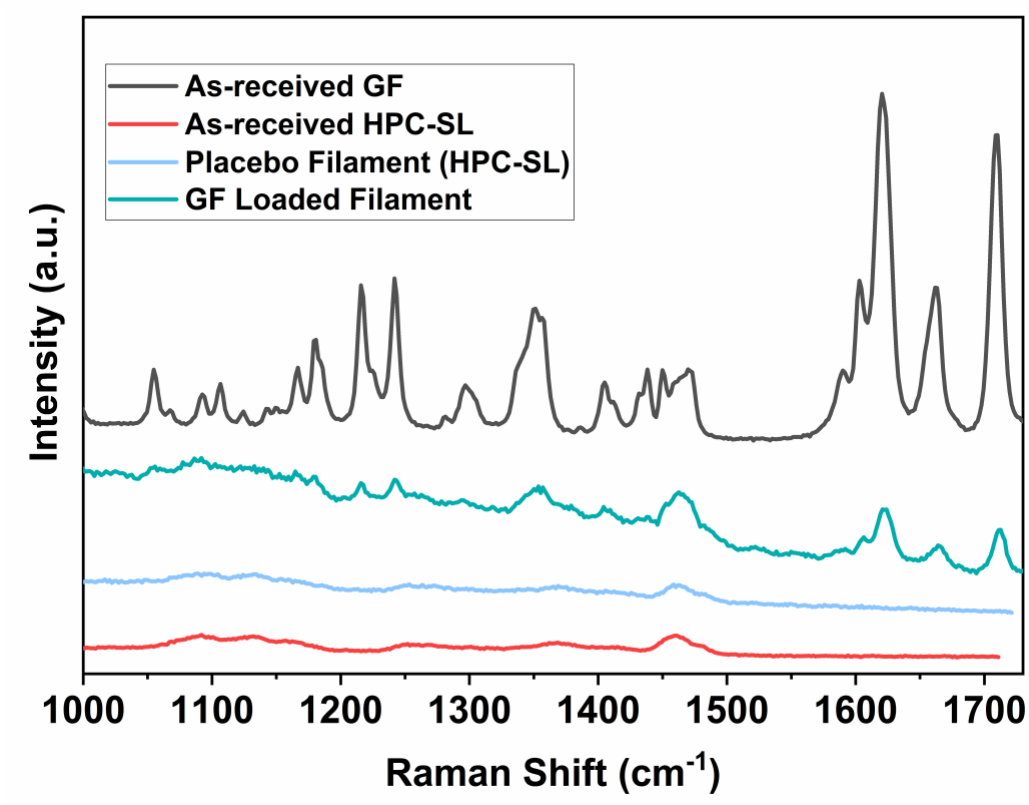

Figure 5.4 Raman spectra of as-received GF particles, as-received HPC-SL, placebo filament, and filament at 15 wt% GF concentration.

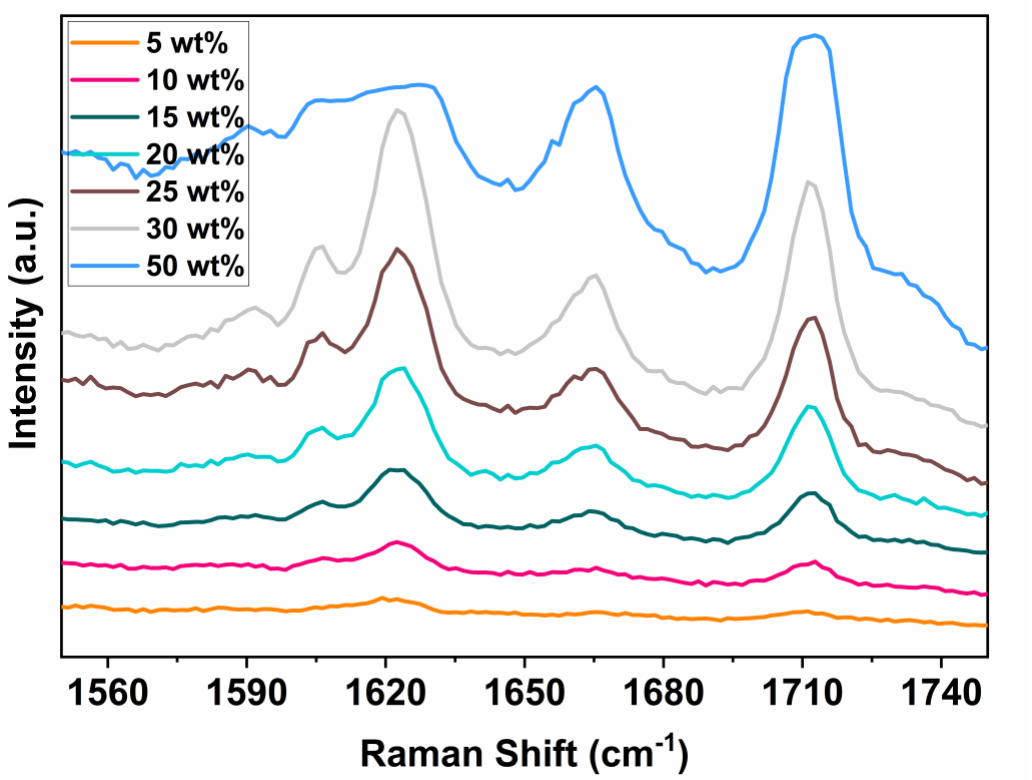

Figure 5.5 Raman spectra of filament containing varying GF concentrations in range 5–50% wt.

5.3.4 Development of qualitative and quantitative models

Baseline, de-trend, and SNV transformations were applied to develop calibration models through PCA and PLS algorithms. The responses are presented in Table 5.2. The pre-treatments of baseline and de-trend explained 99% of the data while SNV explained 91% of the data. Unlike the baseline transformation, de-trend and SNV had one data outside of the 95% confidence interval. In addition, the baseline transformation outperformed the other two pretreatments in the sense of linearity and/or the required number of the latent variables (see Table 5.2). Based on these

assessments, baseline transformation was used for developing quantitative and qualitative models.

Table 5.2 Pre-treatments and Their Responses in PCA and PLS Algorithms

Pre-treatment	PCA (%)		# of data outside of 95% CI	# of Factors*	R^2
	PC-1	PC-2			
Baseline	92	7	0	3	0.975
SNV	56	35	1	4	0.954
De-trend	77	22	1	3	0.968

*Suggested number of factors in PLS algorithm by CAMO software. CI: Confidence interval

The PCA scores plot is presented in Figure 5.6, where the ellipse represents the multivariate 95% confidence interval for the data. The principal components (factors) of PC-1 and PC-2 were used to explain the variations in the spectra obtained from the filaments at varying drug concentrations. The first component of PC-1 accounted for the majority of the variance in Raman spectra i.e., 92% whereas PC-2 explained only 7%. It is considered that PC-1 represents the varying GF concentrations. PC-2 might mainly refer to within-sample spectral variations (ICH, 1997; Zhang et al., 2014) while somewhat differentiate the highest drug concentration amongst others. These outcomes suggested that the drug concentrations in the calibration model could be quantified.

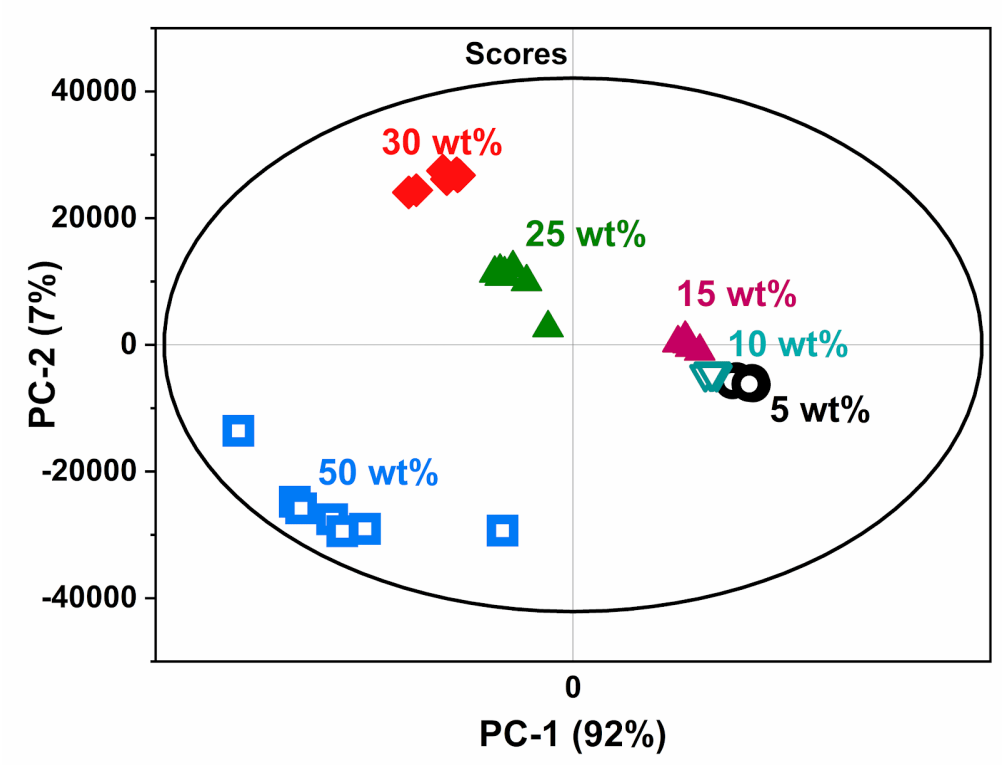

Figure 5.6 PCA of GF loaded filaments showing the effect of varying drug concentration. The ellipse represents the multivariate 95% confidence interval for the spectral variance.

The quantitative calibration models were developed through PLS regression models. The prediction diagnostic for three Factors is presented in Table 5.3. The calibration models were evaluated regarding accuracy, precision and, linearity determined in the ICH guideline (ICH, 1997) for deciding optimum latent variable for the prediction model. Factor-3 and Factor-4 showed higher yet close linearity compared to that of Factor-2. As mentioned earlier, the minimum PRESS value was considered as an indicator of the optimum latent variable in the calibration model (Jouan-Rimbaud et al., 1995; Popo et al., 2002). Similar to the linearity results, Factor-3 and Factor-4 showed close yet lower PRESS values. Thus, it was considered that Factor-2 was not the best candidate for the optimum

latent variable. Regarding the prediction capability, no discernible difference in RMSEP and RMSEC values was noticed between Factor-3 and Factor-4, however, the Factor-3 exhibited a bias value being around 2 times lower than that of Factor-4. Vargas et al. (2018) reported that lower bias implies the high accuracy of the model. Since there is no significant difference between Factor-3 and Factor-4, however, Factor-3 better performed regarding the accuracy, Factor-3 was used to avoid overfitting (Jouan-Rimbaud et al., 1995) in the development of the prediction model. The quantitative model with Factor-3 is demonstrated in Figure 5.7.

Table 5.3 Prediction Diagnostic and Limit of Quantification (LOQ)

Algorithm	Factor	RMSEC	RMSEP	Bias	PRESS	R^2	LOQ
PLS	2	3.099	3.573	0.026	0.085	0.948	10.434
	3	1.940	2.493	0.079	0.059	0.975	7.174
	4	1.768	2.303	0.145	0.055	0.978	6.587

*Pre-treatment: Baseline

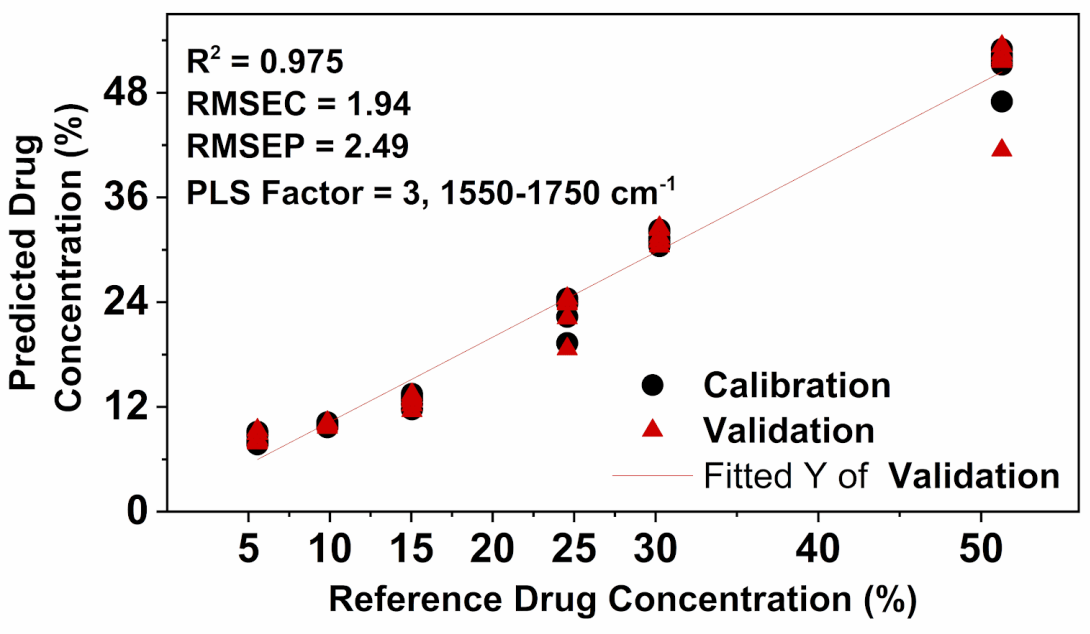

Figure 5.7 PLS algorithm for filaments at varying GF concentrations.

Besides the statistical analysis, the prediction capability of the models was assessed with LOQ values. Interestingly, the LOQ of the model was higher than the minimum value of the reference concentration of being 5.55 wt%, even at Factor-4, see Table 5.3. This is not surprising considering the fact that the model was established with a wide range of drug concentrations, where the difference between the lowest and highest concentration is 45 wt%, which is reasonably large compared to the current literature (Inoue et al., 2020; Zhang et al., 2014). However, that could expand the prediction range for the drug concentration from filaments. Nevertheless, incorporating higher number of spectra into the models developed could be improved the reliability of the model.

5.3.5 Validation of the calibration model

The validation of the calibration model with Factor-3 was performed via predicting the drug concentrations using a separate training set (see Subsection 5.2.3.5 for

details). The prediction results are presented in Table 5.4, where the reference concentrations used in the calibration model were quantified by direct assaying via UV spectroscopy (refer to Subsection 5.2.3.3). In addition, drug concentrations in 3D printed tablets were presented for comparison purposes. As expected, they had strongly similar concentration values to that of filaments, where 50 wt% was not printable, however, investigating the printability of the filaments is beyond the scope of this study. The close values between the reference and predicted drug concentrations indicated the capability of the developed model to perform accurate predictions with small residuals up to 2.58 (see Table 5.4). The predicted lowest drug concentration, 5 wt%, was slightly off from the reference value, which was expected owing to the high LOQ value of the calibration model. However, as aforementioned, that might be improved by incorporating higher number of spectra into the calibration model. Another option would be the use of drug concentrations at a narrow range. It is useful to highlight that the sample left-out, 20 wt% drug concentration, from the calibration set was accurately predicted. This corroborates that the calibration model developed could accurately predict the drug concentration in range of 5–50 wt%.

Table 5.4 Validation of the Filaments at 5–50 wt% GF Concentration

Optimum latent variable (PLS Factor)	Reference Concentration (wt.%)(±std)	Predicted Concentration (wt.%)(±std), n=5	Residuals	3D printed tablets
Factor-3	5.55±0.13	8.13±0.23	-2.58	5.66±0.10
	9.85±0.06	10.02±0.37	-0.18	10.08±0.0
	15.04±0.20	12.71±0.47	2.33	15.17±0.0
	19.78±0.55	18.33±0.65	1.44	20.53±0.9
	24.58±0.16	23.64±2.30	0.94	24.67±0.1
	30.24±0.26	31.13±0.66	-0.89	30.40±0.1
	51.28±0.72	52.33±1.38	-1.04	N/A

5.4 Conclusions

The quantitative and qualitative models were developed for the prediction of drug concentration from the feed materials (filaments) of FDM 3D printing using Raman spectroscopy via chemometric methods. Surface modification of the drug particles helped improve the flowability of the powder blends, which promoted maintaining the amount of material in the production line same, in turn, promoted product uniformity. Using a single transformation in the pre-treatment reduced the complexity of the calibration algorithm. The calibration model developed covered wide range of drug concentrations, which provided an expanded prediction space for drug-loaded filaments with high linearity, accuracy, and prediction capability.

CHAPTER 6

OVERALL CONCLUSIONS AND FUTURE WORK

6.1 Conclusions

Novel FDM 3D printing technology as a drug delivery platform was implemented for manipulating the pharmaceutical tablet properties, where tablet design options with the concern of individual's needs were investigated, and the process for manufacturing of FDM 3D printed tablets loaded with fusion-assisted ASDs were demonstrated for bioavailability enhancement of BCS Class II drugs. In addition, calibration models and PAT methodology were developed for predicting the drug concentration of the printed tablets based on the chemometric analysis of Raman spectroscopy testing of the feed materials.

Tablet design options for FDM 3D printing were explored in Chapter 2 for simultaneous tailoring of drug release and dose. Formulations containing varying drug concentrations were developed for feed materials compatible with FDM 3D printing, offering the required flexibility in producing tablets having a desirable drug release. In Chapter 3, design options for miniature tablets were considered for the pediatric patient population who needs manipulations in the dose per age/body weight or might have swallowing issues. The mini-sized tablets containing very low drug concentration, 1 wt%, enabling micro-dosing, were manufactured using FDM 3D printing. That allowed proper dose titration through the use of multi-unit mini-tablets. Additionally, the size advantage of printed mini-tablets was expected to address the swallowing difficulties. The feature of FDM 3D printing being a thermal

processing was used in Chapter 4 to produce 3D tablets containing fusion-assisted ASDs for enhancing the solubility of poorly soluble drugs. That helped alleviate the challenges of the conventional HME technique in producing the final product. Considering the solubility advantages of fusion-assisted ASDs, the demonstrated technique was shown to be advantageous since it is a single-step production of the final product. Finally, chemometric models for predicting drug concentration from feed materials were developed in Chapter 5. That was expected to address regulatory concerns related to on-demand products.

Overall, this dissertation explored the tailoring of FDM 3D printed tablet properties by considering patient-specific drug therapy and solubility enhancement. In addition, chemometric models were developed to quantitatively determine the drug concentration for on-demand products.

6.2 Future Work

6.2.1 FDM 3D printed mini-tablets loaded with ASDs

FDM 3D printed mini-tablets in Chapter 3 were designed as solid tablets with cylindrical geometry. As a result, relatively slow dissolution profiles were achieved due to their inherent dense structures. It has been reported that the structure design of printed tablets i.e., infill density and shell thickness could control the drug release behavior (Solanki et al., 2018b; Wei et al., 2020; Zhang et al., 2017b). Thus, structured tablets could help enhance the drug release rate if they have a higher available surface area for water penetration. Exploring the design of the structures could be an extension of the mini-tablet study. The smallness of the

tablet size could limit the structure design, however, high layer resolution could help print desired design. In this case, the impact of printing layer resolution on drug release profiles, which was shown for regular solid mini-tablets in Chapter 3, could be different for the structured mini-tablets. Investigation of which could be another extension.

6.2.2 Design of FDM 3D printed tablets loaded with pharmaceutically-favored ASDs

In Chapter 3, the solid-state of the drug within the mini-tablets appeared to be partially crystalline or was under the limit of detection. Since the amorphous form of a drug has a higher solubility than its crystalline form, manipulating the physical form of the drug could be a logical strategy for achieving enhanced release profiles of the mini-tablets. Solubility enhancement in addition to the goal in Subsection 6.2.1, could be an extension of the mini-tablet study. To this end, the approach of formulation development could be applied to produce tablets with ASDs, where highly miscible polymer with drug, which typically produces ASDs, could be used. This option requires polymer screening to assure drug-polymer miscibility. In addition, the feed materials produced from the formulations developed should be compatible with FDM 3D printing. In that case, suitable mechanical properties of the filaments and appropriate formulation would be the main considerations in future studies.

6.2.3 Development of prediction model using PLS algorithm for predicting the printability of the feed materials

The model in Chapter 6 covered the filaments at a wide range of drug concentrations i.e., 5–50 wt%, although the filament at the highest drug

concentration was not printable. The mechanical properties of those filaments could be linked with filament printability. Thus, this correlation could be translated into a prediction model with the help of PLS algorithm, where the reference values are correlated to develop a prediction model. Moreover, the wide range of drug concentrations used would be useful for easily determining the printability range. The limitation of this model would be the dependency of the model on the filament formulation. However, it is useful to mention that HPC is a well-accepted polymer for FDM 3D printing due to its ability to produce filaments with appropriate mechanical properties (Öblom et al., 2019; Pietrzak et al., 2015; Zhang et al., 2017a). Since the model developed in Chapter 6 used the filaments containing largely HPC polymer, using different active substances having intrinsic differences i.e., miscibility with HPC, melting point, molecular weight compares to GF could provide reasonable information for FDM 3D printing literature. Since intrinsic drug properties might affect the mechanical properties of the filaments, the model would cover a wide range of mechanical properties for printing filaments. Thus, another possible extension would be to use different active substances in developing a prediction model for filament printability.

6.2.4 *In-vivo* release behavior of FDM 3D printed tablets loaded with fusion-assisted ASDs

The technique of fusion-assisted ASDs has been demonstrated for FDM 3D printed tablets in Chapter 4. However, all the products in this study were tested under *in-vitro* dissolution conditions. Since the supersaturation level of the drug used was reasonably high compared to the current literature, a simple extension

of this study would be to test the products in an *in-vivo* dissolution environment. That requires selecting a suitable animal model and the testing conditions.

APPENDIX A

SIMILARITY FACTORS AND SWELLING MECHANISM

A.1 Similarity factors for dissolution profiles of case A, case C and, case E

The dissolution profiles of the printed tablets for case A, case C, and case E were compared via bootstrap similarity (f_2) test (Mendyk et al., 2013; Paixão et al., 2017) using PhEq_bootstrap software (Mendyk et al., 2013). This test was used because of the large variability in the dissolution profiles. For each tested case, the time point data beyond 85% dissolution were discarded. The following bootstrapping parameters were applied for all the tested data; the number of bootstraps is 5000, and the confidence interval (CI) was set to 90%. The 4–6 sample for each individual sub-cases was used. The assessment of the results is based on the rule of dissolution profile similarity, where f_2 >50. The similarity statistics for case A, case C and, case E are presented in Table A.1.

Table A.1 Similarity (f_2) Analysis Factor for Dissolution Profiles of Case A, Case C, And Case E

	3D Tablet Design	Similarity factor (f_2)
Case A	**A1-A2**	45.05
	A1-A3	38.72
	A1-A4	27.15
	A2-A3	46.83
	A2-A4	30.90
	A3-A4	36.08
Case C	**C1-C2**	38.87
	C1-C3	41.92
	C1-C4	40.04
	C2-C3	51.76
	C2-C4	50.21
	C3-C4	59.35
Case E	**E1-E2**	65.59
	E1-E3	52.81
	E1-E4	43.81
	E2-E3	55.57
	E2-E4	45.07
	E3-E4	59.43

A.2 Calculation of the swelling and eroding mechanism from printed tablets containing 5 wt% and 30 wt% drug concentration

The swelling and eroding distances were measured from the digital images of the tablet placed on a flat disc with a marker for easier assessment. The thickness and diameter of the marker were used as a reference. The swelling and eroding extent of the tablet were calculated according to Equation (A1) and Equation (A2) in axial and radial directions, respectively.

$$\text{Swelling (or Eroding) Extent} = \frac{final\ tablet\ diameter - initial\ tablet\ diamter}{initial\ tablet\ diameter} \times 100\% \quad \text{(A1)}$$

$$\text{Swelling (or Eroding) Extent} = \frac{final\ tablet\ thickness - initial\ tablet\ thickness}{initial\ tablet\ thickness} \times 100\% \quad \text{(A2)}$$

The results are expressed as a percentage (%) and presented in Table A.2.

Table A.2 The Swelled or Eroded Percentage (%) of the Tablets Containing 5 and 30 wt% Drug Concentration. The Negative Sign Refers to Decreases in the Original Size of the Tablet

Time (h)	Size Changes by 5 wt% Drug (%)		Size Changes by 30 wt% Drug (%)	
	Axial	Radial	Axial	Radial
0	0.00	0.00	0.00	0.0
3	3.59	5.71	87.20	4.0
7	17.48	2.86	112.96	7.3
24	-33.22	5.71	46.54	-4.7

APPENDIX B

SIMILARITY FACTORS

The dissolution profiles of the printed tablets for mini-tablets and large tablets were analyzed through bootstrap similarity (f_2) test (Mendyk et al., 2013; Paixão et al., 2017) using PhEq_bootstrap software (Mendyk et al., 2013) by following the same processing parameters in Section A.1 of Appendix A. The results were deemed statistically similar when f_2 >50. The outcomes for similarity statistics are presented in Table B.1.

Table B.1 Similarity (f_2) Analysis

Run	Differences in Compared Couples			Similarity factor (f_2)
	Number of units	Drug concentration %wt	Tablet size	
1	1-5			53.63
2	1-10			45.68
3	1-15			47.89
4	1-20			45.64
5	5-10	1.0-1.0	M-M	59.06
6	5-15			59.04
7	5-20			55.22
8	10-15			68.42
9	10-20			67.44
10	15-20			64.04
11	1-0.5		F-H	28.66
12	1-0.25	1.0-1.0	F-Q	26.77
13	0.5-0.25		H-Q	40.67
14		1.0-10.0		32.79
15	1-1	1.0-20.0	M-M	27.45
16		1.0-20.0		52.94

*All the tablets were printed at 0.2 mm layer resolution. M: Mini-tablet, F: Full-size H: Half-size Q: Quart-size tablet

B.2 Digital Images of Split Tablets vs. mini tablets at the same total drug amounts

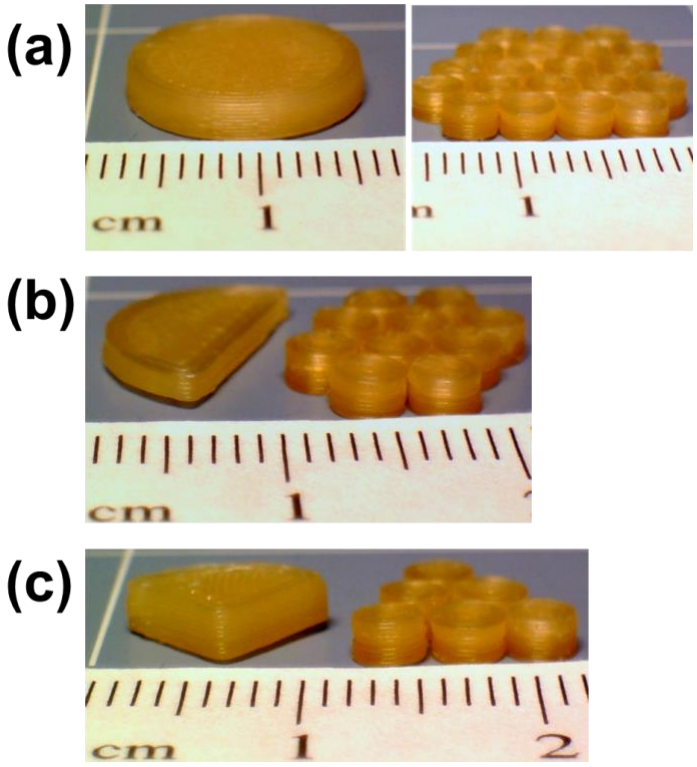

Figure B.1 Digital Images of (a) full tablet vs. 20 units mini-tablets containing 0.99, (b) half-split tablet vs. 10 units mini-tablets, and quartered tablet vs. 5 units mini-tablets, each sub-case contained similar drug amounts.

APPENDIX C

AMORPHOUS SOLID DISPERSION LOADED THREE DIMENSIONAL TABLETS

C.1 Extent of GF supersaturation and dissolution mechanism of the printed tablets

Table C.1 Extent of GF Supersaturation for Various Tablet Designs along with the Fitting Parameters of the Corresponding Fitting Dissolution Curves

Run	*Extent of Supersaturation (%)	Fitting Parameters		
		k ($\%/min^n$)	n	R^2
F240	153.3	0.16	0.94	0.988
F240a	246.8	5.07	0.46	0.975
F240b	214.9	1.86	0.58	0.988
F240c	225.6	1.71	0.59	0.977
F240d	293.0	7.13	0.38	0.918

*The values for the extent of supersaturation are calculated from the dissolution curves at the time points between 9–12h

REFERENCES

Afseth, N. K., Segtnan, V. H., & Wold, J. P. (2006). Raman spectra of biological samples: A study of preprocessing methods. *Applied Spectroscopy, 60*(12), 1358-1367.

Ahmad, A., Jaya, M., Derek, C., & Ahmad, M. (2011). Synthesis and characterization of TiO2 membrane with palladium impregnation for hydrogen separation. *Journal of Membrane Science, 366*(1-2), 166-175.

Aho, J., Van Renterghem, J., Arnfast, L., De Beer, T., & Rantanen, J. (2017). The flow properties and presence of crystals in drug-polymer mixtures: Rheological investigation combined with light microscopy. *International Journal of Pharmaceutics, 528*(1-2), 383-394.

Al-Obaidi, H., & Buckton, G. (2009). Evaluation of griseofulvin binary and ternary solid dispersions with HPMCAS. *AAPS PharmSciTech, 10*(4), 1172.

Aleksovski, A., Dreu, R., Gašperlin, M., & Planinšek, O. (2015). Mini-tablets: a contemporary system for oral drug delivery in targeted patient groups. *Expert opinion on drug delivery, 12*(1), 65-84.

Alhijjaj, M., Nasereddin, J., Belton, P., & Qi, S. (2019). Impact of processing parameters on the quality of pharmaceutical solid dosage forms produced by Fused Deposition Modeling (FDM). *Pharmaceutics, 11*(12), 633.

Alhnan, M. A., Okwuosa, T. C., Sadia, M., Wan, K.-W., Ahmed, W., & Arafat, B. (2016). Emergence of 3D printed dosage forms: opportunities and challenges. *Pharmaceutical Research, 33*(8), 1817-1832.

Amidon, G. L., Lennernäs, H., Shah, V. P., & Crison, J. R. (1995). A theoretical basis for a biopharmaceutic drug classification: the correlation of in vitro drug product dissolution and in vivo bioavailability. *Pharmaceutical Research, 12*(3), 413-420.

Arafat, B., Qinna, N., Cieszynska, M., Forbes, R. T., & Alhnan, M. A. (2018a). Tailored on demand anti-coagulant dosing: An in vitro and in vivo evaluation of 3D printed purpose-designed oral dosage forms. *European Journal of Pharmaceutics and Biopharmaceutics, 128*, 282-289.

Arafat, B., Wojsz, M., Isreb, A., Forbes, R. T., Isreb, M., Ahmed, W., Arafat, T., & Alhnan, M. A. (2018b). Tablet fragmentation without a disintegrant: A novel design approach for accelerating disintegration and drug release from 3D printed cellulosic tablets. *European Journal of Pharmaceutical Sciences, 118*, 191-199.

Augustijns, P., & Brewster, M. E. (2012). Supersaturating drug delivery systems: fast is not necessarily good enough. *Journal of Pharmaceutical Sciences, 101*(1), 7-9.

Baggi, R. B., & Kilaru, N. B. (2016). Calculation of predominant drug release mechanism using Peppas-Sahlin model, Part-I (substitution method): A linear regression approach. *Asian Journal of Pharmacy and Technology, 6*(4), 223-230.

Baghel, S., Cathcart, H., & O'Reilly, N. J. (2016). Polymeric amorphous solid dispersions: a review of amorphization, crystallization, stabilization, solid-state characterization, and aqueous solubilization of biopharmaceutical classification system class II drugs. *Journal of Pharmaceutical Sciences, 105*(9), 2527-2544.

Baird, J. A., Van Eerdenbrugh, B., & Taylor, L. S. (2010). A classification system to assess the crystallization tendency of organic molecules from undercooled melts. *Journal of Pharmaceutical Sciences, 99*(9), 3787-3806.

Barimani, S., & Kleinebudde, P. (2017). Evaluation of in–line Raman data for end-point determination of a coating process: Comparison of Science–Based Calibration, PLS-regression and univariate data analysis. *European Journal of Pharmaceutics and Biopharmaceutics, 119*, 28-35.

Barnes, R., Dhanoa, M. S., & Lister, S. J. (1989). Standard normal variate transformation and de-trending of near-infrared diffuse reflectance spectra. *Applied Spectroscopy, 43*(5), 772-777.

Bayan, M. F., Sbaih, H. M., & Saadh, M. J. (2021). Pharmaceutical mini-tablets overview. *Indian Journal of Forensic Medicine and Toxicology, 15*(1).

Bennett, R. C., Keen, J. M., Bi, Y., Porter, S., Dürig, T., & McGinity, J. W. (2015). Investigation of the interactions of enteric and hydrophilic polymers to enhance dissolution of griseofulvin following hot melt extrusion processing. *Journal of Pharmacy and Pharmacology, 67*(7), 918-938.

Bhakay, A., Azad, M., Bilgili, E., & Dave, R. (2014). Redispersible fast dissolving nanocomposite microparticles of poorly water-soluble drugs. *International Journal of Pharmaceutics, 461*(1-2), 367-379.

Blanco, M., Coello, J., Iturriaga, H., Maspoch, S., & Pou, N. (2001). Influence of the procedure used to prepare the calibration sample set on the performance of near infrared spectroscopy in quantitative pharmaceutical analyses. *Analyst, 126*(7), 1129-1134.

Boggie, D. T., DeLattre, M. L., Schaefer, M. G., Morreale, A. P., & Plowman, B. K. (2004). Accuracy of splitting unscored valdecoxib tablets. *American Journal of Health-system Pharmacy, 61*(14), 1482-1483.

Borujeni, S. H., Mirdamadian, S. Z., Varshosaz, J., & Taheri, A. (2020). Three-dimensional (3D) printed tablets using ethyl cellulose and hydroxypropyl cellulose to achieve zero order sustained release profile. *Cellulose, 27*(3), 1573-1589.

Breitkreutz, J., & Boos, J. (2007). Paediatric and geriatric drug delivery. *Expert Opinion on Drug delivery, 4*(1), 37-45.

Brenken, B., Favaloro, A., Barocio, E., DeNardo, N. M., & Pipes, R. B. (2016). Development of a model to predict temperature history and crystallization behavior of 3D printed parts made from fiber-reinforced thermoplastic polymers. Paper presented at the *Society for the Advancement of Material and Process Engineering Conference.*

Brown, D., Ford, J., Nunn, A., & Rowe, P. (2004). An assessment of dose-uniformity of samples delivered from paediatric oral droppers. *Journal of Clinical Pharmacy and Therapeutics, 29*(6), 521-529.

Bühler, V. (2007). *Kollicoat grades: functional polymers for the pharmaceutical industry*. Ludwigshafen, Germany: BASF SE Chemical Company.

Buyukgoz, G. G., Soffer, D., Defendre, J., Pizzano, G. M., & Davé, R. N. (2020). Exploring tablet design options for tailoring drug release and dose via Fused Deposition Modeling (FDM) 3D printing. *International Journal of Pharmaceutics*, 119987.

Callister, W. D. (2007). *Materials science and engineering: an introduction.* (seventh ed.). New York, NY: John Willey & Sons, Inc.

Capece, M., Huang, Z., & Davé, R. (2017). Insight into a novel strategy for the design of tablet formulations intended for direct compression. *Journal of Pharmaceutical Sciences, 106*(6), 1608-1617.

Capece, M., Huang, Z., To, D., Aloia, M., Muchira, C., Davé, R., & Yu, A. (2014). Prediction of porosity from particle scale interactions: surface modification of fine cohesive powders. *Powder Technology, 254*, 103-113.

Castellanos, A. (2005). The relationship between attractive interparticle forces and bulk behaviour in dry and uncharged fine powders. *Advances in Physics, 54*(4), 263-376.

Censi, R., Gigliobianco, M. R., Casadidio, C., & Di Martino, P. (2018). Hot melt extrusion: Highlighting physicochemical factors to be investigated while designing and optimizing a hot melt extrusion process. *Pharmaceutics, 10*(3), 89.

Cetindag, E., Pentangelo, J., Cespedes, T. A., & Davé, R. N. (2020). Effect of solvents and cellulosic polymers on quality attributes of films loaded with a poorly water-soluble drug. *Carbohydrate Polymers, 250*, 117012.

Chai, X., Chai, H., Wang, X., Yang, J., Li, J., Zhao, Y., Cai, W., Tao, T., & Xiang, X. (2017). Fused deposition modeling (FDM) 3D printed tablets for intragastric floating delivery of domperidone. *Scientific Reports, 7*(1), 1-9.

Chen, H., Wang, C., Liu, S., & Sun, C. C. (2020). Development of piroxicam mini-tablets enabled by spherical cocrystallization. *International Journal of Pharmaceutics, 590*, 119953.

Chen, Y., Yang, J., Dave, R. N., & Pfeffer, R. (2008). Fluidization of coated group C powders. *AIChE Journal, 54*(1), 104-121.

Chiou, W. L., & Riegelman, S. (1971). Pharmaceutical applications of solid dispersion systems. *Journal of Pharmaceutical Sciences, 60*(9), 1281-1302.

Chowhan, Z. (1980). The effect of low-and high-humidity ageing on the hardness, disintegration time and dissolution rate of dibasic calcium phosphate-based tablets. *Journal of Pharmacy and Pharmacology, 32*(1), 10-14.

Cogdill, R. P., Anderson, C. A., Delgado, M., Chisholm, R., Bolton, R., Herkert, T., Afnan, A. M., & Drennen, J. K. (2005). Process analytical technology case study: part II. Development and validation of quantitative near-infrared calibrations in support of a process analytical technology application for real-time release. *AAPS PharmSciTech, 6*(2), E273-E283.

Cohen, J. S. (2002). Tablet splitting: imperfect perhaps, but better than excessive dosing. *Journal of the American Pharmaceutical Association, 42*(2), 160-162.

Collier, J., Shah, R., Bryant, A., Habib, M., Khan, M., & Faustino, P. (2011). Development and application of a validated HPLC method for the analysis of dissolution samples of levothyroxine sodium drug products. *Journal of Pharmaceutical and Biomedical Analysis, 54*(3), 433-438.

Davé, R. N., Beach, L., Scicolone, J., & Gurumurthy, L. (2011). Particle engineering via dry coating: development of a novel material sparing technology for pharmaceutical powders. Paper presented at the *American Institute of Chemical Engineers Annual Meeting*, Pittsburgh.

Ernest, T. B., Craig, J., Nunn, A., Salunke, S., Tuleu, C., Breitkreutz, J., Alex, R., & Hempenstall, J. (2012). Preparation of medicines for children–a hierarchy of classification. *International Journal of Pharmaceutics, 435*(2), 124-130.

Esbensen, K. H., & Geladi, P. (2010). Principles of proper validation: Use and abuse of re-sampling for validation. *Journal of Chemometrics, 24*(3-4), 168-187.

Fawell, N. G., Cookson, T. L., & Scranton, S. S. (1999). Relationship between tablet splitting and compliance, drug acquisition cost, and patient acceptance. *American Journal of Health-system Pharmacy, 56*(24), 2542-2545.

FDA. (2009). Guidance for industry: Q8 (R2) pharmaceutical development. *Center for Drug Evaluation and Research*.

FDA. (2013). Best practice of tablet splitting. Retrieved from https://www.fda.gov/drugs/ensuring-safe-use-medicine/best-practices-tablet-splitting.

FDA, & Lostritto, R. (2014). Content uniformity (CU) testing for the 21st century: CDER perspective, October 17, 2012. Paper presented at the *American Association of Pharmaceutical Scientists Annual Meeting*. http://www.fda.gov/downloads/AboutFDA/CentersOffices/OfficeofMedicalProductsandTobacco/CDER/UCM341168. pdf.

Ford, J. L., Mitchell, K., Rowe, P., Armstrong, D. J., Elliott, P. N., Rostron, C., & Hogan, J. E. (1991). Mathematical modelling of drug release from hydroxypropylmethylcellulose matrices: Effect of temperature. *International Journal of Pharmaceutics, 71*(1-2), 95-104.

Ford, J. L., Rubinstein, M. H., & Hogan, J. E. (1985). Dissolution of a poorly water soluble drug, indomethacin, from hydroxypropylmethylcellulose controlled release tablets. *Journal of Pharmacy and Pharmacology, 37*(S12), 33P-33P.

Gaber, D. M., Nafee, N., & Abdallah, O. Y. (2015). Mini-tablets versus pellets as promising multiparticulate modified release delivery systems for highly soluble drugs. *International Journal of Pharmaceutics, 488*(1-2), 86-94.

Gazzaniga, A., Cerea, M., Cozzi, A., Foppoli, A., Maroni, A., & Zema, L. (2011). A novel injection-molded capsular device for oral pulsatile delivery based on swellable/erodible polymers. *AAPS PharmSciTech, 12*(1), 295-303.

Gioumouxouzis, C. I., Baklavaridis, A., Katsamenis, O. L., Markopoulou, C. K., Bouropoulos, N., Tzetzis, D., & Fatouros, D. G. (2018). A 3D printed bilayer oral solid dosage form combining metformin for prolonged and glimepiride for immediate drug delivery. *European Journal of Pharmaceutical Sciences, 120*, 40-52.

Gioumouxouzis, C. I., Katsamenis, O. L., Bouropoulos, N., & Fatouros, D. G. (2017). 3D printed oral solid dosage forms containing hydrochlorothiazide for controlled drug delivery. *Journal of Drug Delivery Science and Technology, 40*, 164-171.

Gogos, C. G., Liu, H., & Wang, P. (2012). Laminar dispersive and distributive mixing with dissolution and applications to hot-Melt Extrusion. *Hot-Melt Extrusion: Pharmaceutical Applications*, 261-284.

Goh, H. P., Heng, P. W. S., & Liew, C. V. (2017). Understanding die fill variation during mini-tablet production. *International Journal of Pharmaceutics, 534*(1-2), 279-286.

Govender, R., Abrahmsén-Alami, S., Folestad, S., & Larsson, A. (2020). High content solid dispersions for dose window extension: A basis for design flexibility in Fused Deposition Modelling. *Pharmaceutical Research, 37*(1), 9.

Goyanes, A., Allahham, N., Trenfield, S. J., Stoyanov, E., Gaisford, S., & Basit, A. W. (2019). Direct powder extrusion 3D printing: Fabrication of drug products using a novel single-step process. *International Journal of Pharmaceutics, 567*, 118471.

Goyanes, A., Buanz, A. B., Basit, A. W., & Gaisford, S. (2014). Fused-filament 3D printing (3DP) for fabrication of tablets. *International Journal of Pharmaceutics, 476*(1-2), 88-92.

Goyanes, A., Buanz, A. B., Hatton, G. B., Gaisford, S., & Basit, A. W. (2015a). 3D printing of modified-release aminosalicylate (4-ASA and 5-ASA) tablets. *European Journal of Pharmaceutics and Biopharmaceutics, 89*, 157-162.

Goyanes, A., Chang, H., Sedough, D., Hatton, G. B., Wang, J., Buanz, A., Gaisford, S., & Basit, A. W. (2015b). Fabrication of controlled-release budesonide tablets via desktop (FDM) 3D printing. *International Journal of Pharmaceutics, 496*(2), 414-420.

Goyanes, A., Fina, F., Martorana, A., Sedough, D., Gaisford, S., & Basit, A. W. (2017). Development of modified release 3D printed tablets (printlets) with pharmaceutical excipients using additive manufacturing. *International Journal of Pharmaceutics, 527*(1-2), 21-30.

Goyanes, A., Kobayashi, M., Martínez-Pacheco, R., Gaisford, S., & Basit, A. W. (2016). Fused-filament 3D printing of drug products: microstructure analysis and drug release characteristics of PVA-based caplets. *International Journal of Pharmaceutics, 514*(1), 290-295.

Goyanes, A., Martinez, P. R., Buanz, A., Basit, A. W., & Gaisford, S. (2015c). Effect of geometry on drug release from 3D printed tablets. *International Journal of Pharmaceutics, 494*(2), 657-663.

Goyanes, A., Wang, J., Buanz, A., Martínez-Pacheco, R., Telford, R., Gaisford, S., & Basit, A. W. (2015d). 3D printing of medicines: engineering novel oral devices with unique design and drug release characteristics. *Molecular Pharmaceutics, 12*(11), 4077-4084.

Gupta, P., Kakumanu, V. K., & Bansal, A. K. (2004). Stability and solubility of celecoxib-PVP amorphous dispersions: a molecular perspective. *Pharmaceutical Research, 21*(10), 1762-1769.

Gupta, S. S., Meena, A., Parikh, T., & Serajuddin, A. T. (2016). Investigation of thermal and viscoelastic properties of polymers relevant to hot melt extrusion-I: Polyvinylpyrrolidone and related polymers. *Journal of Excipients and Food Chemicals, 5*(1), 1001.

Han, X., Ghoroi, C., & Davé, R. (2013). Dry coating of micronized API powders for improved dissolution of directly compacted tablets with high drug loading. *International Journal of Pharmaceutics, 442*(1-2), 74-85.

Han, X., Ghoroi, C., To, D., Chen, Y., & Davé, R. (2011). Simultaneous micronization and surface modification for improvement of flow and dissolution of drug particles. *International Journal of Pharmaceutics, 415*(1-2), 185-195.

Hancock, B. C., & Zografi, G. (1997). Characteristics and significance of the amorphous state in pharmaceutical systems. *Journal of Pharmaceutical Sciences, 86*(1), 1-12.

Huang, Z., Scicolone, J. V., Han, X., & Davé, R. N. (2015). Improved blend and tablet properties of fine pharmaceutical powders via dry particle coating. *International Journal of Pharmaceutics, 478*(2), 447-455.

Huang, Z., Xiong, W., Kunnath, K., Bhaumik, S., & Davé, R. N. (2017). Improving blend content uniformity via dry particle coating of micronized drug powders. *European Journal of Pharmaceutical Sciences, 104*, 344-355.

Hülsmann, S., Backensfeld, T., Keitel, S., & Bodmeier, R. (2000). Melt extrusion–an alternative method for enhancing the dissolution rate of 17β-estradiol hemihydrate. *European Journal of Pharmaceutics and Biopharmaceutics, 49*(3), 237-242.

ICH. (1997). *Q2B validation of analytical procedures: Methodology.* Paper presented at the *International Conference on Harmonization*.

Ilyés, K., Balogh, A., Casian, T., Igricz, T., Borbás, E., Démuth, B., Vass, P., Menyhárt, L., Kovács, N. K., & Marosi, G. (2019a). 3D floating tablets: Appropriate 3D design from the perspective of different in vitro dissolution testing methodologies. *International Journal of Pharmaceutics, 567*, 118433.

Ilyés, K., Kovács, N. K., Balogh, A., Borbás, E., Farkas, B., Casian, T., Marosi, G., Tomuță, I., & Nagy, Z. K. (2019b). The applicability of pharmaceutical polymeric blends for the fused deposition modelling (FDM) 3D technique: Material considerations–printability–process modulation, with consecutive effects on in vitro release, stability and degradation. *European Journal of Pharmaceutical Sciences, 129*, 110-123.

Inoue, M., Kiefer, O., Fischer, B., & Breitkreutz, J. (2020). Raman monitoring of semi-continuously manufactured orodispersible films for individualized dosing. *Journal of Drug Delivery Science and Technology*, 102224.

Isreb, A., Baj, K., Wojsz, M., Isreb, M., Peak, M., & Alhnan, M. A. (2019). 3D printed oral theophylline doses with innovative 'radiator-like'design: Impact of polyethylene oxide (PEO) molecular weight. *International Journal of Pharmaceutics, 564*, 98-105.

Jallo, L. J., Ghoroi, C., Gurumurthy, L., Patel, U., & Davé, R. N. (2012). Improvement of flow and bulk density of pharmaceutical powders using surface modification. *International Journal of Pharmaceutics, 423*(2), 213-225.

Jambhrunkar, S., Qu, Z., Popat, A., Karmakar, S., Xu, C., & Yu, C. (2014). Modulating in vitro release and solubility of griseofulvin using functionalized mesoporous silica nanoparticles. *Journal of Colloid and Interface Science, 434*, 218-225.

Jamróz, W., Kurek, M., Czech, A., Szafraniec, J., Gawlak, K., & Jachowicz, R. (2018). 3D printing of tablets containing amorphous aripiprazole by filaments co-extrusion. *European Journal of Pharmaceutics and Biopharmaceutics, 131*, 44-47.

Jamróz, W., Kurek, M., Łyszczarz, E., Szafraniec, J., Knapik-Kowalczuk, J., Syrek, K., Paluch, M., & Jachowicz, R. (2017). 3D printed orodispersible films with Aripiprazole. *International Journal of Pharmaceutics, 533*(2), 413-420.

Janssens, S., & Van den Mooter, G. (2009). Physical chemistry of solid dispersions. *Journal of Pharmacy and Pharmacology, 61*(12), 1571-1586.

Jouan-Rimbaud, D., Walczak, B., Massart, D., Last, I., & Prebble, K. (1995). Comparison of multivariate methods based on latent vectors and methods based on wavelength selection for the analysis of near-infrared spectroscopic data. *Analytica Chimica Acta, 304*(3), 285-295.

Kadry, H., Al-Hilal, T. A., Keshavarz, A., Alam, F., Xu, C., Joy, A., & Ahsan, F. (2018). Multi-purposable filaments of HPMC for 3D printing of medications with tailored drug release and timed-absorption. *International Journal of Pharmaceutics, 544*(1), 285-296.

Kandpal, L. M., Tewari, J., Gopinathan, N., Boulas, P., & Cho, B.-K. (2016). In-process control assay of pharmaceutical microtablets using hyperspectral imaging coupled with multivariate analysis. *Analytical Chemistry, 88*(22), 11055-11061.

Kao, C.-C., Chen, S.-C., & Sheu, M.-T. (1997). Lag time method to delay drug release to various sites in the gastrointestinal tract. *Journal of Controlled Release, 44*(2-3), 263-270.

Kearns, G. L., Abdel-Rahman, S. M., Alander, S. W., Blowey, D. L., Leeder, J. S., & Kauffman, R. E. (2003). Developmental pharmacology—drug disposition, action, and therapy in infants and children. *New England Journal of Medicine, 349*(12), 1157-1167.

Kempin, W., Domsta, V., Brecht, I., Semmling, B., Tillmann, S., Weitschies, W., & Seidlitz, A. (2018). Development of a dual extrusion printing technique for an acid-and thermo-labile drug. *European Journal of Pharmaceutical Sciences, 123*, 191-198.

Kempin, W., Franz, C., Koster, L.-C., Schneider, F., Bogdahn, M., Weitschies, W., & Seidlitz, A. (2017). Assessment of different polymers and drug loads for fused deposition modeling of drug loaded implants. *European Journal of Pharmaceutics and Biopharmaceutics, 115*, 84-93.

Khaled, S. A., Burley, J. C., Alexander, M. R., & Roberts, C. J. (2014). Desktop 3D printing of controlled release pharmaceutical bilayer tablets. *International Journal of Pharmaceutics, 461*(1-2), 105-111.

Khaled, S. A., Burley, J. C., Alexander, M. R., Yang, J., & Roberts, C. J. (2015a). 3D printing of five-in-one dose combination polypill with defined immediate and sustained release profiles. *Journal of Controlled Release, 217*, 308-314.

Khaled, S. A., Burley, J. C., Alexander, M. R., Yang, J., & Roberts, C. J. (2015b). 3D printing of tablets containing multiple drugs with defined release profiles. *International Journal of Pharmaceutics, 494*(2), 643-650.

Kitazawa, S., Johno, I., Ito, Y., Teramura, S., & Okada, J. (1975). Effects of hardness on the disintegration time and the dissolution rate of uncoated caffeine tablets. *Journal of Pharmacy and Pharmacology, 27*(10), 765-770.

Klingmann, V. (2017). Acceptability of mini-tablets in young children: Results from three prospective cross-over studies. *AAPS PharmSciTech, 18*(2), 263-266.

Klingmann, V., Seitz, A., Meissner, T., Breitkreutz, J., Moeltner, A., & Bosse, H. M. (2015). Acceptability of uncoated mini-tablets in neonates—a randomized controlled trial. *The Journal of Pediatrics, 167*(4), 893-896. e892.

Knop, K., & Kleinebudde, P. (2013). PAT-tools for process control in pharmaceutical film coating applications. *International Journal of Pharmaceutics, 457*(2), 527-536.

Kolter, K., Karl, M., Gryczke, A., & Ludwigshafen am Rhein, B. (2012). Hot-melt extrusion with BASF pharma polymers: Extrusion compendium (Second ed.): Ludwigshafen, Germany: BASF SE Chemical company.

Korsmeyer, R. W., Gurny, R., Doelker, E., Buri, P., & Peppas, N. A. (1983). Mechanisms of solute release from porous hydrophilic polymers. *International Journal of Pharmaceutics, 15*(1), 25-35.

Korte, C., & Quodbach, J. (2018). Formulation development and process analysis of drug-loaded filaments manufactured via hot-melt extrusion for 3D-printing of medicines. *Pharmaceutical Development and Technology, 23*(10), 1117-1127.

Krull, S. M., Moreno, J., Li, M., Bilgili, E., & Davé, R. N. (2017). Critical material attributes (CMAs) of strip films loaded with poorly water-soluble drug nanoparticles: III. Impact of drug nanoparticle loading. *International Journal of Pharmaceutics, 523*(1), 33-41.

Kunnath, K., Huang, Z., Chen, L., Zheng, K., & Davé, R. (2018). Improved properties of fine active pharmaceutical ingredient powder blends and tablets at high drug loading via dry particle coating. *International Journal of Pharmaceutics, 543*(1-2), 288-299.

Lakshman, J. P., Cao, Y., Kowalski, J., & Serajuddin, A. T. (2008). Application of melt extrusion in the development of a physically and chemically stable high-energy amorphous solid dispersion of a poorly water-soluble drug. *Molecular Pharmaceutics, 5*(6), 994-1002.

Langer, R., & Peppas, N. A. (1981). Present and future applications of biomaterials in controlled drug delivery systems. *Biomaterials, 2*(4), 201-214.

Laukamp, E. J., Thommes, M., & Breitkreutz, J. (2014). Hot-melt extruded drug-loaded rods: Evaluation of the mechanical properties for individual dosing via the Solid Dosage Pen. *International Journal of Pharmaceutics, 475*(1-2), 344-350.

Lennartz, P., & Mielck, J. (1998). Minitabletting: improving the compactability of paracetamol powder mixtures. *International Journal of Pharmaceutics, 173*(1-2), 75-85.

Leuner, C., & Dressman, J. (2000). Improving drug solubility for oral delivery using solid dispersions. *European Journal of Pharmaceutics and Biopharmaceutics, 50*(1), 47-60.

Li, M., Ioannidis, N., Gogos, C., & Bilgili, E. (2017a). A comparative assessment of nanocomposites vs. amorphous solid dispersions prepared via nanoextrusion for drug dissolution enhancement. *European Journal of Pharmaceutics and Biopharmaceutics, 119*, 68-80.

Li, N., & Taylor, L. S. (2018). Tailoring supersaturation from amorphous solid dispersions. *Journal of Controlled Release, 279*, 114-125.

Li, Q., Wen, H., Jia, D., Guan, X., Pan, H., Yang, Y., Yu, S., Zhu, Z., Xiang, R., & Pan, W. (2017b). Preparation and investigation of controlled-release glipizide novel oral device with three-dimensional printing. *International Journal of Pharmaceutics, 525*(1), 5-11.

Lipinski, C. (2002). Poor aqueous solubility—an industry wide problem in drug discovery. *American Pharmaceutical Review, 5*(3), 82-85.

Liu, F., Ranmal, S., Batchelor, H. K., Orlu-Gul, M., Ernest, T. B., Thomas, I. W., Flanagan, T., & Tuleu, C. (2014). Patient-centered pharmaceutical design to improve acceptability of medicines: similarities and differences in paediatric and geriatric populations. *Drugs, 74*(16), 1871-1889.

Loftsson, T., Fri, H., & Gu, T. K. (1996). The effect of water-soluble polymers on aqueous solubility of drugs. *International Journal of Pharmaceutics, 127*(2), 293-296.

Long, J., Gholizadeh, H., Lu, J., Bunt, C., & Seyfoddin, A. (2017). Application of fused deposition modelling (FDM) method of 3D printing in drug delivery. *Current Pharmaceutical Design, 23*(3), 433-439.

Lopez, F. L., Ernest, T. B., Tuleu, C., & Gul, M. O. (2015). Formulation approaches to pediatric oral drug delivery: benefits and limitations of current platforms. *Expert Opinion on Drug Delivery, 12*(11), 1727-1740.

Loreti, G., Maroni, A., Del Curto, M. D., Melocchi, A., Gazzaniga, A., & Zema, L. (2014). Evaluation of hot-melt extrusion technique in the preparation of HPC matrices for prolonged release. *European Journal of Pharmaceutical Sciences, 52*, 77-85.

Macchi, E., Zema, L., Maroni, A., Gazzaniga, A., & Felton, L. (2015). Enteric-coating of pulsatile-release HPC capsules prepared by injection molding. *European Journal of Pharmaceutical Sciences, 70*, 1-11.

Maniruzzaman, M., Boateng, J. S., Snowden, M. J., & Douroumis, D. (2012). A review of hot-melt extrusion: process technology to pharmaceutical products. *International Scholarly Research Notices, 2012*.

Mazurek, S., & Szostak, R. (2006). Quantitative determination of captopril and prednisolone in tablets by FT-Raman spectroscopy. *Journal of Pharmaceutical and Biomedical Analysis, 40*(5), 1225-1230.

McDevitt, J. T., Gurst, A. H., & Chen, Y. (1998). Accuracy of tablet splitting. *Pharmacotherapy: The Journal of Human Pharmacology and Drug Therapy, 18*(1), 193-197.

Melocchi, A., Parietti, F., Loreti, G., Maroni, A., Gazzaniga, A., & Zema, L. (2015). 3D printing by fused deposition modeling (FDM) of a swellable/erodible capsular device for oral pulsatile release of drugs. *Journal of Drug Delivery Science and Technology, 30*, 360-367.

Melocchi, A., Parietti, F., Maroni, A., Foppoli, A., Gazzaniga, A., & Zema, L. (2016). Hot-melt extruded filaments based on pharmaceutical grade polymers for 3D printing by fused deposition modeling. *International Journal of Pharmaceutics, 509*(1-2), 255-263.

Mendonsa, N., Almutairy, B., Kallakunta, V. R., Sarabu, S., Thipsay, P., Bandari, S., & Repka, M. A. (2020). Manufacturing strategies to develop amorphous solid dispersions: An overview. *Journal of Drug Delivery Science and Technology, 55*, 101459.

Mendyk, A., Pacławski, A., Szlek, J., & Jachowicz, R. (2013). PhEq_bootstrap: open-source software for the simulation of f2 distribution in cases of large variability in dissolution profiles. *Dissolution Technology, 20*(1), 13-17.

Meza, C. P., Santos, M. A., & Romañach, R. J. (2006). Quantitation of drug content in a low dosage formulation by transmission near infrared spectroscopy. *AAPS PharmSciTech, 7*(1), E206-E214.

Mitra, B., Chang, J., Wu, S.-J., Wolfe, C. N., Ternik, R. L., Gunter, T. Z., & Victor, M. C. (2017). Feasibility of mini-tablets as a flexible drug delivery tool. *International Journal of Pharmaceutics, 525*(1), 149-159.

Mitra, B., Thool, P., Meruva, S., Aycinena, J. A., Li, J., Patel, J., Patel, K., Agarwal, A., Karki, S., & Bowen, W. (2020). Decoding the small size challenges of mini-tablets for enhanced dose flexibility and micro-dosing. *International Journal of Pharmaceutics, 574*, 118905.

Moseson, D. E., Parker, A. S., Beaudoin, S. P., & Taylor, L. S. (2020). Amorphous solid dispersions containing residual crystallinity: Influence of seed properties and polymer adsorption on dissolution performance. *European Journal of Pharmaceutical Sciences*, 105276.

Nasereddin, J. M., Wellner, N., Alhijjaj, M., Belton, P., & Qi, S. (2018). Development of a simple mechanical screening method for predicting the feedability of a pharmaceutical FDM 3D printing filament. *Pharmaceutical Research, 35*(8), 151.

Newman, A., Knipp, G., & Zografi, G. (2012). Assessing the performance of amorphous solid dispersions. *Journal of Pharmaceutical Sciences, 101*(4), 1355-1377.

Norman, J., Madurawe, R. D., Moore, C. M., Khan, M. A., & Khairuzzaman, A. (2017). A new chapter in pharmaceutical manufacturing: 3D-printed drug products. *Advanced Drug Delivery Reviews, 108*, 39-50.

Nukala, P. K., Palekar, S., Patki, M., & Patel, K. (2019). Abuse deterrent immediate release egg-shaped tablet (egglets) using 3D printing technology: quality by design to optimize drug release and extraction. *AAPS PharmSciTech, 20*(2), 80.

Öblom, H., Zhang, J., Pimparade, M., Speer, I., Preis, M., Repka, M., & Sandler, N. (2019). 3D-printed isoniazid tablets for the treatment and prevention of tuberculosis—Personalized dosing and drug release. *AAPS PharmSciTech, 20*(2), 52.

Okwuosa, T. C., Pereira, B. C., Arafat, B., Cieszynska, M., Isreb, A., & Alhnan, M. A. (2017). Fabricating a shell-core delayed release tablet using dual FDM 3D printing for patient-centred therapy. *Pharmaceutical Research, 34*(2), 427-437.

Okwuosa, T. C., Stefaniak, D., Arafat, B., Isreb, A., Wan, K.-W., & Alhnan, M. A. (2016). A lower temperature FDM 3D printing for the manufacture of patient-specific immediate release tablets. *Pharmaceutical Research, 33*(11), 2704-2712.

Ozaki, S., Kushida, I., Yamashita, T., Hasebe, T., Shirai, O., & Kano, K. (2012). Evaluation of drug supersaturation by thermodynamic and kinetic approaches for the prediction of oral absorbability in amorphous pharmaceuticals. *Journal of Pharmaceutical Sciences, 101*(11), 4220-4230.

Paixão, P., Gouveia, L. F., Silva, N., & Morais, J. A. (2017). Evaluation of dissolution profile similarity–Comparison between the f2, the multivariate statistical distance and the f2 bootstrapping methods. *European Journal of Pharmaceutics and Biopharmaceutics, 112*, 67-74.

Palekar, S., Nukala, P. K., Mishra, S. M., Kipping, T., & Patel, K. (2019). Application of 3D printing technology and quality by design approach for development of age-appropriate pediatric formulation of baclofen. *International Journal of Pharmaceutics, 556*, 106-116.

Pawar, J. N., Fule, R. A., Maniruzzaman, M., & Amin, P. D. (2017). Solid crystal suspension of Efavirenz using hot melt extrusion: Exploring the role of crystalline polyols in improving solubility and dissolution rate. *Materials Science and Engineering: C, 78*, 1023-1034.

Peppas, N. A., & Narasimhan, B. (2014). Mathematical models in drug delivery: How modeling has shaped the way we design new drug delivery systems. *Journal of Controlled Release, 190*, 75-81.

Peppas, N. A., & Sahlin, J. J. (1989). A simple equation for the description of solute release. III. Coupling of diffusion and relaxation. *International Journal of Pharmaceutics, 57*(2), 169-172.

Picker-Freyer, K. M., & Dürig, T. (2007). Physical mechanical and tablet formation properties of hydroxypropylcellulose: in pure form and in mixtures. *AAPS PharmSciTech, 8*(4), 82.

Pietrzak, K., Isreb, A., & Alhnan, M. A. (2015). A flexible-dose dispenser for immediate and extended release 3D printed tablets. *European Journal of Pharmaceutics and Biopharmaceutics, 96*, 380-387.

Popo, M., Romero-Torres, S., Conde, C., & Romañach, R. J. (2002). Blend uniformity analysis using stream sampling and near infrared spectroscopy. *AAPS PharmSciTech, 3*(3), 61-71.

Prasad, L. K., & Smyth, H. (2016). 3D Printing technologies for drug delivery: a review. *Drug Development and Industrial Pharmacy, 42*(7), 1019-1031.

Preis, M. (2015). Orally disintegrating films and mini-tablets—innovative dosage forms of choice for pediatric use. *AAPS PharmSciTech, 16*(2), 234-241.

Price, D. J., Ditzinger, F., Koehl, N. J., Jankovic, S., Tsakiridou, G., Nair, A., Holm, R., Kuentz, M., Dressman, J. B., & Saal, C. (2019). Approaches to increase mechanistic understanding and aid in the selection of precipitation inhibitors for supersaturating formulations–a PEARRL review. *Journal of Pharmacy and Pharmacology, 71*(4), 483-509.

Priyanka, P., Kumar, K., & Teotia, D. (2018). A comprehensive review on pharmaceutical mini tablets. *Journal of Drug Delivery and Therapeutics, 8*(6), 382-390.

Quinzler, R., Gasse, C., Schneider, A., Kaufmann-Kolle, P., Szecsenyi, J., & Haefeli, W. (2006). The frequency of inappropriate tablet splitting in primary care. *European Journal of Clinical Pharmacology, 62*(12), 1065-1073.

Rahman, M., Ahmad, S., Tarabokija, J., & Bilgili, E. (2020a). Roles of surfactant and polymer in drug release from spray-dried hybrid nanocrystal-amorphous solid dispersions (HyNASDs). *Powder Technology, 361*, 663-678.

Rahman, M., Ahmad, S., Tarabokija, J., Parker, N., & Bilgili, E. (2020b). Spray-Dried Amorphous Solid Dispersions of Griseofulvin in HPC/Soluplus/SDS: Elucidating the Multifaceted Impact of SDS as a Minor Component. *Pharmaceutics, 12*(3), 197.

Rahman, M., Arevalo, F., Coelho, A., & Bilgili, E. (2019). Hybrid nanocrystal–amorphous solid dispersions (HyNASDs) as alternative to ASDs for enhanced release of BCS Class II drugs. *European Journal of Pharmaceutics and Biopharmaceutics, 145*, 12-26.

Rahman, M., Coelho, A., Tarabokija, J., Ahmad, S., Radgman, K., & Bilgili, E. (2020c). Synergistic and Antagonistic Effects of Various Amphiphilic Polymer Combinations in Enhancing Griseofulvin Release from Ternary Amorphous Solid Dispersions. *European Journal of Pharmaceutical Sciences*, 105354.

Ranmal, S. R., Cram, A., & Tuleu, C. (2016). Age-appropriate and acceptable paediatric dosage forms: Insights into end-user perceptions, preferences and practices from the Children's Acceptability of Oral Formulations (CALF) Study. *International Journal of Pharmaceutics, 514*(1), 296-307.

Rattanakit, P., Moulton, S. E., Santiago, K. S., Liawruangrath, S., & Wallace, G. G. (2012). Extrusion printed polymer structures: A facile and versatile approach to tailored drug delivery platforms. *International Journal of Pharmaceutics, 422*(1-2), 254-263.

Richey, R. H., Hughes, C., Craig, J. V., Shah, U. U., Ford, J. L., Barker, C. E., Peak, M., Nunn, A. J., & Turner, M. A. (2017). A systematic review of the use of dosage form manipulation to obtain required doses to inform use of manipulation in paediatric practice. *International Journal of Pharmaceutics, 518*(1-2), 155-166.

Ritger, P. L., & Peppas, N. A. (1987). A simple equation for description of solute release II. Fickian and anomalous release from swellable devices. *Journal of Controlled Release, 5*(1), 37-42.

Rood, J. M., Engels, M. J., Ciarkowski, S. L., Wagenknecht, L. D., Dickinson, C. J., & Stevenson, J. G. (2014). Variability in compounding of oral liquids for pediatric patients: a patient safety concern. *Journal of the American Pharmacists Association, 54*(4), 383-389.

Rowe, C., Katstra, W., Palazzolo, R., Giritlioglu, B., Teung, P., & Cima, M. (2000). Multimechanism oral dosage forms fabricated by three dimensional printing™. *Journal of Controlled Release, 66*(1), 11-17.

Rumondor, A. C., Ivanisevic, I., Bates, S., Alonzo, D. E., & Taylor, L. S. (2009a). Evaluation of drug-polymer miscibility in amorphous solid dispersion systems. *Pharmaceutical Research, 26*(11), 2523-2534.

Rumondor, A. C., Marsac, P. J., Stanford, L. A., & Taylor, L. S. (2009b). Phase behavior of poly (vinylpyrrolidone) containing amorphous solid dispersions in the presence of moisture. *Molecular Pharmaceutics, 6*(5), 1492-1505.

Rycerz, K., Stepien, K. A., Czapiewska, M., Arafat, B. T., Habashy, R., Isreb, A., Peak, M., & Alhnan, M. A. (2019). Embedded 3D printing of novel bespoke soft dosage form concept for pediatrics. *Pharmaceutics, 11*(12), 630.

Sadia, M., Arafat, B., Ahmed, W., Forbes, R. T., & Alhnan, M. A. (2018a). Channelled tablets: An innovative approach to accelerating drug release from 3D printed tablets. *Journal of Controlled Release, 269*, 355-363.

Sadia, M., Isreb, A., Abbadi, I., Isreb, M., Aziz, D., Selo, A., Timmins, P., & Alhnan, M. A. (2018b). From 'fixed dose combinations' to 'a dynamic dose combiner': 3D printed bi-layer antihypertensive tablets. *European Journal of Pharmaceutical Sciences, 123*, 484-494.

Sadia, M., Sośnicka, A., Arafat, B., Isreb, A., Ahmed, W., Kelarakis, A., & Alhnan, M. A. (2016). Adaptation of pharmaceutical excipients to FDM 3D printing for the fabrication of patient-tailored immediate release tablets. *International Journal of Pharmaceutics, 513*(1-2), 659-668.

Saerens, L., Dierickx, L., Lenain, B., Vervaet, C., Remon, J. P., & De Beer, T. (2011). Raman spectroscopy for the in-line polymer–drug quantification and solid state characterization during a pharmaceutical hot-melt extrusion process. *European Journal of Pharmaceutics and Biopharmaceutics, 77*(1), 158-163.

Salunke, S., & Tuleu, C. (2016). Formulating better medicines for children—Still too far to walk. *International Journal of Pharmaceutics, 511*(2), 1124-1126.

Sánchez-Paternina, A., Sierra-Vega, N. O., Cárdenas, V., Méndez, R., Esbensen, K. H., & Romañach, R. J. (2019). Variographic analysis: a new methodology for quality assurance of pharmaceutical blending processes. *Computers & Chemical Engineering, 124*, 109-123.

Sandler, N., & Preis, M. (2016). Printed drug-delivery systems for improved patient treatment. *Trends in pharmacological sciences, 37*(12), 1070-1080.

Sarode, A., Wang, P., Cote, C., & Worthen, D. R. (2013a). Low-viscosity hydroxypropylcellulose (HPC) grades SL and SSL: versatile pharmaceutical polymers for dissolution enhancement, controlled release, and pharmaceutical processing. *AAPS PharmSciTech, 14*(1), 151-159.

Sarode, A. L., Malekar, S. A., Cote, C., & Worthen, D. R. (2014). Hydroxypropyl cellulose stabilizes amorphous solid dispersions of the poorly water soluble drug felodipine. *Carbohydrate Polymers, 112*, 512-519.

Sarode, A. L., Sandhu, H., Shah, N., Malick, W., & Zia, H. (2013b). Hot melt extrusion for amorphous solid dispersions: temperature and moisture activated drug–polymer interactions for enhanced stability. *Molecular Pharmaceutics, 10*(10), 3665-3675.

Sathigari, S. K., Radhakrishnan, V. K., Davis, V. A., Parsons, D. L., & Babu, R. J. (2012). Amorphous-state characterization of efavirenz—polymer hot-melt extrusion systems for dissolution enhancement. *Journal of Pharmaceutical Sciences, 101*(9), 3456-3464.

Schulze, D. (2008). Powders and bulk solids. Behaviour, characterization, storage and flow. Newyork, NY: Springer-Verlag Berlin Heidelberg.

Scoutaris, N., Ross, S. A., & Douroumis, D. (2018). 3D printed “Starmix” drug loaded dosage forms for paediatric applications. *Pharmaceutical Research, 35*(2), 34.

Serajuddin, A. T. (1999). Solid dispersion of poorly water-soluble drugs: Early promises, subsequent problems, and recent breakthroughs. *Journal of Pharmaceutical Sciences, 88*(10), 1058-1066.

Shah, R. B., Collier, J. S., Sayeed, V. A., Bryant, A., Habib, M. J., & Khan, M. A. (2010). Tablet splitting of a narrow therapeutic index drug: a case with levothyroxine sodium. *AAPS PharmSciTech, 11*(3), 1359-1367.

Shah, S., Maddineni, S., Lu, J., & Repka, M. A. (2013). Melt extrusion with poorly soluble drugs. *International Journal of Pharmaceutics, 453*(1), 233-252.

Siddiqui, A., Rahman, Z., Bykadi, S., & Khan, M. A. (2014). Chemometric methods for the quantification of crystalline tacrolimus in solid dispersion by powder X-ray diffractrometry. *Journal of Pharmaceutical Sciences, 103*(9), 2819-2828.

Siepmann, J., Karrout, Y., Gehrke, M., Penz, F., & Siepmann, F. (2013). Predicting drug release from HPMC/lactose tablets. *International Journal of Pharmaceutics, 441*(1-2), 826-834.

Siepmann, J., & Peppas, N. (2000). Hydrophilic matrices for controlled drug delivery: an improved mathematical model to predict the resulting drug release kinetics (the “sequential layer” model). *Pharmaceutical Research, 17*(10), 1290-1298.

Siepmann, J., & Siepmann, F. (2012). Modeling of diffusion controlled drug delivery. *Journal of Controlled Release, 161*(2), 351-362.

Siepmann, J., Streubel, A., & Peppas, N. (2002). Understanding and predicting drug delivery from hydrophilic matrix tablets using the “sequential layer” model. *Pharmaceutical Research, 19*(3), 306-314.

Sievens-Figueroa, L., Bhakay, A., Jerez-Rozo, J. I., Pandya, N., Romañach, R. J., Michniak-Kohn, B., Iqbal, Z., Bilgili, E., & Davé, R. N. (2012). Preparation and characterization of hydroxypropyl methyl cellulose films containing stable BCS Class II drug nanoparticles for pharmaceutical applications. *International Journal of Pharmaceutics, 423*(2), 496-508.

Skowyra, J., Pietrzak, K., & Alhnan, M. A. (2015). Fabrication of extended-release patient-tailored prednisolone tablets via fused deposition modelling (FDM) 3D printing. *European Journal of Pharmaceutical Sciences, 68*, 11-17.

Smirnova, I., Suttiruengwong, S., & Arlt, W. (2004). Feasibility study of hydrophilic and hydrophobic silica aerogels as drug delivery systems. *Journal of Non-Crystalline Solids, 350*, 54-60.

Solanki, N., Gupta, S. S., & Serajuddin, A. T. (2018a). Rheological analysis of itraconazole-polymer mixtures to determine optimal melt extrusion temperature for development of amorphous solid dispersion. *European Journal of Pharmaceutical Sciences, 111*, 482-491.

Solanki, N. G., Gumaste, S. G., Shah, A. V., & Serajuddin, A. T. (2019a). Effects of surfactants on itraconazole-hydroxypropyl methylcellulose acetate succinate solid dispersion prepared by hot melt extrusion. II: rheological analysis and extrudability testing. *Journal of Pharmaceutical Sciences, 108*(9), 3063-3073.

Solanki, N. G., Lam, K., Tahsin, M., Gumaste, S. G., Shah, A. V., & Serajuddin, A. T. (2019b). Effects of surfactants on itraconazole-HPMCAS solid dispersion prepared by hot-melt extrusion I: miscibility and drug release. *Journal of Pharmaceutical Sciences, 108*(4), 1453-1465.

Solanki, N. G., Tahsin, M., Shah, A. V., & Serajuddin, A. T. (2018b). Formulation of 3D printed tablet for rapid drug release by fused deposition modeling: screening polymers for drug release, drug-polymer miscibility and printability. *Journal of Pharmaceutical Sciences, 107*(1), 390-401.

Strickley, R. G. (2019). Pediatric oral formulations: an updated review of commercially available pediatric oral formulations since 2007. *Journal of Pharmaceutical Sciences, 108*(4), 1335-1365.

Sujja-Areevath, J., Munday, D., Cox, P., & Khan, K. (1998). Relationship between swelling, erosion and drug release in hydrophillic natural gum mini-matrix formulations. *European Journal of Pharmaceutical Sciences, 6*(3), 207-217.

Sun, D. D., Ju, T.-c. R., & Lee, P. I. (2012). Enhanced kinetic solubility profiles of indomethacin amorphous solid dispersions in poly (2-hydroxyethyl methacrylate) hydrogels. *European Journal of Pharmaceutics and Biopharmaceutics, 81*(1), 149-158.

Sun, D. D., & Lee, P. I. (2013). Evolution of supersaturation of amorphous pharmaceuticals: the effect of rate of supersaturation generation. *Molecular Pharmaceutics, 10*(11), 4330-4346.

Sun, D. D., & Lee, P. I. (2015). Probing the mechanisms of drug release from amorphous solid dispersions in medium-soluble and medium-insoluble carriers. *Journal of Controlled Release, 211*, 85-93.

Sun, D. D., Wen, H., & Taylor, L. S. (2016). Non-sink dissolution conditions for predicting product quality and in vivo performance of supersaturating drug delivery systems. *Journal of Pharmaceutical Sciences, 105*(9), 2477-2488.

Tagami, T., Fukushige, K., Ogawa, E., Hayashi, N., & Ozeki, T. (2017). 3D printing factors important for the fabrication of polyvinylalcohol filament-based tablets. *Biological and Pharmaceutical Bulletin, 40*(3), 357-364.

Tagami, T., Nagata, N., Hayashi, N., Ogawa, E., Fukushige, K., Sakai, N., & Ozeki, T. (2018). Defined drug release from 3D-printed composite tablets consisting of drug-loaded polyvinylalcohol and a water-soluble or water-insoluble polymer filler. *International Journal of Pharmaceutics, 543*(1-2), 361-367.

Tan, D. K., Maniruzzaman, M., & Nokhodchi, A. (2020). Development and optimisation of novel polymeric compositions for sustained release theophylline caplets (PrintCap) via FDM 3D printing. *Polymers, 12*(1), 27.

Tatavarti, A. S., Fahmy, R., Wu, H., Hussain, A. S., Marnane, W., Bensley, D., Hollenbeck, G., & Hoag, S. W. (2005). Assessment of NIR spectroscopy for nondestructive analysis of physical and chemical attributes of sulfamethazine bolus dosage forms. *AAPS PharmSciTech, 6*(1), E91-E99.

Teng, J., Song, C. K., Williams, R. L., & Polli, J. E. (2002). Lack of medication dose uniformity in commonly split tablets. *Journal of the American Pharmaceutical Association (1996), 42*(2), 195-199.

Terán, M. M., & Flament, M. (2016). Development of multiparticulate orodispersible tablets for pediatric use. *International Journal of Pharmaceutics, 2*(511), 1143.

Tewari, J., Dixit, V., & Malik, K. (2010). On-line monitoring of residual solvent during the pharmaceutical drying process using non-contact infrared sensor: a process analytical technology (PAT) approach. *Sensors and Actuators B: Chemical, 144*(1), 104-111.

Thommes, M., Ely, D. R., Carvajal, M. T., & Pinal, R. (2011). Improvement of the dissolution rate of poorly soluble drugs by solid crystal suspensions. *Molecular Pharmaceutics, 8*(3), 727-735.

Thomson, S. A., Tuleu, C., Wong, I. C., Keady, S., Pitt, K. G., & Sutcliffe, A. G. (2009). Minitablets: new modality to deliver medicines to preschool-aged children. *Pediatrics, 123*(2), e235-e238.

Tidau, M., Kwade, A., & Finke, J. H. (2019). Influence of high, disperse API load on properties along the Fused-Layer Modeling process chain of solid dosage forms. *Pharmaceutics, 11*(4), 194.

Tumuluri, V. S., Kemper, M. S., Lewis, I. R., Prodduturi, S., Majumdar, S., Avery, B. A., & Repka, M. A. (2008). Off-line and on-line measurements of drug-loaded hot-melt extruded films using Raman spectroscopy. *International Journal of Pharmaceutics, 357*(1-2), 77-84.

Uekama, K., Ikegami, K., Wang, Z., Horiuchi, Y., & Hirayama, F. (1992). Inhibitory effect of 2-hydroxypropyl-β-cyclodextrin on crystal-growth of nifedipine during storage: Superior dissolution and oral bioavailability compared with polyvinylpyrrolidone K-30. *Journal of Pharmacy and Pharmacology, 44*(2), 73-78.

Van den Mooter, G. (2012). The use of amorphous solid dispersions: A formulation strategy to overcome poor solubility and dissolution rate. *Drug Discovery Today: Technologies, 9*(2), e79-e85.

van Riet-Nales, D. A., Doeve, M. E., Nicia, A. E., Teerenstra, S., Notenboom, K., Hekster, Y. A., & van den Bemt, B. J. (2014). The accuracy, precision and sustainability of different techniques for tablet subdivision: breaking by hand and the use of tablet splitters or a kitchen knife. *International Journal of Pharmaceutics, 466*(1-2), 44-51.

Vargas, J. M., Nielsen, S., Cárdenas, V., Gonzalez, A., Aymat, E. Y., Almodovar, E., Classe, G., Colón, Y., Sanchez, E., & Romañach, R. J. (2018). Process analytical technology in continuous manufacturing of a commercial pharmaceutical product. *International Journal of Pharmaceutics, 538*(1-2), 167-178.

Vasconcelos, T., Sarmento, B., & Costa, P. (2007). Solid dispersions as strategy to improve oral bioavailability of poor water soluble drugs. *Drug Discovery Today, 12*(23-24), 1068-1075.

Verstraete, G., Samaro, A., Grymonpré, W., Vanhoorne, V., Van Snick, B., Boone, M., Hellemans, T., Van Hoorebeke, L., Remon, J. P., & Vervaet, C. (2018). 3D printing of high drug loaded dosage forms using thermoplastic polyurethanes. *International Journal of Pharmaceutics, 536*(1), 318-325.

Wang, S., Capoen, L., D'hooge, D. R., & Cardon, L. (2018). Can the melt flow index be used to predict the success of fused deposition modelling of commercial poly (lactic acid) filaments into 3D printed materials? *Plastics, Rubber and Composites, 47*(1), 9-16.

Wei, C., Solanki, N. G., Vasoya, J. M., Shah, A. V., & Serajuddin, A. T. (2020). Development of 3D printed tablets by Fused Deposition Modeling using polyvinyl alcohol as polymeric matrix for rapid drug release. *Journal of Pharmaceutical Sciences*.

Wening, K., & Breitkreutz, J. (2011). Oral drug delivery in personalized medicine: unmet needs and novel approaches. *International Journal of Pharmaceutics, 404*(1-2), 1-9.

Workman, J. (1997). Optical spectrometers. *Applied spectroscopy: A Compact Reference for Practitioners*, 3-28.

Xu, G., & Sunada, H. (1995). Influence of formulation change on drug release kinetics from hydroxypropylmethylcellulose matrix tablets. *Chemical and Pharmaceutical Bulletin, 43*(3), 483-487.

Yadav, V., & Yadav, A. (2009). Effect of different stabilizers and polymers on spherical agglomerates of gresiofulvine by emulsion solvent diffusion (ESD) system. *International Journal of PharmTech Research, 1*(2), 149-150.

Yang, Y., Chen, Y., Wei, Y., & Li, Y. (2016). 3D printing of shape memory polymer for functional part fabrication. *The International Journal of Advanced Manufacturing Technology, 84*(9-12), 2079-2095.

Yang, Y., Wang, H., Li, H., Ou, Z., & Yang, G. (2018). 3D printed tablets with internal scaffold structure using ethyl cellulose to achieve sustained ibuprofen release. *European Journal of Pharmaceutical Sciences, 115*, 11-18.

Yu, D. G., Shen, X. X., Branford-White, C., Zhu, L. M., White, K., & Yang, X. L. (2009). Novel oral fast-disintegrating drug delivery devices with predefined inner structure fabricated by Three-Dimensional Printing. *Journal of Pharmacy and Pharmacology, 61*(3), 323-329.

Zaldivar, R., Mclouth, T., Ferrelli, G., Patel, D., Hopkins, A., & Witkin, D. (2018). Effect of initial filament moisture content on the microstructure and mechanical performance of ULTEM® 9085 3D printed parts. *Additive Manufacturing, 24*, 457-466.

Żarów, A., Zhou, B., Wang, X., Pinal, R., & Iqbal, Z. (2011). Spectroscopic and X-ray diffraction study of structural disorder in cryomilled and amorphous griseofulvin. *Applied Spectroscopy, 65*(2), 135-143.

Zhang, J., Feng, X., Patil, H., Tiwari, R. V., & Repka, M. A. (2017a). Coupling 3D printing with hot-melt extrusion to produce controlled-release tablets. *International Journal of Pharmaceutics, 519*(1-2), 186-197.

Zhang, J., Yang, W., Vo, A. Q., Feng, X., Ye, X., Kim, D. W., & Repka, M. A. (2017b). Hydroxypropyl methylcellulose-based controlled release dosage by melt extrusion and 3D printing: Structure and drug release correlation. *Carbohydrate Polymers, 177*, 49-57.

Zhang, J., Ying, Y., Pielecha-Safira, B., Bilgili, E., Ramachandran, R., Romañach, R., Davé, R. N., & Iqbal, Z. (2014). Raman spectroscopy for in-line and off-line quantification of poorly soluble drugs in strip films. *International Journal of Pharmaceutics, 475*(1-2), 428-437.

Zhang, L., Alfano, J., Race, D., & Davé, R. N. (2018). Zero-order release of poorly water-soluble drug from polymeric films made via aqueous slurry casting. *European Journal of Pharmaceutical Sciences, 117*, 245-254.

Zhao, J., Yin, D., Rowe, J., Badawy, S., Nikfar, F., & Pandey, P. (2018). Understanding the factors that control the quality of mini-tablet compression: flow, particle size, and tooling dimension. *Journal of Pharmaceutical Sciences, 107*(4), 1204-1208.

Zheng, K., Lin, Z., Capece, M., Kunnath, K., Chen, L., & Davé, R. N. (2019). Effect of particle size and polymer loading on dissolution behavior of amorphous griseofulvin powder. *Journal of Pharmaceutical Sciences, 108*(1), 234-242.

Zipdose®, A. (2015). The world's first 3DP dosage form. Retrieved from https://www.aprecia.com/technology/zipdose